Modelling the Effects of Climate Change on the Surface and Subsurface Hydrology of the Grand River Watershed

by

Dennis Colautti

A thesis
presented to the University of Waterloo
in fulfillment of the
thesis requirement for the degree of
Doctor of Philosophy
in
Earth Sciences

Waterloo, Ontario, Canada, 2010

AUTHOR'S DECLARATION

I hereby declare that I am the sole author of this thesis. This is a true copy of the thesis, including any required final revisions, as accepted by my examiners.
I understand that my thesis may be made electronically available to the public.

Abstract

A numerical modelling analysis of climate change's precipitation effects on the long-term, averaged surface and subsurface hydrology of the Grand River Watershed (GRW) was undertaken in order to assess possible areas of concern for decision makers in the water management sector. The physically-based, fully-integrated and variably-saturated 3-D surface-subsurface numerical simulator, HydroGeoSphere, was used to drive five mid-21st century climate change scenarios, developed from multiple general circulation models. Calibration involved altering measured and literature-derived hydraulic conductivity and precipitation distribution estimates, resulting in very good matching between observed and simulated long-term average surface flow at all gauge stations. Subsurface head results, too, matched observed heads quite well, though groundwater linkage to neighbouring watersheds was not included. When groundwater linkage to neighbouring watersheds was allowed, *via* regional Dirichlet boundary conditions used in a parent study, groundwater throughput was deemed to be unrealistic.

All but one of the climate change scenarios caused an increase in both river discharge and water table elevation, with the greatest climate perturbations causing the greatest increases. For Scenario 1 (5% less precipitation than the 1960-to-1999 average), percentage discharge changes averaged -15% over all gauge stations. For the other scenarios (more precipitation than average), the inter-scenario discharge response ranged from approximately +12% to +59%. In general the range of inter-

subcatchment response was greater than was the range for intra-subcatchment response; the greatest percentage response was consistently in the Speed River subcatchment, while the least was consistently in the Nith and Conestogo subcatchments. The exception was the application of less-than-average precipitation to the Grand River, whose gauge stations reported percentage changes in discharge that varied more substantially from one another.

Subsurface hydrology reacted to the climate change scenarios in much the same manner as did the surface hydrology, with all climate change scenarios associated with a precipitation increase unsurprisingly resulting in higher total hydraulic heads throughout the entire domain. Specifically, the minimum and maximum mean head increases among the climate change scenarios were 0.41 m and 1.25 m respectively, while the only decrease was an average of 0.55 m. Similarly, the depth from the ground surface to the water table decreased in most scenarios, the maximum water table rise being 1.08 m and the minimum 0.36 m. When precipitation was allowed to decrease by 5% relative to the long-term average, the average water table elevation decreased by 0.48 m. However the water table's pattern of high and low points remained very much the same among all climate change scenarios, suggesting that basin-wide groundwater flow patterns may not be among the hydrological measures most sensitive to climate change. Groundwater recharge, like almost all other components of the water budget, changed in linear proportion to the climate forcing and in agreement with GRW recharge estimates

developed by others. Evapotranspiration, which met potential evapotranspiration in all scenarios due to the constant application of precipitation, was the only element of the water budget that did not increase, even though the water table was elevated closer to the rooting zone by most of the climate scenarios.

On a smaller scale, changes in flow patterns may well be expected, given that zones of infiltration were observed to intensify with most of the climate forcing.

Acknowledgements

I extend my sincere gratitude to the following people:

• Ed Sudicky for giving me the opportunity to be part of his group of modellers, and for his patience and helpful advice. This work was funded with a NSERC Discovery Grant, a grant from the Canadian Water Network, and a Tier I Canada Research Chair awarded to Dr. Sudicky;
• Rob McLaren for the truly countless occasions when he dropped whatever he was doing to give me technical assistance in many aspects of the modelling process;
•Young-Jin Park for his assistance with the HydroGeoSphere code, and especially for his assistance during the model calibration phase;
• Jianming (Jeremy) Chen, for taking a keen, insightful, and very helpful interest in my work, even when his own work demanded much of him;
• advisory committee members, Jon Sykes and Andre Unger, for their helpful advice;
• and of course my family, without whose patience, support, and occasional helpful nudge, the present work might never have materialized.

Contents

List of Figures

List of Tables

Chapter 1: Introduction

While the percentage contribution of factors, such as greenhouse gas emissions (Loáiciga, 2003), to large-scale climate change are still being determined, there exists much concern over the degree of large-scale temporal and spatial changes in temperature, precipitation, and evapotranspiration (ET). Despite this and the recognition that climate change may be one of the greatest influences stressing the hydrologic system, relatively little research has been undertaken regarding the potential impacts to groundwater (IPCC, 2007). Unconfined groundwater systems can be strongly correlated with temperature and precipitation (Chen *et al*., 2004), but these parameters' effects on deeper groundwater and surface water flow systems of large areas require further investigation. The same is true of effects on groundwater-surface water interaction, and on baseflow into streams. Several studies (Alcamo *et al.*, 2003; Kundzewicz *et al.*, 2008; Howard and Griffith, 2009; Nyenje and Batelaan, 2009) have examined these influences to some extent, but not at both decadal time scales and spatial scales on the order of several thousand square kilometers. Furthermore, the flow models used in these studies often neither couple the groundwater system simultaneously and physically to the surface water system, nor are they coupled (Sudicky *et al.*, 2008; Partington *et al*., 2009) to general circulation models (GCMs) that model primarily link atmospheric-oceanic-land surface processes. Output from GCMs -- temperature, precipitation, and ET, for example -- can be used as hydrological model input. Better model integration, combined with

the larger scales, should enable the instructive prediction of, as just one example, the changes in river discharge that can be expected to accompany climate change. Greater discharge might allow increased pollution from continued urbanization to be mitigated by the surface system's increased ability to flush away contaminants, thus allaying fears that sewage output to the river system cannot grow. On the other hand, prediction of a lowering of the regional water table may further convince water managers that drinking water alternatives to the groundwater system should be sought, and that further water use and protection restrictions should be set in place. Thus, the principal objective of the present work is to link the averaged, long-term-predicted precipitation output of several GCMs to a fully-integrated surface-subsurface hydrological model, so as to assess the effects of various climate change scenarios on the surface and subsurface hydrology of the Grand River Watershed (GRW). The following two sections provide some further insight into related studies, as well as describing the present work's study area, numerical model, objectives, and limitations in more detail. These are followed by an analysis of the model application's results, which in turn are followed by some concluding remarks, including a discussion of the areas of potential improvement in future, related research efforts.

Chapter 2: Background

2.1 Previous Studies

The most obvious and pertinent work relating to the present study was commissioned by the Grand River Conservation Authority (GRCA), produced in 2001 (Holysh *et al*., 2001), and which continues to be updated (Graham and Banks, 2004; AquaResource Inc., 2007). This ongoing effort forms the basis of the present study's conceptual model, *via* borrowed hydrostratigraphy and material properties, as clarified later. It consists of a FEFLOW (Diersch, 2002) groundwater flow model whose recharge is provided *via* linkage to a GAWSER (Schroeter, 1989) surface runoff model designed for flood prediction. Although this linkage is not physically-based, GAWSER usefully takes into account such important factors as freezing, melting, and hence infiltration capacity. Because of the non-physicality, the computational load is decreased, and simulation times are kept reasonable, even when undertaking transient simulations. Further GRW-related studies (though not in the context of climate change) are summarized by Singer (1997).

The body of climate change-related hydrological studies is considerable, and includes studies situated even within the GRW, such as Brouwers (2007), which simulated climate change by altering recharge and then using the HELP3 system (Schroeder *et al.*, 1994b) to feed that recharge into HydroGeoSphere's (HGS's) subsurface simulator, as a transient boundary condition. An advantage of this

approach is the ability to simulate near-surface hydrological processes under freezing temperatures. Another GRW-related study (Jyrkama and Sykes, 2007) focussed on the distribution and timing of recharge. Arnell (2003), like many others, modelled catchment surface runoff at several locations around the world, in response to several climate change scenarios. Like Jyrkama and Sykes, Arnell found that climate change brought both positive and negative hydrological changes, depending on location.

HGS was used by Goderniaux *et al*. (2009) in a 480 km^2 catchment in Belgium to estimate the impacts of climate change on groundwater reserves; it was predicted that groundwater levels could decrease by up to 8 m, and that streamflow could decrease by between 9% and 33% by 2080. Discretization was approximately the same as in the present work, although the uppermost layers each were no less than 1 m thick, compared the 0.25 m lower limit here. Their approach involved the calculation of evapotranspiration as a function of the soil moisture at each node, and downscaled the output of GCMs, thus improving on the present study's approach, though at a much smaller spatial scale both horizontally and vertically.

Minville *et al*. (2008) took a similar approach to the present work in terms of climate change scenarios (five GCMs considered, most predicting between 10% and 20% increase in precipitation by 2080). The spatial scale of the Chute-du-Diable watershed in south-central Quebec was 9700 km^2, and the past climate was based on a 1961 to 1990 record, using basin-averaged values of weather data. Snow accumulation, melt, and aging, and soil freezing and thawing were among the

mechanisms taken into account using HSAMI, a 23-parameter, lumped, conceptual, rainfall-runoff model. The modelling allowed for seasonal prediction and produced close monthly-averaged hydrograph matches between 1978 and 2003. Spring flooding was predicted to take place between one and five weeks earlier than at present; however, changes in the subsurface flow system were not presented.

Jha *et al*. (2004) examined the impact of climate change on streamflow in the Upper Mississippi River Basin by coupling a regional climate model, rather than a global-scale climate model, to the hydrologic model, SWAT. A climate change scenario with 20% increased precipitation was favoured, resulting annually in a 51% increase in surface runoff and a 43% increase in groundwater recharge, although again the subsurface was not examined in any detail.

Scibek and Allen (2006) used HELP to apply GCM-based recharge to a MODFLOW groundwater model. Four climate change scenarios were simulated for the purpose of predicting groundwater levels. It was found that spatial rather than temoral variation of recharge affected groundwater levels primarily.

In a study of 22 Australian catchments, Jones *et al*. (2006) estimated the sensitivity of two lumped-parameter rainfall-runoff models and an empirical model to predicted changes in rainfall and potential evaporation. They found that "a first-order relationship can be used to give a rough estimate of changes in runoff using estimates of change in rainfall and potential evaporation representing small to modest changes in climate."

Milly *et al.* (2005) summarized the predicted multidecadal changes in streamflow on many continents, resulting from climate change. Results from twelve climate models showed 10% to 40% increases in runoff in the region considered in the present work.

Eight Belgian watersheds with varying characteristics were studied by Gellens and Roulin (1998) to determine how climate change might impact surface water flow. Precipitation change drove stream flow impact, whose direction in most cases matched that of the precipitation forcing.

2.2 Study Area

The GRW (Figures 2.1 and 2.2) was chosen principally due to data availability and its status as a key heritage watershed. It is home to a rapidly growing population of roughly 900,000 people, about 82% of whom rely on groundwater for everyday

Figure 2.1: Location of the Grand River Watershed (GRW)

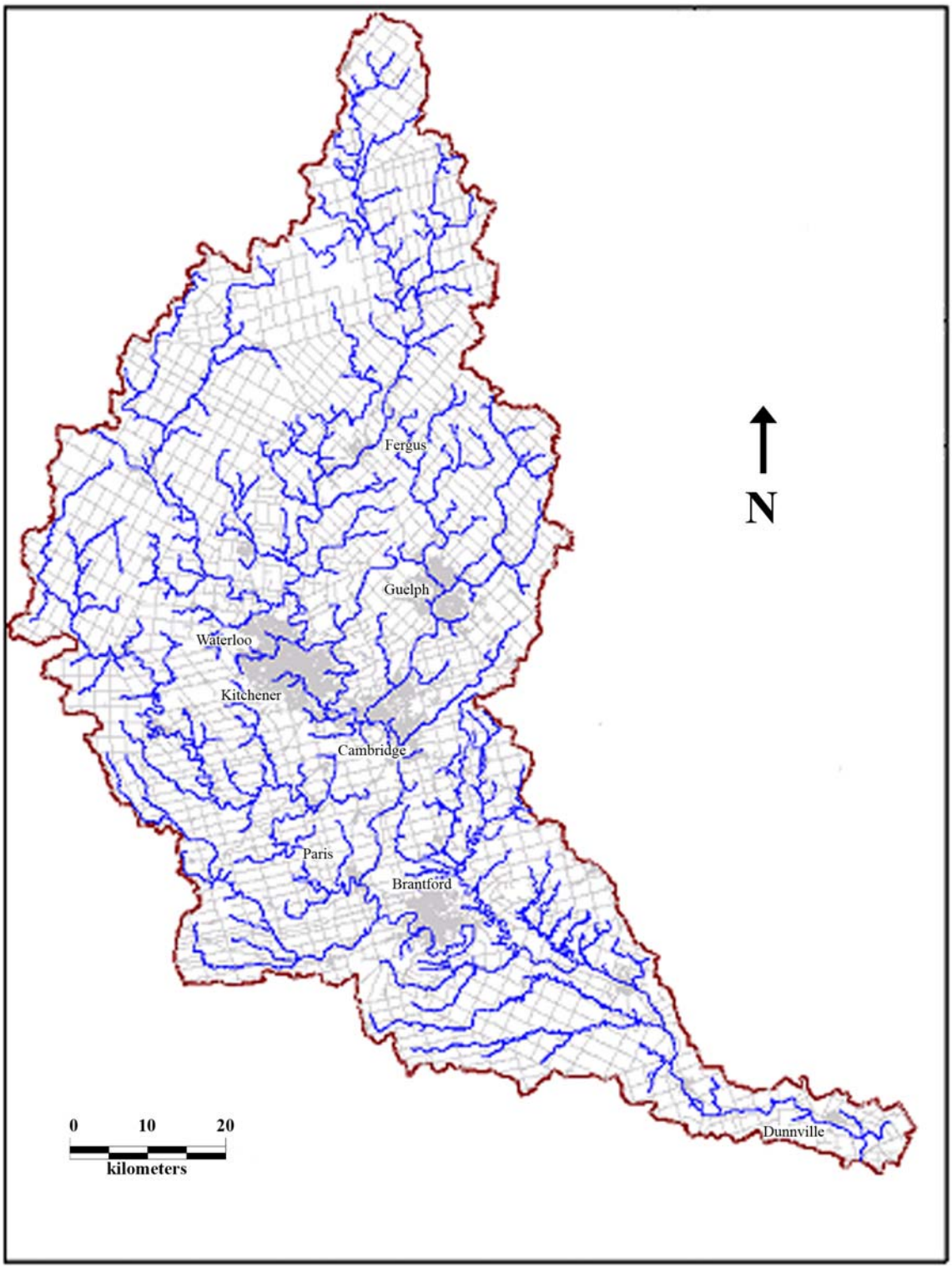

Figure 2.2: Grand River Watershed surficial boundary and river network.

domestic water requirements (Holysh *et al*., 2001). Because of the population size, the watershed is significantly instrumented and managed by way of reservoirs, and thus numerous datasets are available; examples (see Figure 3.7) include databases of pumping rates, water levels, and lithologic descriptions from thousands of wells, available from either Ontario's Ministry of the Environment, the GRCA, or the Region of Waterloo. The most significant example is the study (Graham and Banks, 2004) which forms the basis for much of the conceptual model of the present work, and from which several datasets have been obtained.

Optimal operation of the GRW's water management facilities relies on knowing the timing and quantity of both short-term and long-term hydrological phenomena such as snowmelt and groundwater recharge/discharge zones, respectively. (The present work focuses fully on long-term average conditions, although this focus nonetheless provides some generalized information on short-term processes.) Proper management arguably will become even more important as the watershed's cities – principally Kitchener, Waterloo, Cambridge, Guelph, and Brantford -- continue to rapidly expand both spatially and in terms of population, which is expected to reach approximately 1.2 million people by 2027 (AquaResource Inc., 2007). This growth already has prompted the GRW's regional planners to consider significantly changing the source of drinking water from the subsurface to the surface – for example from groundwater wells to the Great Lakes system, via a pipeline extending to Lake Erie.

The GRW's main tributary, the approximately 290 km-long Grand River, runs through each of the Watershed's main cities except for Guelph (Speed River). Other important rivers are the Conestogo, Nith, and Speed, whose waters eventually spill into Lake Erie *via* the Grand River at Port Maitland. This southern region of the GRW is characterized by glaciolacustrine clay plains (southernmost region in Figure 2.5) and a low point of 175 m above sea level (Figure 2.3), which contrast against the higher-permeability, higher-relief central area lying just to the north, where sand- and gravel kame moraines are abundant (Figures 2.4, 2.5, and 2.7). Here, greater groundwater recharge is facilitated by the relatively high-permeability material, although there are depressions here lined by lower permeability materials, rendering them practically hydrologically unconnected, and encouraging surface storage rather than runoff. In large part, the northern portion of the GRW, with its high point being more than 500m above sea level, consists of lower-permeability till plains (northernmost region in Figure 2.5). Figure 2.6 shows the bedrock elevation change throughout the watershed.

While there are average meteorological differences, too, between the southern and more northern sections of the GRW, on average the study area receives approximately 950 mm of precipitation per year, and has been estimated to experience 500 mm to 550 mm of evapotranspiration annually (AquaResource Inc., 2007). Snow accumulation and melt are important in determining especially the

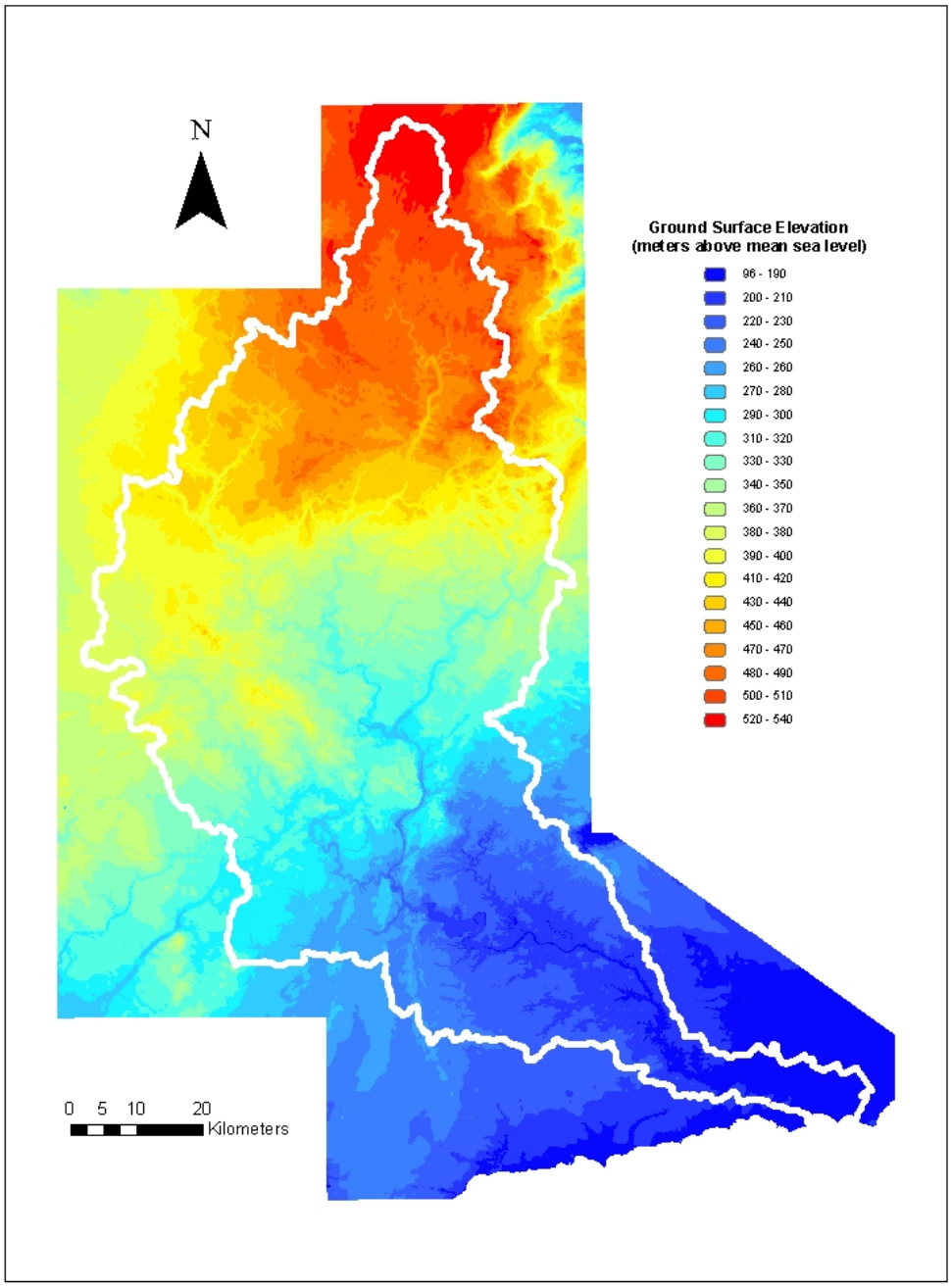

Figure 2.3: Grand River Watershed ground surface elevation (published by the Grand River Conservation Authority, 2000)

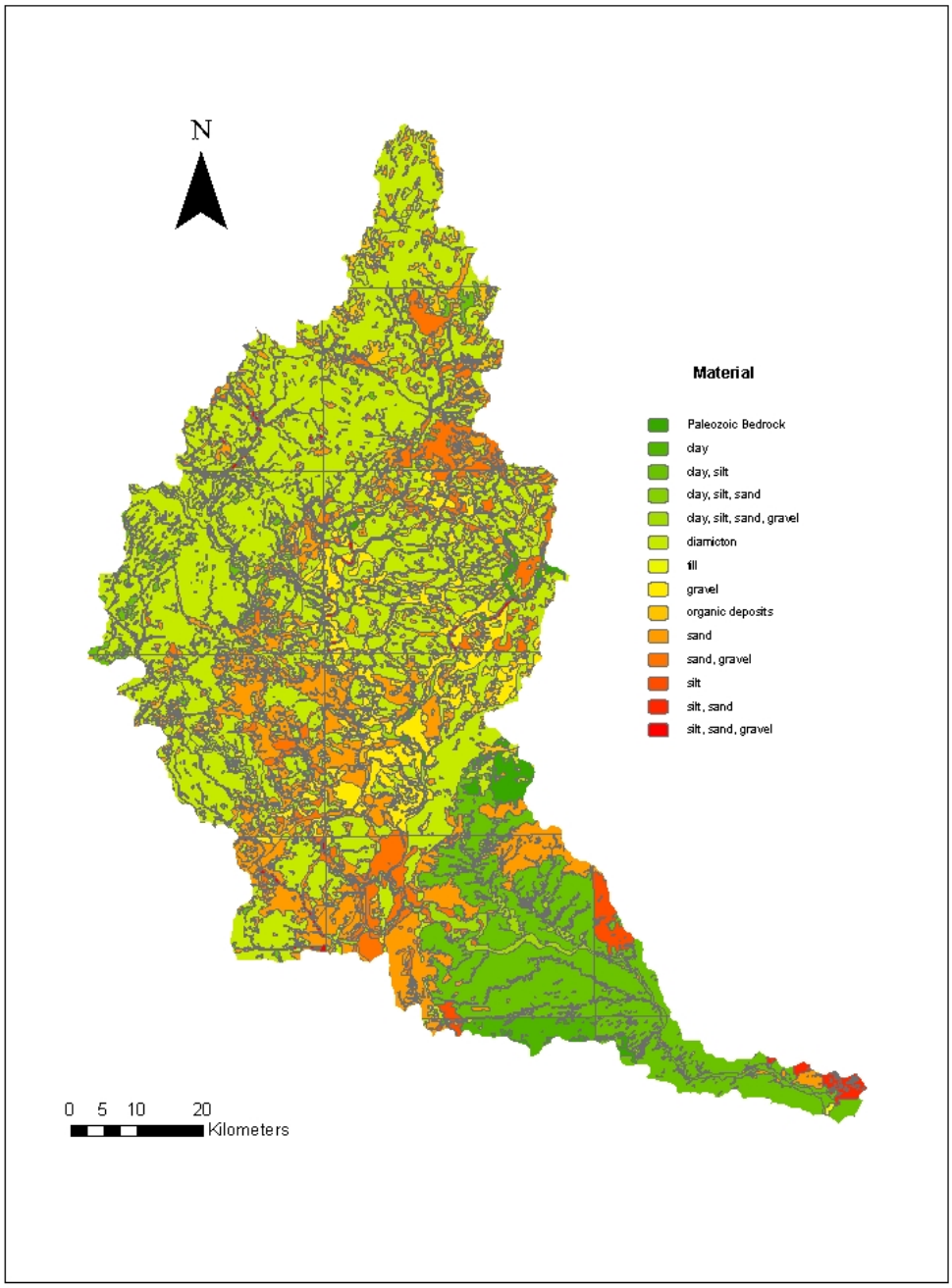

Figure 2.4: Grand River Watershed surface geological materials (published by the Grand River Conservation Authority, 2000)

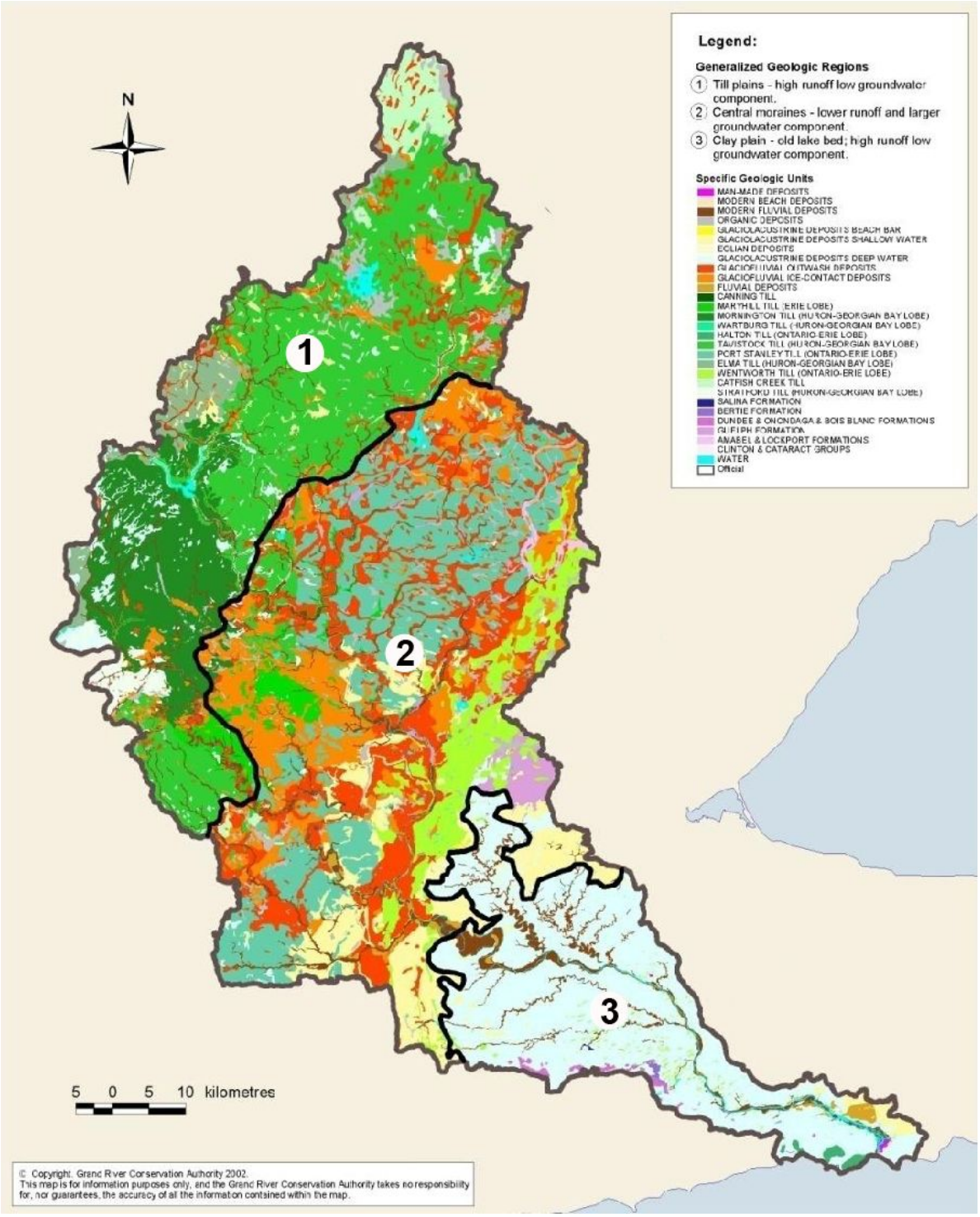

Figure 2.5: Grand River Watershed's three generalized geologic regions (published by the Grand River Conservation Authority, 2002)

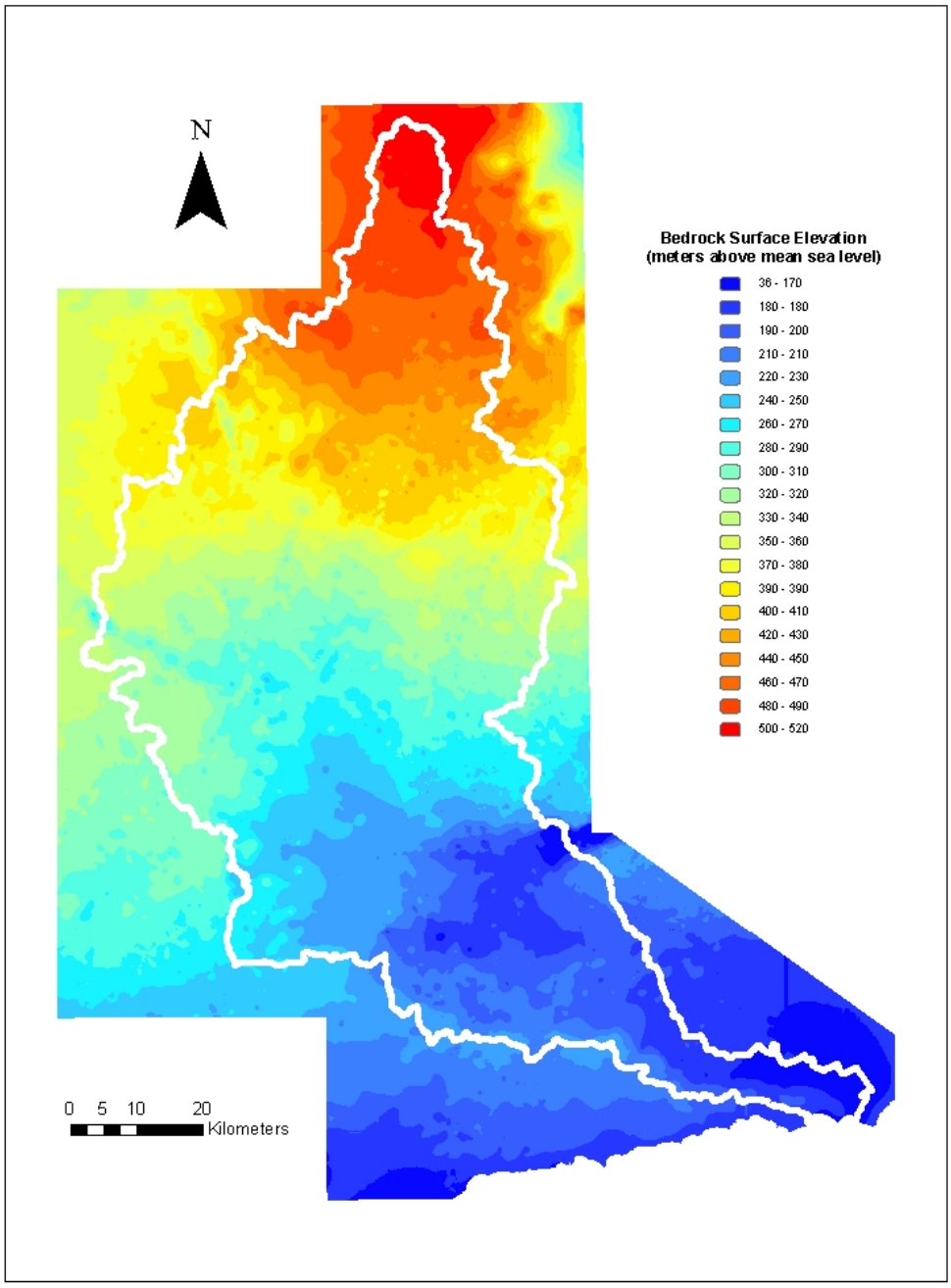

Figure 2.6: Grand River Watershed bedrock surface elevation (published by the Grand River Conservation Authority, 2000)

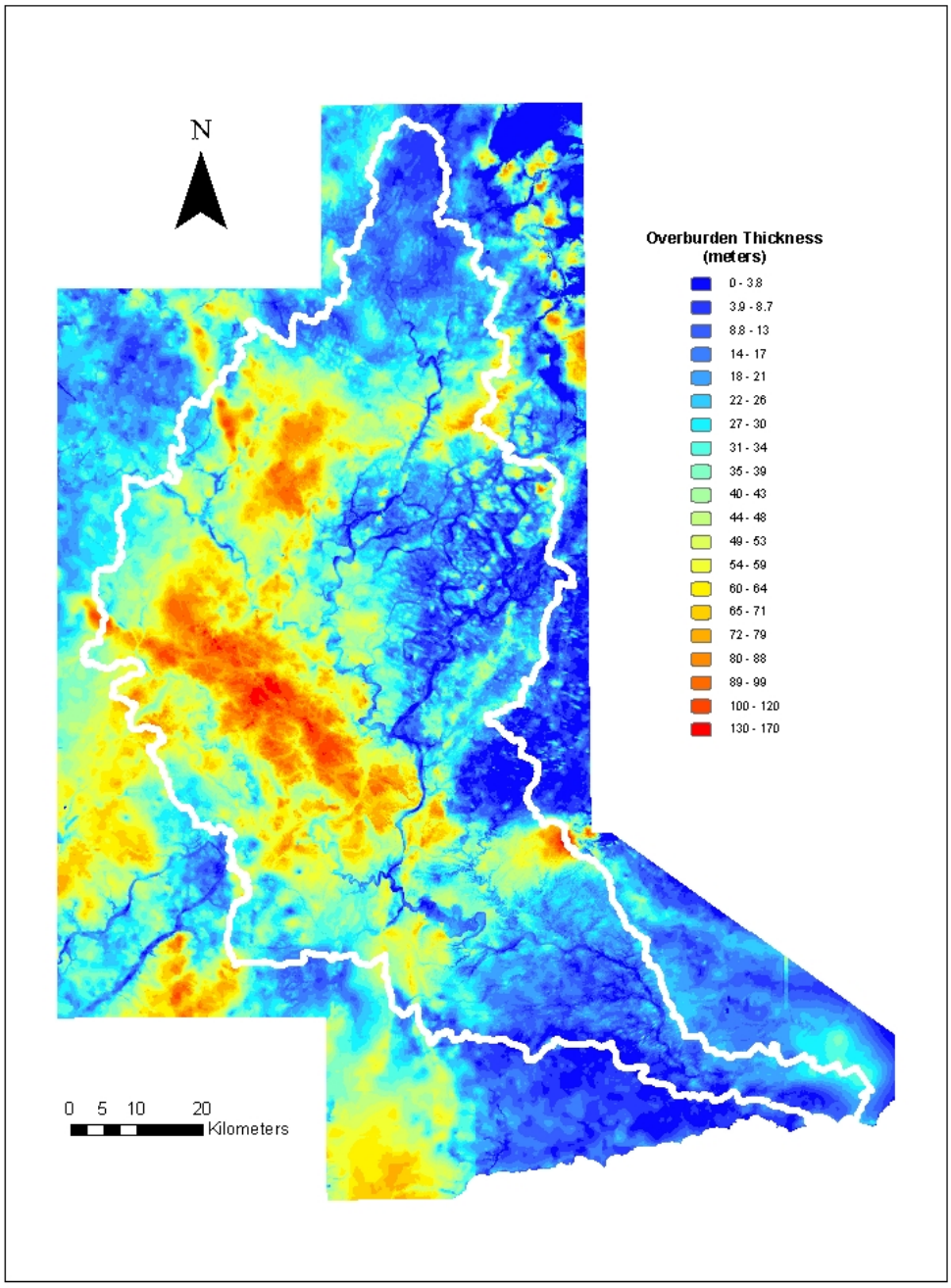

Figure 2.7: Grand River Watershed overburden thickness (after the Grand River Conservation Authority, 2000)

short-term timing of hydrological change within the GRW, as is the operation of the watershed's seven water control structures (reservoirs); these were ignored in the present work, since the focus was on long-term rather than short-term phenomena. However, the average variation of weather across the approximately 6700 km^2 area was included, *via* zones of uniform meteorology (Jyrkama, 2003).

2.3 Objectives

The primary objective of the present work is to estimate, via numerical modelling using HGS, the effects of five climate scenarios on the surface and subsurface hydrology of the GRW. Groundwater and surface water quantity and quality, and flow timing and direction, are potentially influenced by climate change, via changes in recharge, with the greatest of any such effects expected near the water table. Thus, the present study focuses on how new recharge patterns can change the near-surface and subsurface hydrology, namely streamflow, water table elevation and orientation, and recharge/discharge zones. The uniqueness of the climate scenarios arises specifically from differences in precipitation, which in turn result from climate change predictions made by multiple GCMs (IPCC, 2007). Calibrating to a longer temporal scale is meant as a first step toward a future goal of using shorter temporal scales for the purpose of for example flood prediction in the context of climate change.

An additional aim is to compare some of the steady-state results to those obtained by two related studies. The first (Jyrkama, 2003) focussed on recharge, including in the context of climate change somewhat similar to that presented herein. The second (Graham and Banks, 2004) applied a GAWSER recharge boundary condition to a FEFLOW subsurface saturated flow model, as noted earlier. Even if such comparisons were to show no improvement in the accuracy of results, generation of results *via* more physically-based interaction of groundwater and surface water (i.e., *via* HGS) should be seen as an important development. Furthermore, modelling this interaction allows for an understanding of infiltration and exfiltration patterns that cannot be developed *via* less physically realistic methods.

Finally, the present study represents the largest-scale application to date of a three-dimensional, fully-integrated surface/subsurface flow model. While physically-based hydrologic models such as HydroGeoSphere are gaining attention in the literature and in practice, previous applications have been limited to much smaller watersheds of a few tens to a few hundred km^2 in size (e.g., Li *et al*., 2008). Thus, this study represents a major step forward in applying such models to large-scale flow systems.

2.4 Numerical Model

The physically based numerical simulator HydroGeoSphere (Therrien *et al*., 2007), which three-dimensionally integrates and describes subsurface and surface flow, was used for the simulations. HGS is control-volume finite-element code that solves the 3-D Richards' equation for subsurface flow while, for surface flow, simultaneously solves the 2-D diffusion-wave approximation to the Saint-Venant equations. The surface flow and subsurface flow domains are solved simultaneously with an iterative Newton-Raphson scheme to linearize the equations.

The following modified form of Richards' equation is used to describe three-dimensional transient subsurface flow in a variably-saturated porous medium:

$$-\nabla \cdot (w_m q) + \sum \Gamma_{ex} \pm Q = w_m \frac{\partial}{\partial t}(\theta_s S_w) \tag{1}$$

where w_m [dimensionless] is the volumetric fraction of the total porosity occupied by the porous medium (or primary continuum). This volumetric fraction is always equal to 1.0 except when a second porous continuum is considered for a simulation, which is the case when the dual continuum option is used to represent existing fractures or macropores. The fluid flux **q** [LT^{-1}] is given by:

$$q = -K \cdot k_r \nabla(\psi + z) \tag{2}$$

where $k_r = k_r(S_w)$ represents the relative permeability [dimensionless] of the medium with respect to the degree of water saturation S_w [dimensionless], ψ is the pressure head [L], z is the elevation head [L], and θ_s is the saturated water content

[dimensionless], which is assumed equal to the porosity. Fluid injection or withdrawal is represented by Q [$L^3L^{-3}T^{-1}$], which is a volumetric fluid flux per unit volume representing a source (positive) or a sink (negative) to the porous medium system.

The hydraulic conductivity tensor, **K** [LT^{-1}], is given by:

$$\mathrm{K} = \frac{\rho g}{\mu}\mathrm{k} \tag{3}$$

where g is the gravitational acceleration [LT^{-2}], μ is the viscosity of water [$ML^{-1}T^{-1}$], **k** is the permeability tensor [L^2] of the porous medium, and ρ is the density [ML^{-3}] of water, which can be a function of the concentration C [ML^{-3}] of any given solute such that $\rho = \rho(C)$.

Water saturation is related to the water content θ [dimensionless] according to:

$$S_w = \frac{\theta}{\theta_s} \tag{4}$$

In Equation 3, Γ_{ex} represents the volumetric fluid exchange rate [$L^3L^{-3}T^{-1}$] between the subsurface domain and all other types of domains supported by the model such as infiltration or exfiltration across the land surface.

The primary variable used in solving the non-linear flow Equation 1 is the pressure head, and constitutive relations must be established that relate the primary unknown ψ to the secondary variables S_w and k_r.

The storage term forming the right-hand side of Equation 1 can be expanded as follows:

$$\frac{\partial}{\partial t}(\theta_s S_w) \approx S_w S_s \frac{\partial \psi}{\partial t} + \theta_s \frac{\partial S_w}{\partial t} \tag{5}$$

assuming that the bulk compressibility of the medium is constant for saturated and nearly-saturated conditions. For unsaturated conditions, it is assumed that the compressibility effects on storage of water are negligible compared to the effect of changes in saturation. S_s is the specific storage coefficient of the porous medium [L^{-1}]. The specific storage is related to both porous media compressibility α_{pm}, and water compressibility α_w:

$$S_s = \rho g(\alpha_{pm} + n\alpha_w) \tag{6}$$

The surface flow equation used is the diffusion wave approximation of the Saint-Venant equations. In addition to neglecting the inertial terms, the assumptions associated with the diffusion wave equation are those of the Saint-Venant equations, which are depth-averaged flow velocities, a vertical hydrostatic pressure distribution, mild slope, and dominant bottom shear stresses. Furthermore, it is assumed that Manning, Chezy, or Darcy-Weisbach formulae are valid for calculating frictional resistance forces for unsteady flow. The diffusion wave approximation of the Saint-Venant equations is:

$$\frac{\partial \phi_o h_o}{\partial t} - \frac{\partial}{\partial x}(d_o K_{ox} \frac{\partial h_o}{\partial x}) - \frac{\partial}{\partial y}(d_o K_{oy} \frac{\partial h_o}{\partial y}) + d_o \Gamma_o \pm Q_o = 0 \quad (7)$$

where d_o is the depth of flow [L], z_o is the bed (land surface) elevation [L], h_o is the water surface elevation [L] $\{h_o = z_o + d_o\}$, Q_o is a volumetric flow rate per unit area representing external sources and sinks [LT^{-1}], and ϕ_o is a surface flow domain porosity which is unity for flow over a flat plane, and varies between zero at the land surface and unity at the top of all rills and obstructions, for flow over an uneven surface. K_{oz} and K_{oy} are surface conductances [LT^{-1}] that depend on the equation used to approximate the friction slopes. Conductances for the Manning equation are given by:

$$K_{ox} = \frac{d_o^{2/3}}{n_x}) \frac{1}{[\partial h_o / \partial s]^{1/2}} \quad (8)$$

and:

$$K_{oy} = \frac{d_o^{2/3}}{n_y}) \frac{1}{[\partial h_o / \partial s]^{1/2}} \quad (9)$$

where s is distance taken in the direction of maximum slope. The parameters n_z and n_y are the Manning roughness coefficients [$L^{-1/3}T$] in the x and y directions.

When the dual node approach is chosen to represent simultaneous flow in the subsurface porous medium and the surface domain, the exchange term is given by:

$$d_o \Gamma_o = k_{ro} K_{so} (h - h_o) \quad (10)$$

where a positive Γ_o represents flow from the subsurface system to the surface system, h_o is the surface water head, h is the subsurface water head which now has an additional connection to the surface flow system via K_{so}, the leakance factor [T^{-1}] across the ground surface to the modelled subsurface, defined as the conductivity of the bottom divided by the thickness of the bottom surface across which flow occurs. The term k_{ro}, which accounts for rill storage effects, is zero when the surface domain is completely dry.

Chapter 3: Steady-State Simulation of GRW Hydrological Conditions Under Historical Perspective

3.1 Modelling Set-up and Approach

The conceptual model includes two surficial aquifers and four bedrock aquifers, alternating with aquitards, and forming a total of twelve hydrostratigraphic layers (i.e., thirteen slices), or four overburden layers and eight bedrock layers, as shown in Figures 3.1 through 3.3. The model's minimum layer thickness was set to 0.25 m, which is reached primarily and often in the topmost few layers of the domain. This finer discretization allows for a more accurate representation of the unsaturated zone and the connection between the surface domain and the subsurface domain (i.e., recharge processes). Downer and Ogden (2004) noted that no coarser a near-surface vertical discretization than 2cm is desirable; any coarser and the non-linear response of the vadose zone may not be captured accurately. They further report that such coarseness can result in significant misrepresentation of infiltration, evapotranspiration, and runoff, resulting in a meaningless, physically incorrect solution to the Richards' Equation. Unfortunately, in the present work 25 cm was the minimum thickness that could be achieved while keeping time expenditure (computational effort) during the development of base-case steady-state conditions less than half a year. While this vertical discretization may not be capable of resolving details in the vertical saturation profile, the calculated saturations are

representative of an average over a 25 cm vertical interval. The average layer thicknesses are described in Table 3.1.

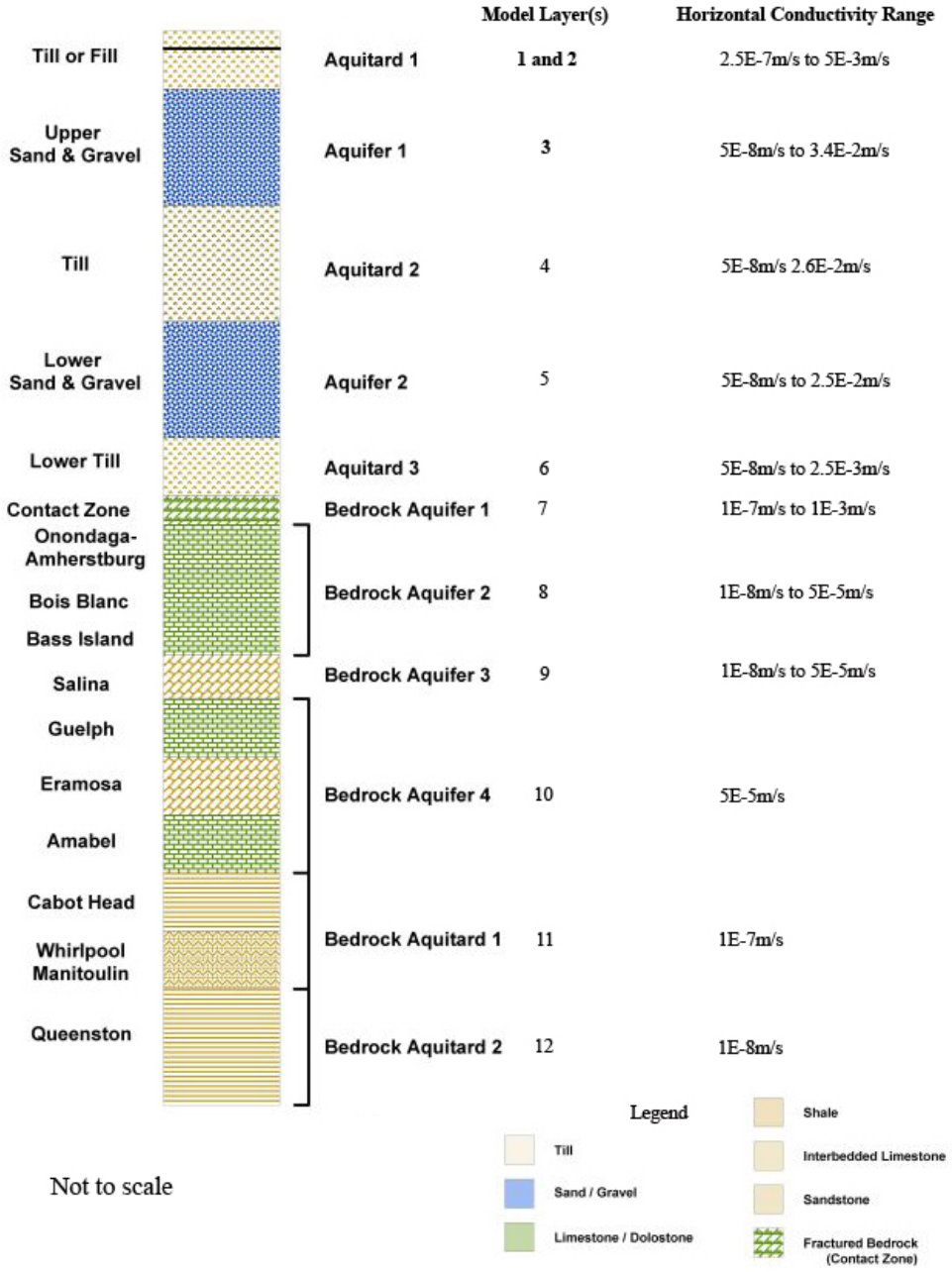

Figure 3.1: Conceptual hydrostratigraphic structure of the Grand River Watershed (after Graham and Banks, 2004).

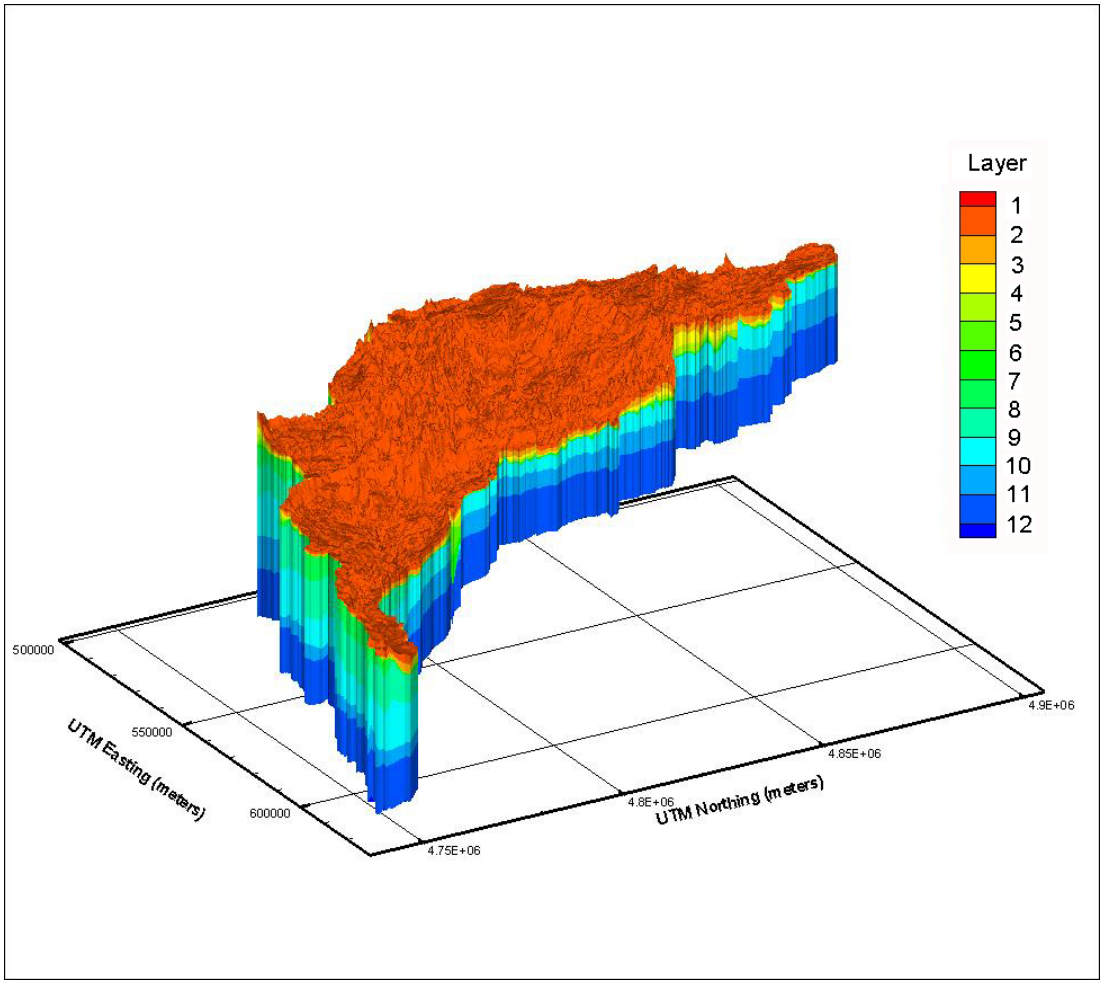

Figure 3.2a: Layers of the GRW model domain (Vertical exaggeration: 100X)

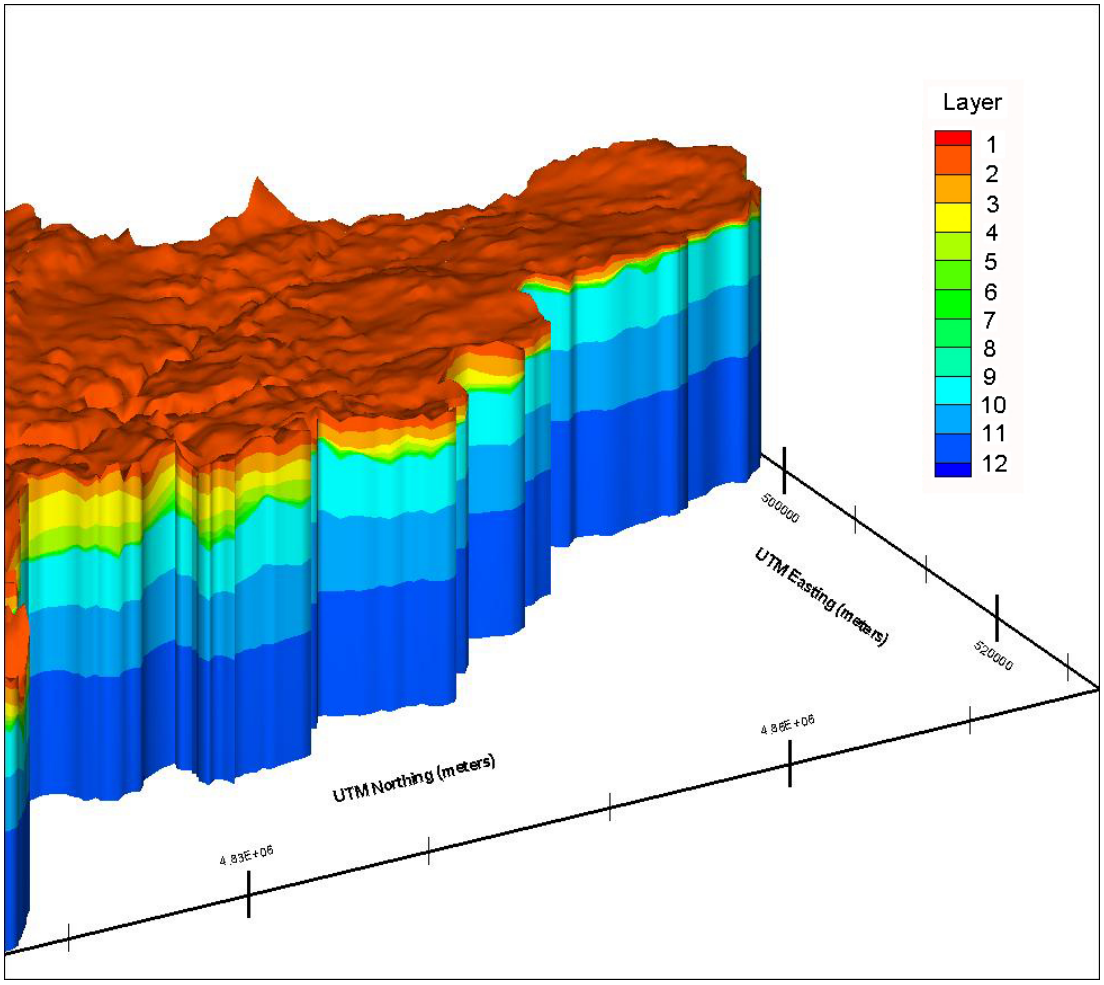

Figure 3.2b: Northern tip of GRW model domain (Vertical exaggeration: 50X)

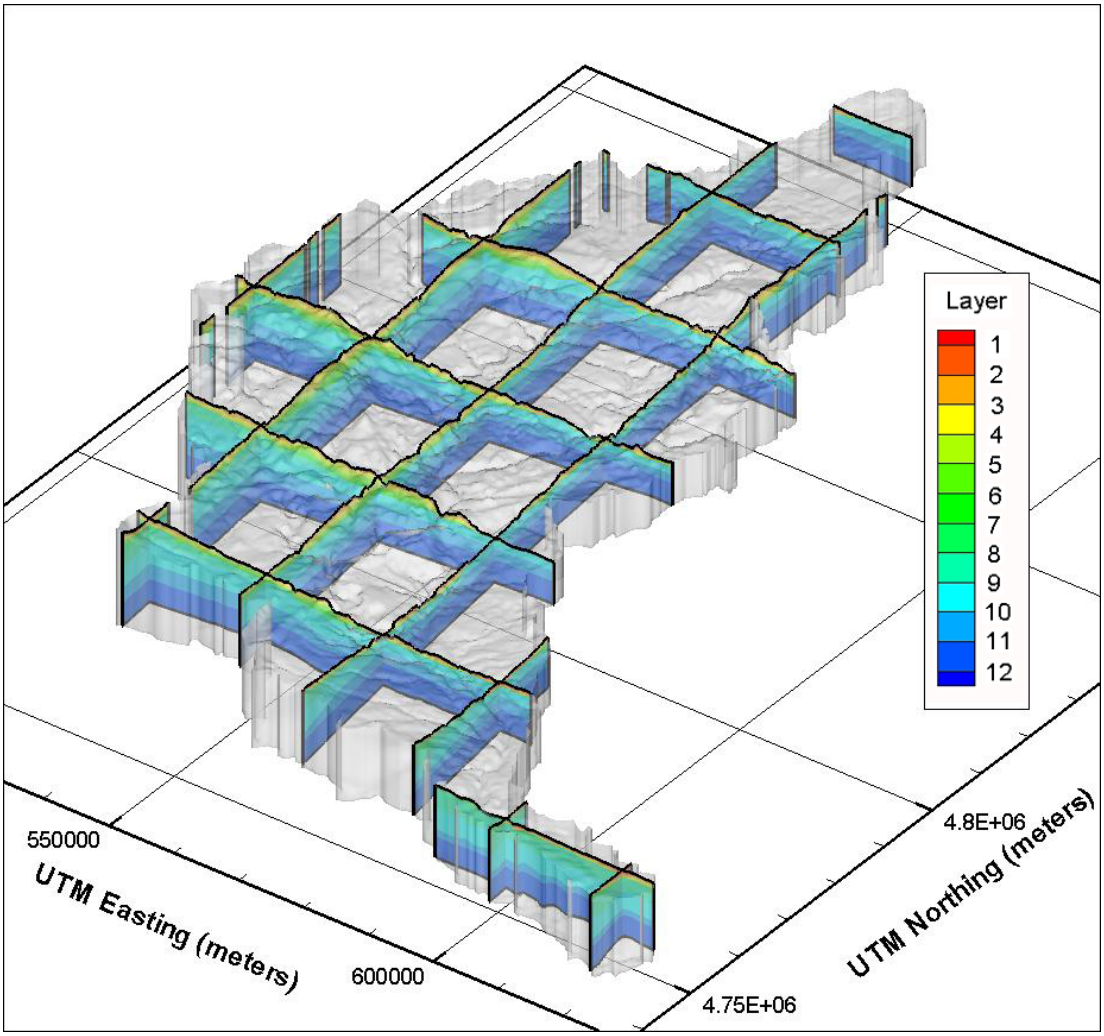

Figure 3.3a: Fence diagram of hydrostratigraphic layers (Vertical exaggeration: 30X)

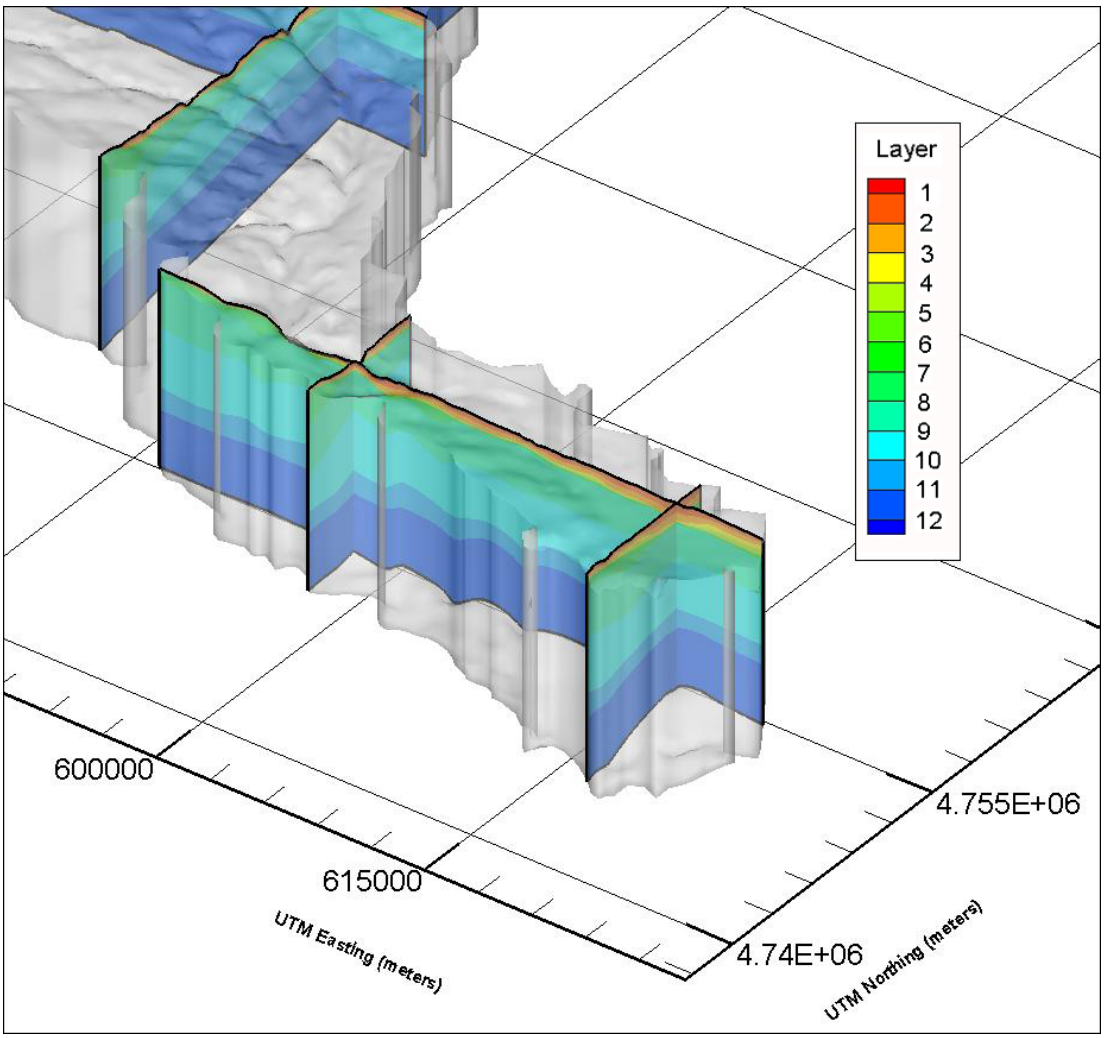

Figure 3.3b: Expanded fence diagram of hydrostratigraphic layers at southern tip of watershed (Vertical exaggeration: 30X)

Hydraulic conductivity is isotropic laterally, and initial trial values were chosen based on Graham and Banks (2004) and on literature values typical of the geologic materials (Figures 3.5a and 3.5b). In addition, the very high concentration of drainage tiles in the northwest of the watershed (see marked area in Figure 3.4) influenced the choice of conductivity values there – vertical and horizontal values

chosen initially were increased by a factor of five in an attempt to mimic the ability of the tiles to quickly deliver subsurface water to channels and streams. That is, rapid, anthropogenic drainage was simulated *via* higher conductivity values. Initially, vertical anisotropy of 10 was assigned throughout the model domain, based on Graham and Banks (2004), and with the goal of changing this value during calibration if necessary. Matrix compressibility was set to 4.4 x 10^{-10} ms^2kg for all elements.

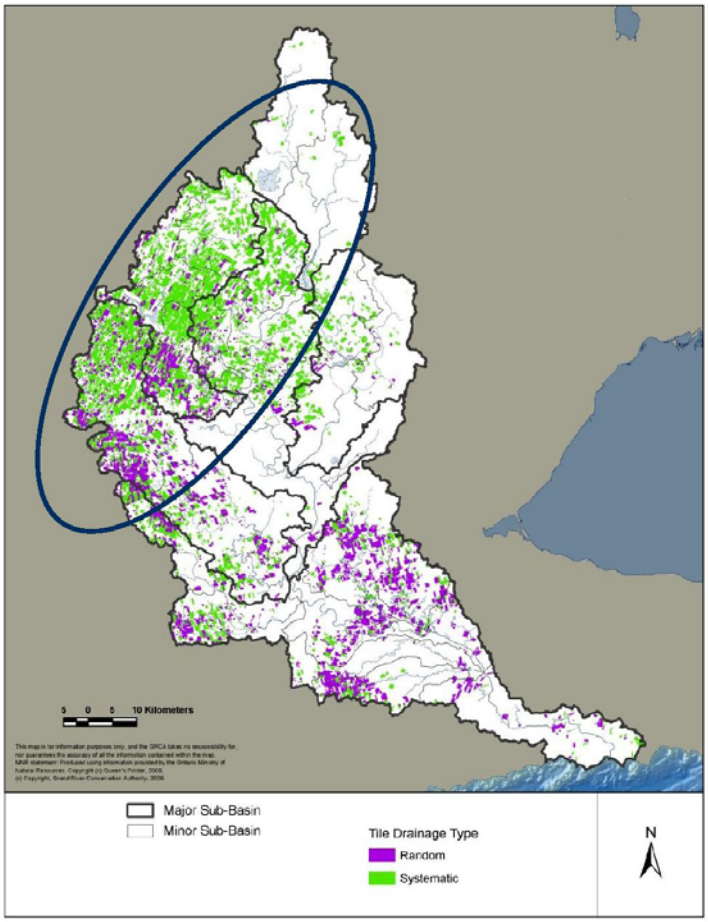

Figure 3.4: Location of zone of highly concentrated tile drainage (see area marked by oval, after Boyd *et al.*, 2009)

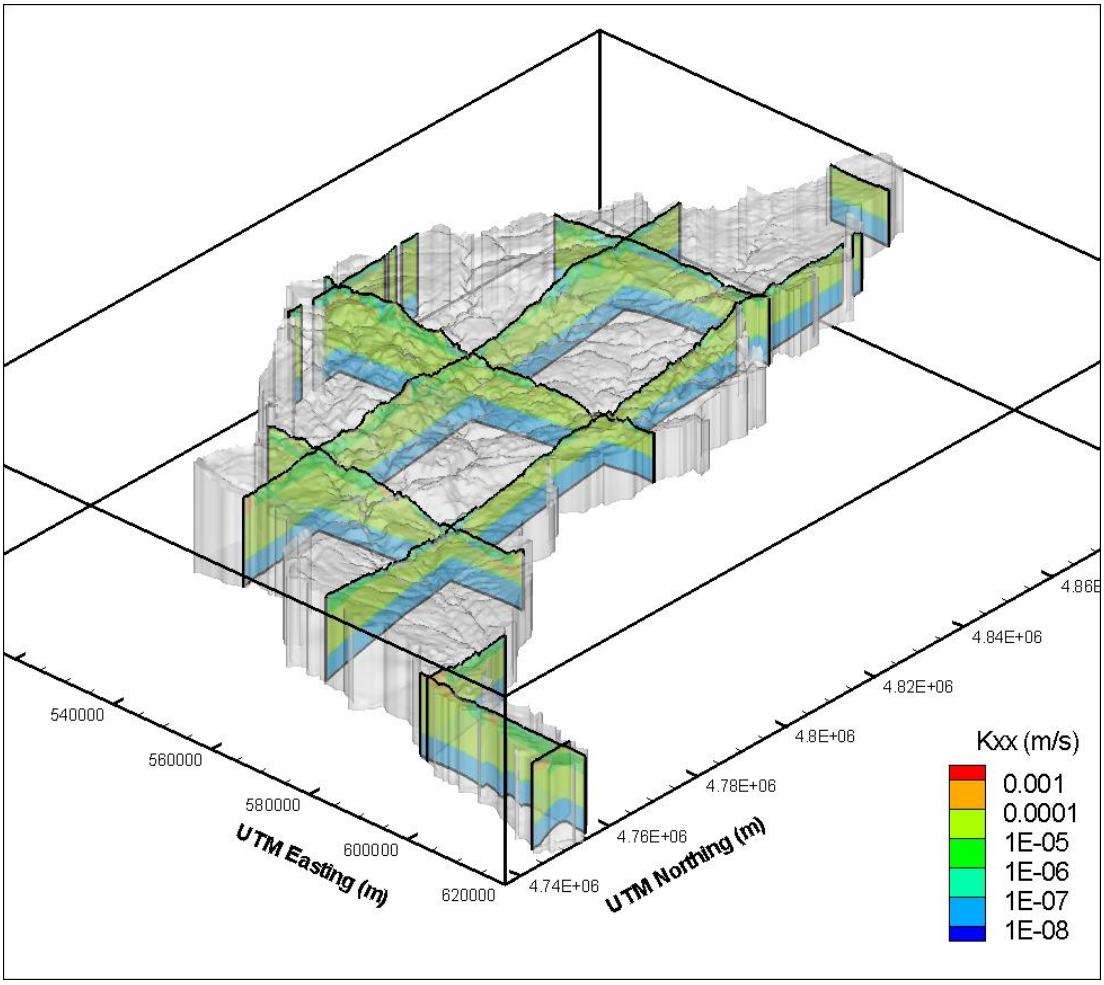

Figure 3.5a: Hydraulic conductivity (K_{xx}) fences (Vertical exaggeration: 30X)

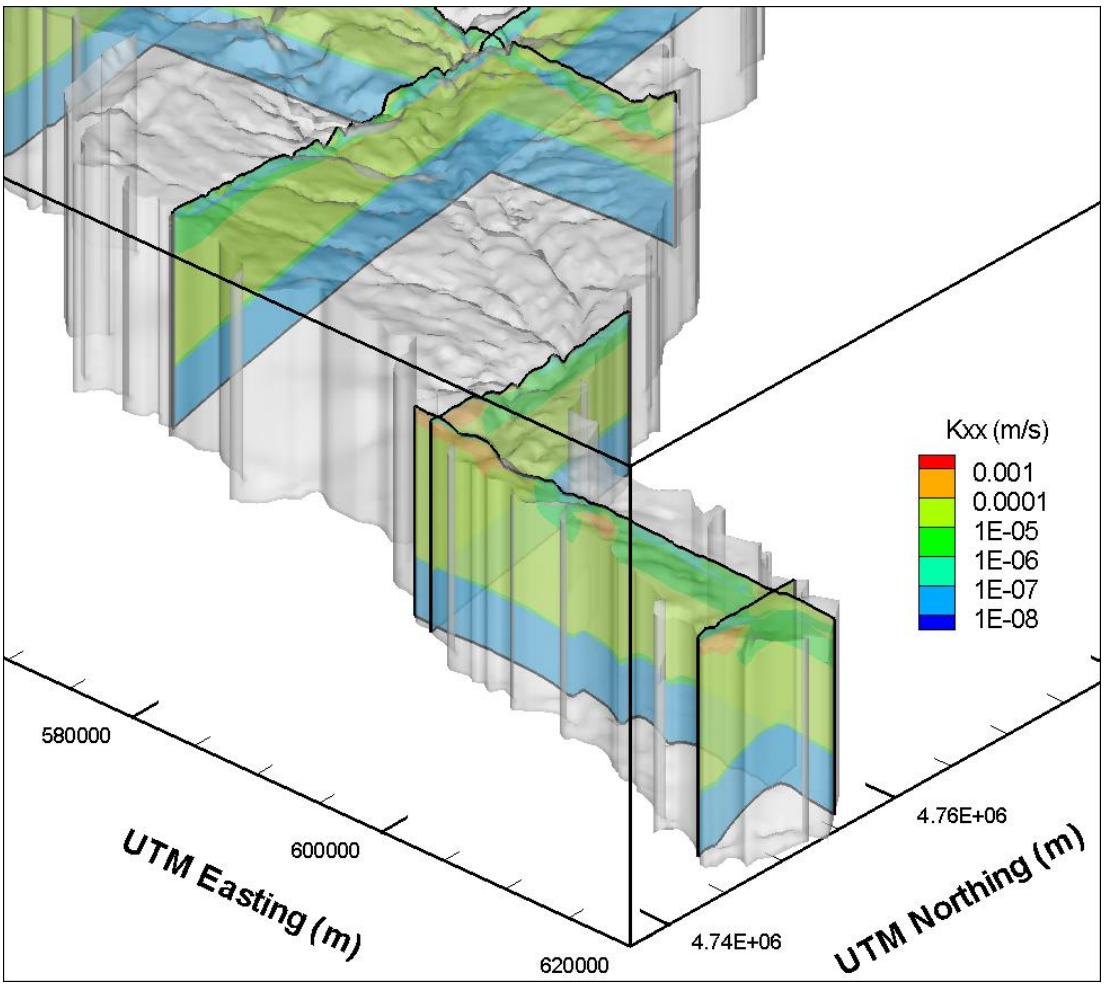

Figure 3.5b: Hydraulic conductivity (Kxx) fences at southern tip of GRW (Vertical exaggeration: 30X)

Table 3.1: Bedrock geology underlying the study area (from Graham and Banks, 2004).

Formation	Sub-Members	Geology	Location	Thickness (m)
Onondaga-Amherstburg		Fossiliferous limestone, variably cherty and shale interbeds	Western boundary near Wellesley to Dunnville	45 – 75
Oriskany		White or grey quartz sandstone	Between Bass	6

Formation	Sub-Members	Geology	Location	Thickness (m)
			Island-Bertie and Bois Blanc near Cayuga	
Bois-Blanc		Grey and greyish brown dolomite, limestone with nodular chert	Western boundary	40 – 60
Bass Islands-Bertie		Cream and tan to greyish-tan dolomite	Inside western boundary	22 – 28
Salina	A	Tan dolomite and grey mudstone	central to western boundary from Drayton to Dunnville	up to 330
	C	Grey and olive green shales with lenses of anhydrite and gypsum		
	E	Tan dolomite with lenses of anhydrite and gypsum		
	F	Grey and red shale containing lenses of anhydrite and gypsum		
Guelph		Brown/tan dolostone	Eastern boundary to central (30 km wide)	15-90
Lockport-Amabel	Eramosa	Dark brown / black bituminous dolostone	Northeastern Boundary, Dundas Valley	30
	Goat Island	Light brown dolostone		
Clinton-Cataract Group	Whirlpool	Grey to reddish sandstone	Dundas Valley	5
	Manitoulin	Grey, medium bedded dolostone with shaley interbeds		5
	Cabot Head	Greenish grey and red-silty shale		10
	Reynales – Fossil Hill	Argillaceous dolostone		2-3
Queenston		Red Shale	Dundas Valley	135-335

Figure 3.2a shows that the lateral boundaries are formed by extending the surficial watershed boundary vertically downwards; the minimum and maximum model domain thicknesses are about 158 m and 484 m, respectively. The average width of the domain is about 36 km, and the surface elevation ranges from a 535 m ASL in the northernmost area to 173 m ASL where the Grand River enters Lake Erie. The bedrock elevation ranges from 525 m ASL to 142 m ASL. Nearly 28,000 well

records (Figure 3.7, Graham and Banks, 2004) were used in developing the conceptual hydrostratigraphic model.

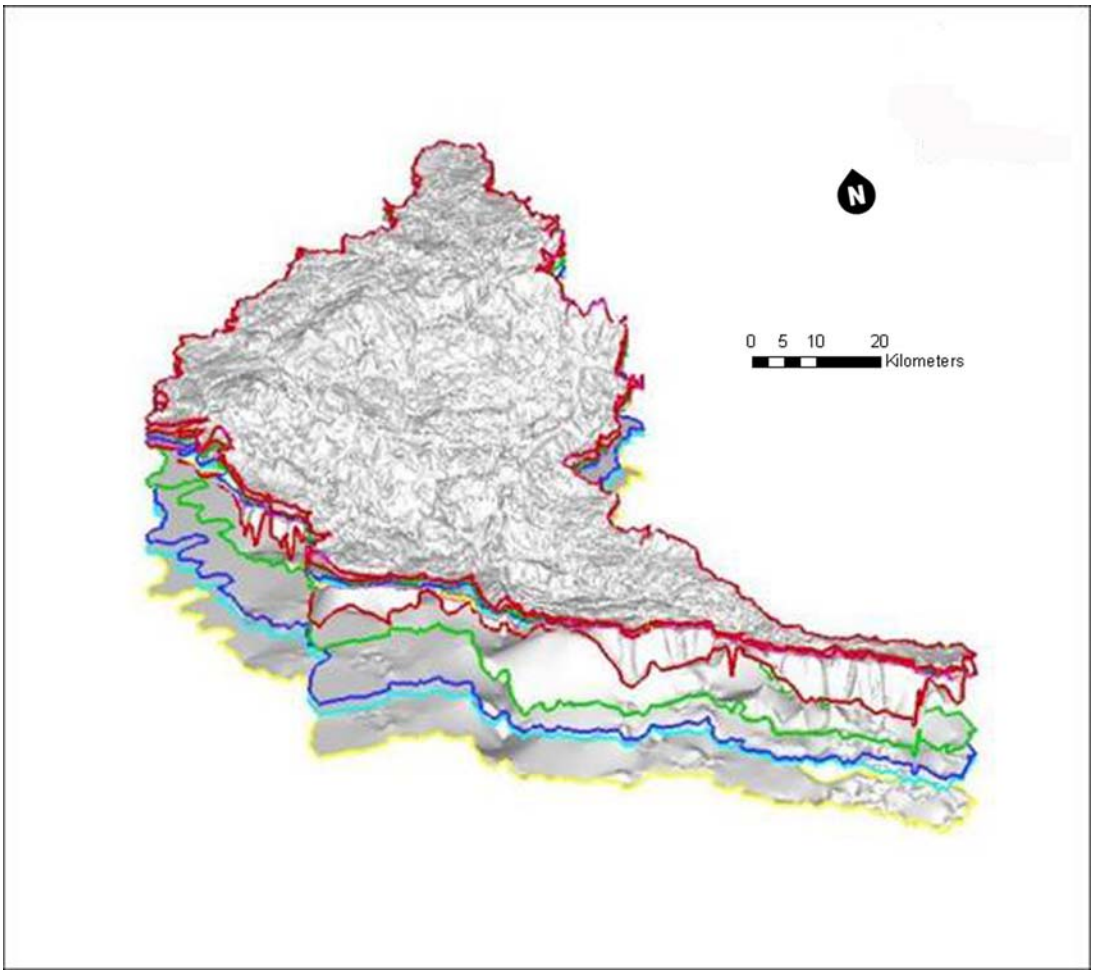

Figure 3.6: GRW slices (layers are between slices). Vertical exaggeration: 70x.

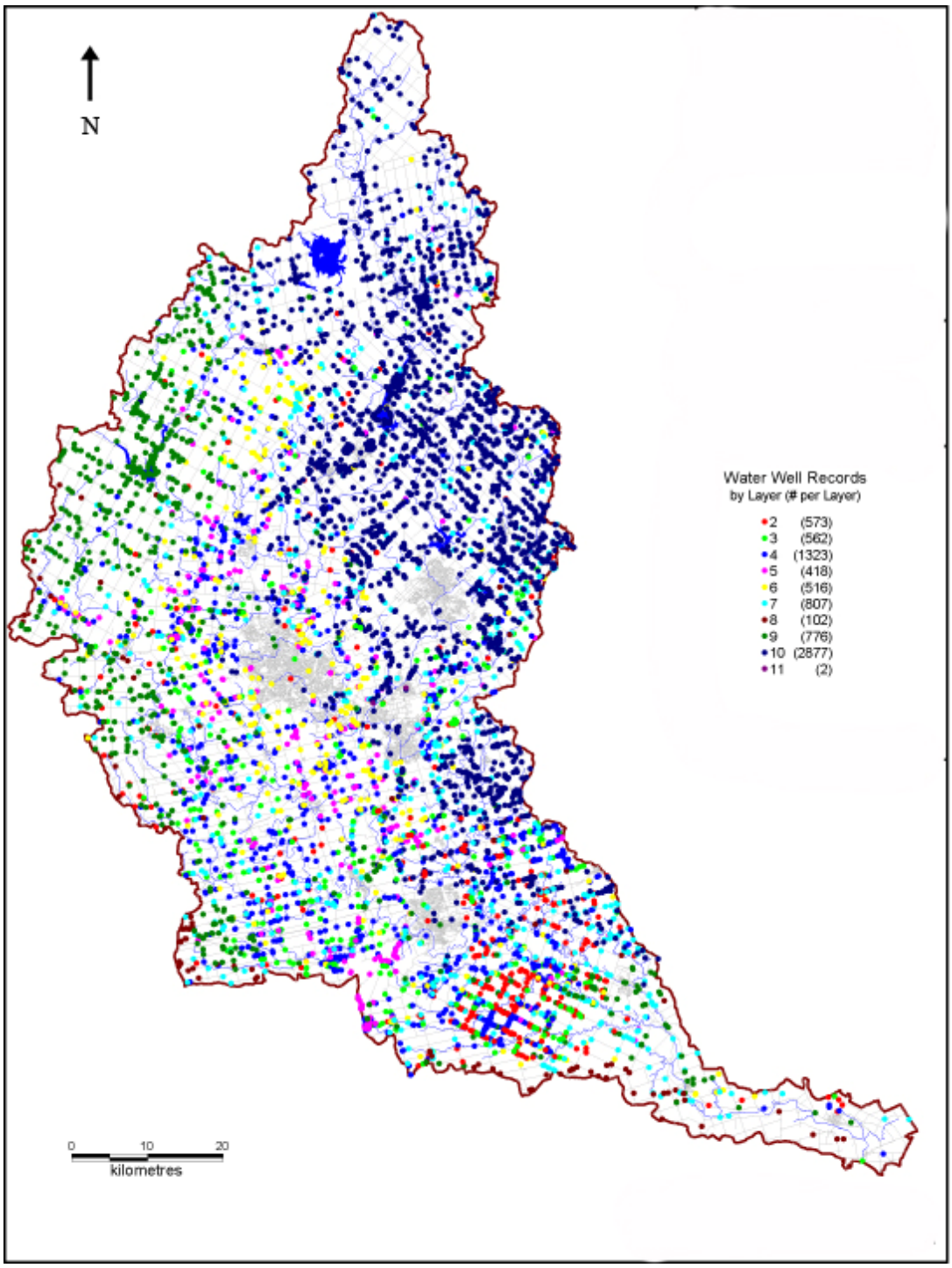

Figure 3.7: Water well records used in construction of model hydrostratigraphy (after Graham and Banks, 2004)

Each of the model's thirteen slices is comprised of 48140 nodes (94885 elements), giving 625,820 nodes (1,233,505 elements) for the entire model, with no horizontal mesh refinement occurring along the river network, and minimum and maximum node-to-node connection lengths of about 200 m and 1 km, respectively. Grid Builder, a 2-D triangular mesh generator (McLaren, 2009), was used to create the mesh, interpolate hydraulic conductivity and elevation values within the mesh, create boundary condition overlays, assign hydrograph and ZUM (Zones of Uniform Meteorology) nodes, and 'correct' waterway node elevations to ensure for a constantly downward slope toward Lake Erie (see Figures 3.8a and 3.8b).

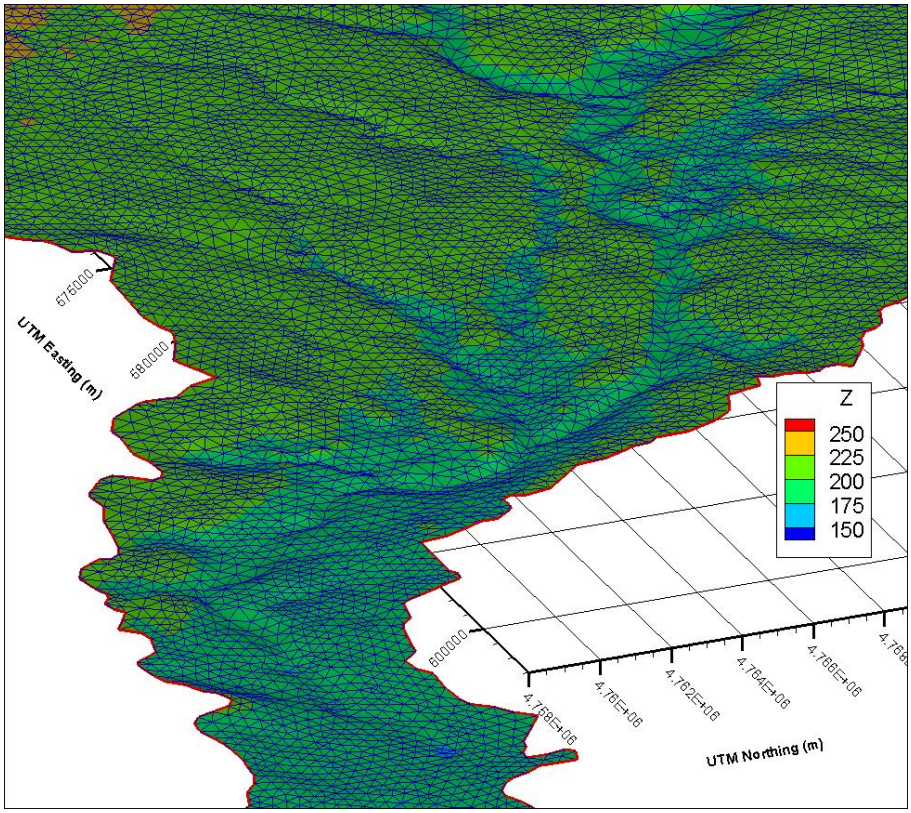

Figure 3.8a: Areal view of model mesh section near southern tip of GRW, including elevation-corrected waterways. (Vertical exaggeration: 50X)

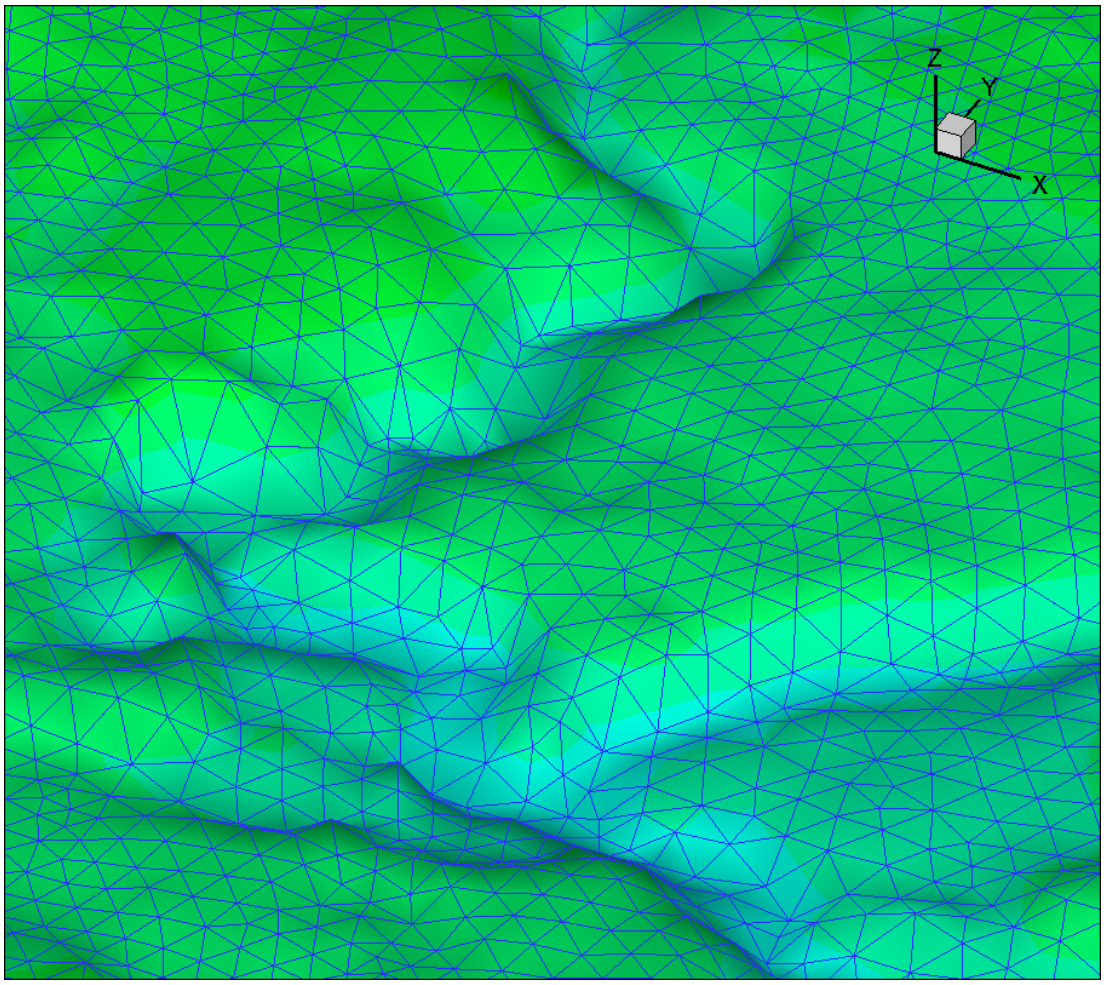

Figure 3.8b: Areal view of small model mesh section, including elevation-corrected waterways. (Vertical exaggeration: 50X)

Although the surface lateral boundary conditions are clearly defined, with the GRW specified flux (Neumann or "type-2") surface boundary matching that of the watershed, the GRW's subsurface boundary type varies in space (and most likely in time also), as indicated by Figures 3.9 and 3.10.

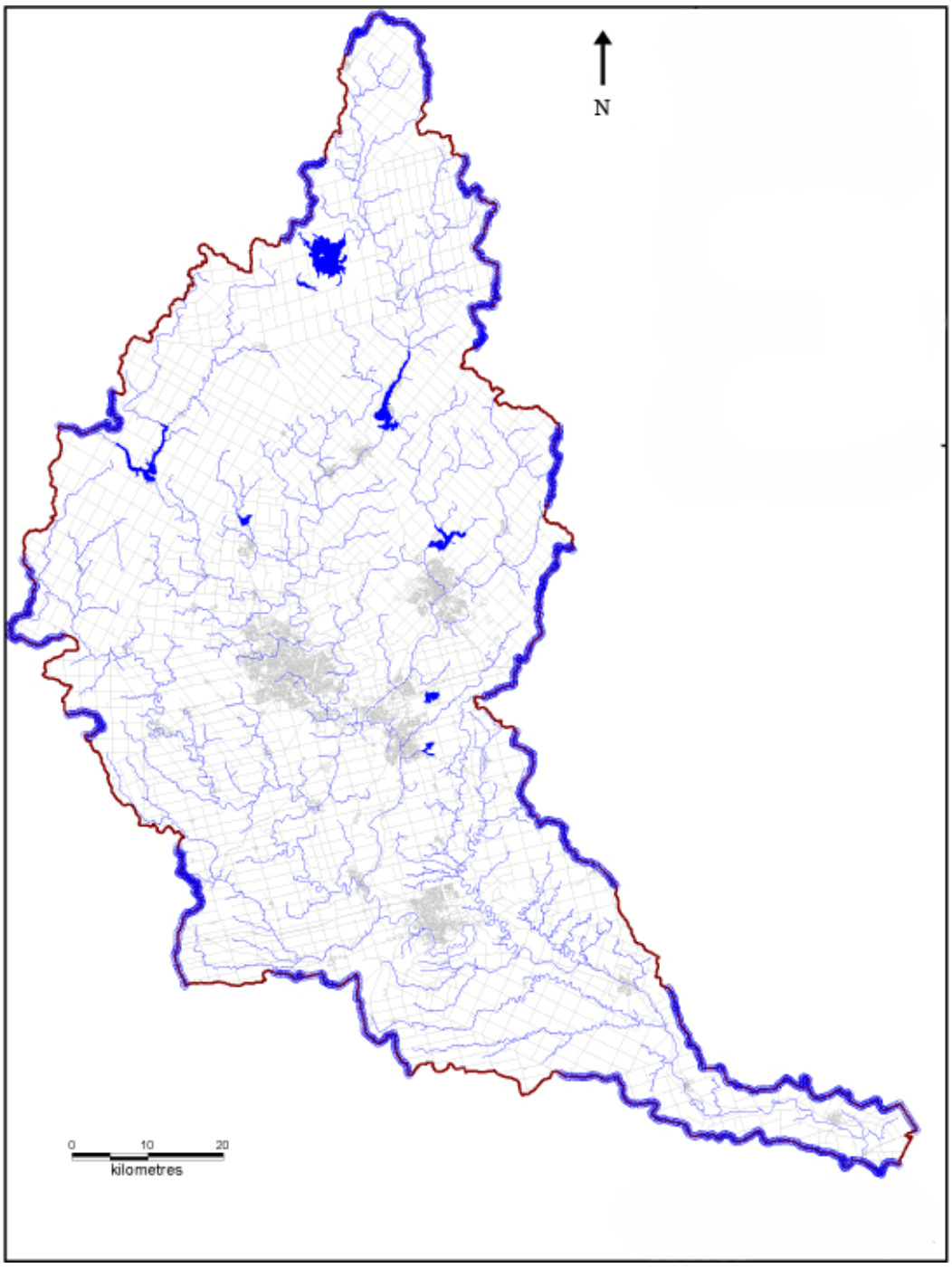

Figure 3.9: Example of hydrostratigraphic layer 3's no-flow boundary conditions and measured, average specified head boundary conditions (no-flow specified flux boundaries coloured brown, while blue indicates specified head boundaries; after Graham and Banks, 2004)

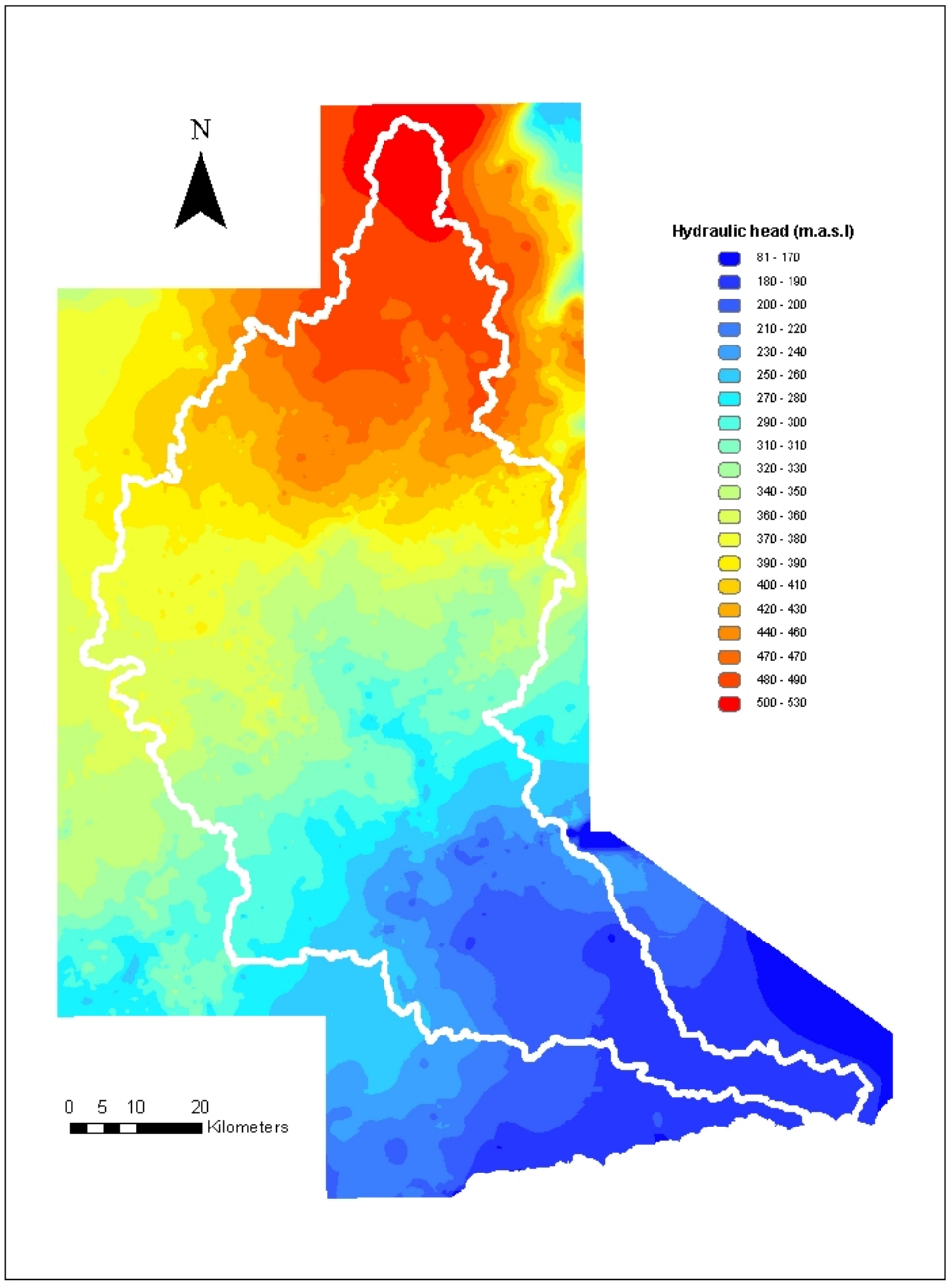

Figure 3.10: Potentiometric surface, based on long-term average (GRCA, 2000)

That is, specified head (Dirichlet or "type-1) and specified (zero) flux boundaries alternate in the subsurface, as estimated by Graham and Banks (2004). Indeed, Figure 3.10, while based on temporally-averaged conditions and thus not reflecting boundary conditions at any particular moment(s) in time, still indicates a probability of some sort of groundwater exchange with surrounding watersheds. However, the application of such boundary conditions, in both preliminary findings in the present study and in Graham and Banks (2004), resulted in such large exchanges (on the order of 120,000,000 m^3/day, dwarfing other input/loss processes) of both groundwater inflow and groundwater outflow to and from the GRW that it was thought more realistic to adopt an entirely no-flow subsurface (lateral and bottom) boundary condition. This approach seems reasonable given that AquaResource Inc. (2007) calculated net groundwater flow out of the GRW to be approximately 1% of precipitation input; future improvement of the model used herein doubtlessly will allow subsurface exchange as long as it approximates that percentage. In all cases, a critical depth surface-water boundary condition was assigned to the entire perimeter of the domain's upper surface. This boundary condition prevents the accumulation of surface water in depressions near the domain's boundary.

Pumping wells (Figure 3.11) and sewage outfall point sources affect the long-term average hydrological regime of the Grand River watershed, although the degree to which they do so is of much less importance than are other components of the GRW's water budget. Graham and Banks (2004) examined two pumping scenarios,

the first of which included only maximum-permitted pumping rates throughout the watershed; the daily amount pumped totalled 638,000 m^3. The second scenario used the same rates but omitted non-municipal wells, resulting in only 211,000 m^3/day. The present effort includes newly available estimates of *actual* pumping rates for approximately 550 pumping wells defined in the model (Amanda Wong, GRCA, personal communication; derived from the Ontario Ministry of the Environment's wells database), which when totalled equals approximately 530,000 m^3/day (Appendix A). The watershed's total pumping rate used by AquaResource Inc. (2007) and based on one GRCA estimate was 300,000 m^3/day, further emphasizing the considerable degree to which pumping estimates vary. However, because pumping comprises only a small fraction (maximum: 3%; minimum: 1.5%) of the watershed's precipitation input, any error in its estimation is not expected to greatly influence the present work's water budget. Data collected from the Ontario Clean Water Association and the City of Guelph indicated that for the GRW, an average approximately 216 m^3/day, or 40% of the watershed's total water taking rate used here, of sewage was pumped back into the hydrologic system, almost exclusively into the surface waterways. Six disparate stream nodes were selected to represent these sewage facilities, and water was injected into the model at rates unique to each facility. Temporally constant pumping was assumed, and code was written to instruct HGS's pre-processor, Grok, to locate aquifer upper and lower boundaries, and to position wells between them. About one third of the watershed's wells,

including most of the high-yield wells, draw water from the overburden. The effects of the GRW's seven water control structures (reservoirs) are assumed to be implicitly accounted for by the present work, since the averaged streamflows used during model calibration include such flow regulation. That is, since these structures augment flow during drought and restrict flow during times of flooding, they in fact drive observed transient flow toward the average value. Consequently, these structures were not explicitly included in the model set-up process.

A steady-state simulation ("base case") was developed using thirteen zones of uniform meteorology (Mikko Jyrkama, personal communication), as shown in Figure 3.12. Each zone, which represents a particular climate station and is assumed to be representative of the average climate throughout each zone, is characterized by a single actual (as opposed to effective) precipitation value. This value is calculated by averaging its daily precipitation values across the period of record, 1960 to 1999 inclusive. Table 3.2 shows each ZUM's value in addition to average monthly values, while watershed-wide monthly-averaged precipitation for this period is displayed in Figure 3.13. Jyrkama and Scott (personal communication) provided meteorological data (rainfall, snowfall), all on a daily basis from 1960 to 1999 inclusive. Liquid and crystalline precipitation forms were treated identically, given the long-term averaged results sought.

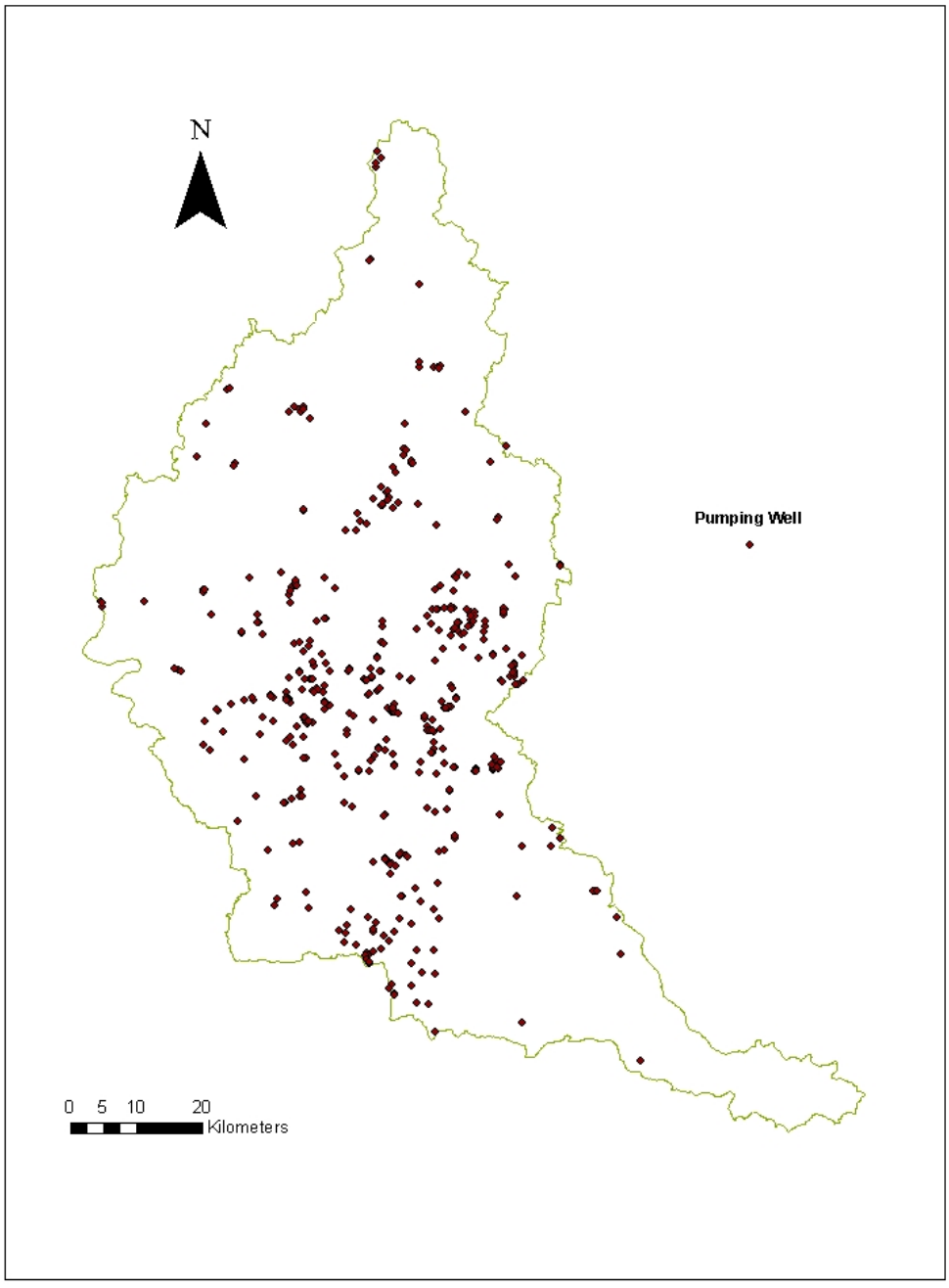

Figure 3.11: Pumping wells (courtesy Amanda Wong, GRCA, 2008)

Table 3.2: Actual precipitation in each zone of uniform meteorology.

Month	Actual Precipitation (mm/year)					
	ZUM 1	ZUM 2	ZUM 3	ZUM 4	ZUM 5	ZUM 6
January	1183	1183	785	1082	814	1053
February	1009	1009	684	933	728	908
March	899	899	760	842	766	848
April	908	908	937	883	937	886
May	883	883	927	987	938	959
June	1022	1022	1063	1006	1009	990
July	952	952	956	896	943	921
August	1126	1126	1082	1091	1157	1031
September	1116	1116	1019	1066	1116	1063
October	1022	1022	880	905	952	886
November	1170	1170	1034	1148	1113	1132
December	1183	1183	867	946	940	968
Average	**1039**	**1039**	**916**	**982**	**951**	**970**

Table 3.2 continued

Month	Actual Precipitation (mm/year)						
	ZUM 7	ZUM 8	ZUM 9	ZUM 10	ZUM 11	ZUM 12	ZUM 13
January	785	703	1113	735	662	665	665
February	684	650	883	697	640	602	602
March	760	792	836	826	757	845	845
April	937	880	1003	971	905	971	971
May	927	864	930	883	855	855	855
June	1063	930	937	1012	899	978	978
July	956	1003	1006	1031	978	952	952
August	1082	1000	1022	1082	930	987	987
September	1019	965	1154	1034	971	1069	1069
October	880	810	940	839	795	914	914
November	1034	987	1230	1041	911	990	990
December	867	829	1271	905	829	858	858
Average	**916**	**868**	**1027**	**921**	**844**	**890**	**890**

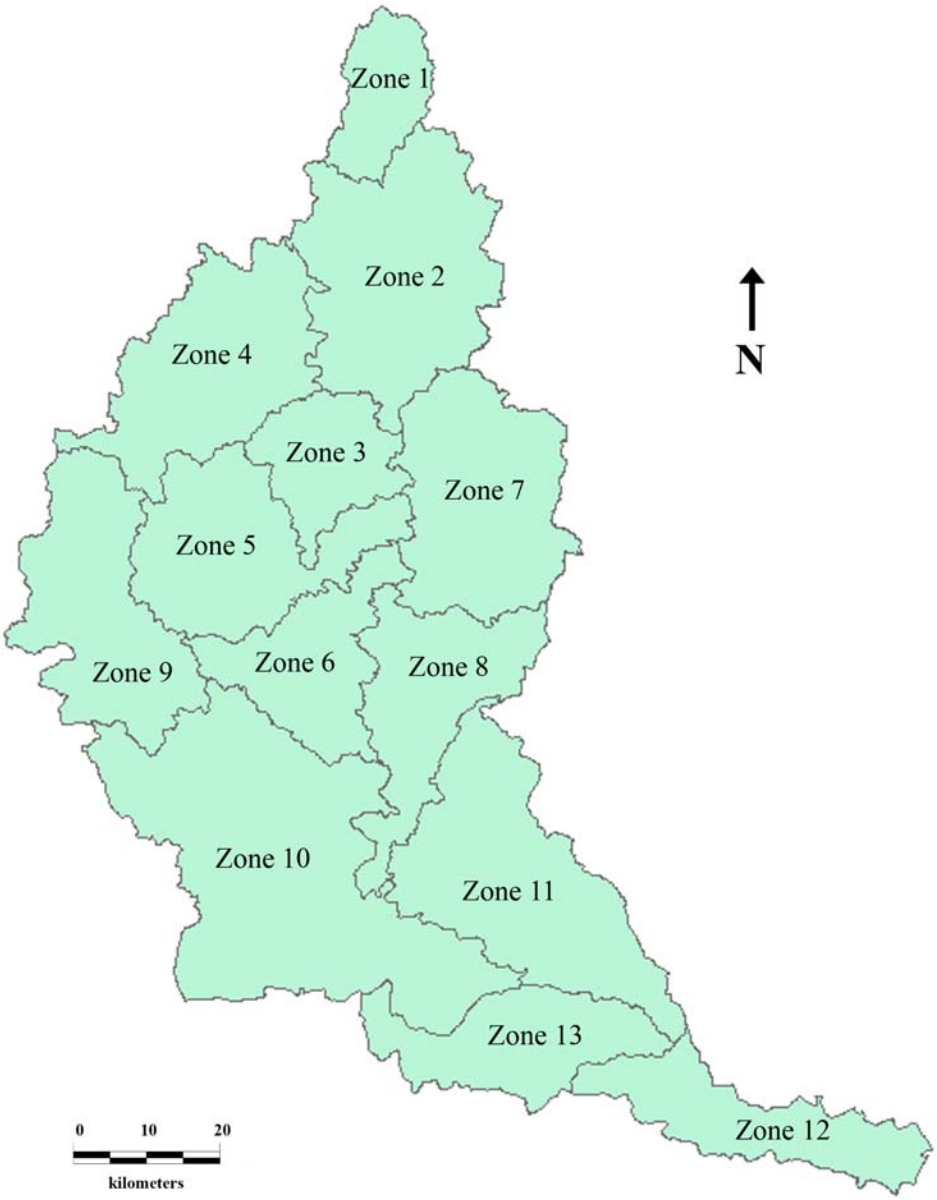

Figure 3.12: Zones of uniform meteorology (ZUMs, after Jyrkyma, 2003)

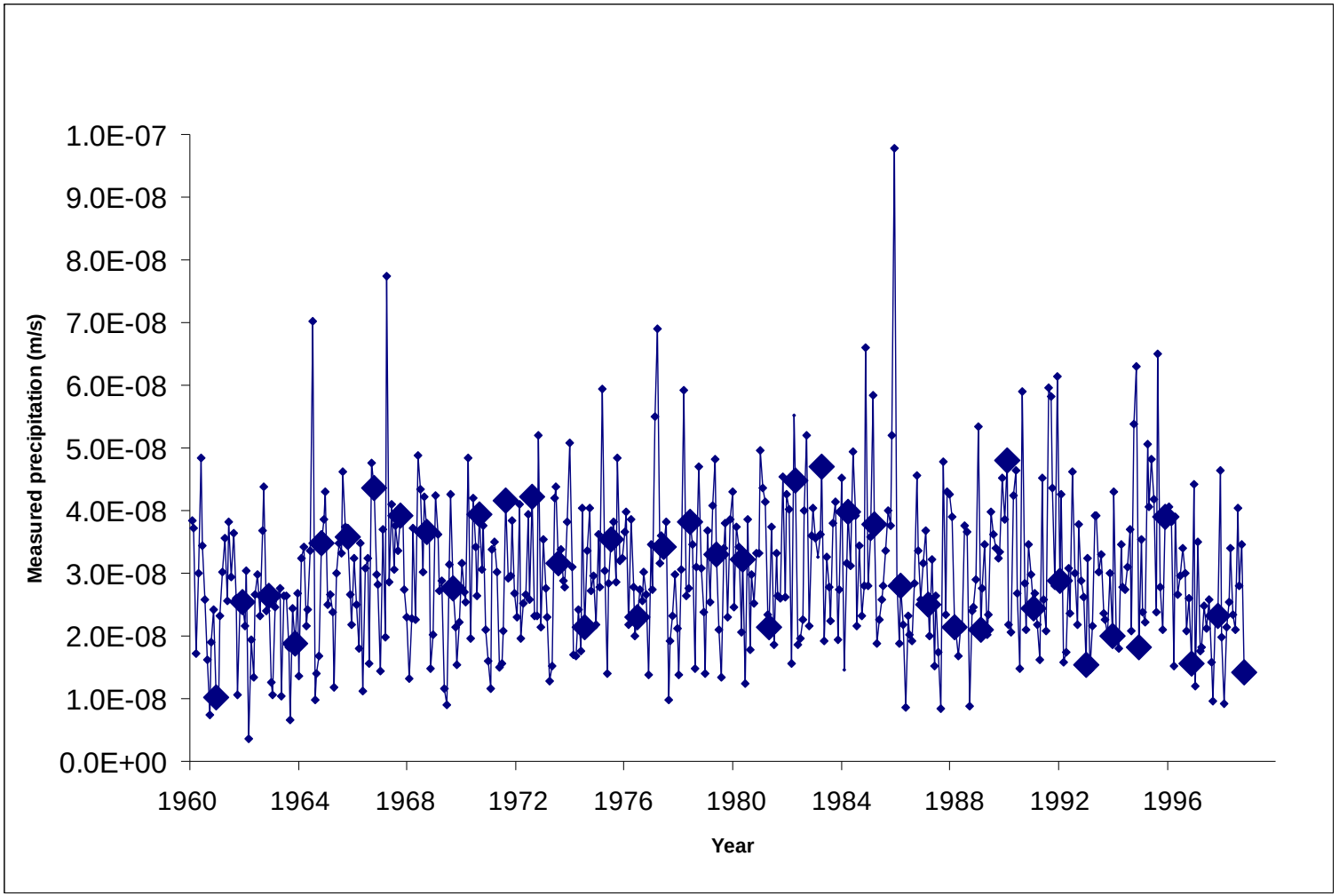

Figure 3.13: Measured, monthly- and spatially-averaged GRW precipitation, 1960 to 1999 inclusive (January depicted by larger diamonds)

Evapotranspiration is modelled explicitly in HGS as a mechanistic process governed by plant and climatic conditions, by applying a non-linear sink term to the model's upper surface (Panday and Huyakorn, 2004). The evapotranspiration was allowed to vary spatially by ZUM, with calculated values equalling long-term average annual estimates. Actual evapotranspiration is calculated by HGS based on a reference (specified) potential evaporation (PET) value, and on evapotranspiration parameters associated with various vegetation types. Water is withdrawn from the land surface *via* evaporation and from the root zone *via* evaporation and transpiration. The uppermost two model layers are as thin as 25 cm in an attempt to account for the vertical distribution of evapotranspiration throughout the root zone. Potential evapotranspiration – the amount of water that *potentially* is lost due to evaporation and plant transpiration – takes into account climatic factors such as solar radiation, temperature, humidity, and wind, and is referred to by HGS as the reference evapotranspiration. Actual evapotranspiration is a function of the potential value, as well as land cover, vegetation type, and soil properties. More specifically, HGS takes into account vegetation type *via* the leaf area index (LAI) and rooting depth, and soil type *via* limiting moisture contents. Both potential and actual evapotranspiration increase from north to south in the GRW, but the degree of this change is uncertain. The Ontario Ministry of Natural Resources (M.O.E., 1984) arrived at an actual evapotranspiration estimate of between 500 mm/year and 600 mm/year for the Grand River Watershed, by subtracting mean annual streamflow

leaving the watershed from mean annual precipitation. In humid regions, actual and potential evapotranspiration often approximate one another quite closely; Arnell (1996) notes that the greatest difference between actual and potential evaporation occurs in the "driest" catchments, where water limitations are greatest. Davies (1971) found that for an Ontario beanfield, actual evapotranspiration never fell below approximately two thirds of potential evapotranspiration, and even reached 90%. Because the average neared 75% in Davies's study, and because the GRW is a nearby system characterized by similar and extensive and agricultural activities, the actual evapotranspiration rate here similarly is considered to be about 75% of the potential rate, making PET on the order of 750 mm/year (changed during calibration to simulate greater PET in the watershed's south). Values of other evapotranspiration parameters were chosen according to those found in Canadell *et al.* 1996 (rooting depth), Scurlock *et al.*, 2001 and Jyrkama (2003) (leaf area index), and Li *et al.* (2008) and Goderniaux *et al*. (2009) (transpiration fitting parameters). Cubic decay with depth was favoured for all land cover types in the contexts of both the evaporation distribution function and the root distribution function (Panday and Huyakorn, 2004). Also universally used were single values of evaporation depth (2 meters), evaporation-limiting saturations (minimum: 0.2; maximum: 0.32), and the canopy interception parameter (1×10^{-5}). Table 3.3 lists the evapotranspiration parameters that varied spatially.

Table 3.3: Root depth, leaf area index (L.A.I.), and empirical transpiration fitting parameters (C1, C2, C3) for various land cover types.

Parameter	Type of land cover					
	Urban	*Crop*	*Deciduous forest*	*Coniferous forest*	*Plantation*	*Grass*
Root depth (m)	0	2.1	2.9	3.9	3.9	0.2
Max. L.A.I.	0.40	1.0	4.0	4.5	2.0	1.0
C1	0.3	0.3	0.3	0.3	0.3	0.5
C2	0.2	0.2	0.2	0.2	0.2	0
C3	10	10	10	10	10	1

The following domain-wide datasets were obtained via the GRCA study (Graham and Banks, 2004): observed well water levels, specific storage, and porosity. Aside from the uppermost two model layers, all elements were assigned a specific storage value of 1×10^{-4} and a porosity value of 0.3. Whereas the saturation-relative permeability relationship had been linearized by Graham and Banks, so as to link the GRCA subsurface-only model to surface recharge values given by GAWSER, the present study instead uses the more physically meaningful, non-linear van Genuchten pressure-saturation relationships shown in Figures 3.14a to 3.14j (van Genuchten *et al*., 1989; Mace *et al*., 1998; Carsel and Parrish, 1988; Bouwer and Rice, 1983). Table 3.4 lists the van Genuchten parameters, as well as porosity (Mercer *et al*., 1982) and specific storage values (Jones, 2005) for the uppermost two model layers.

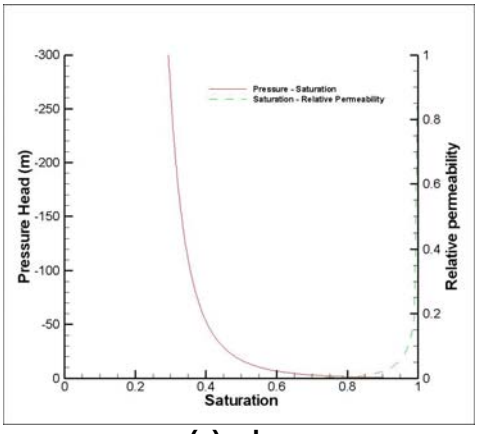

(a): clay

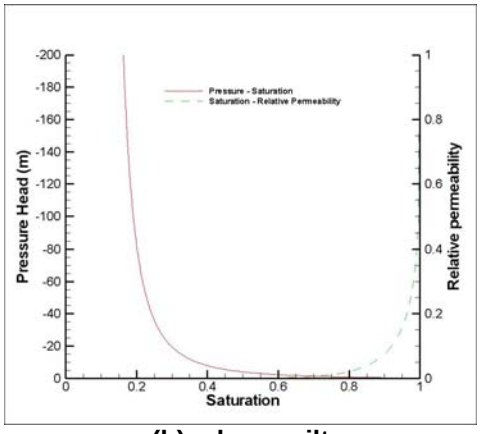

(b): clayey silt

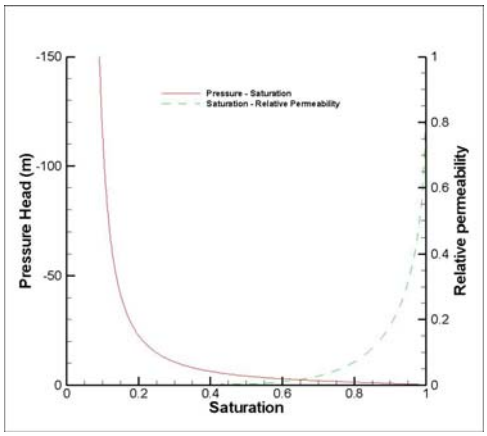

(c): silt

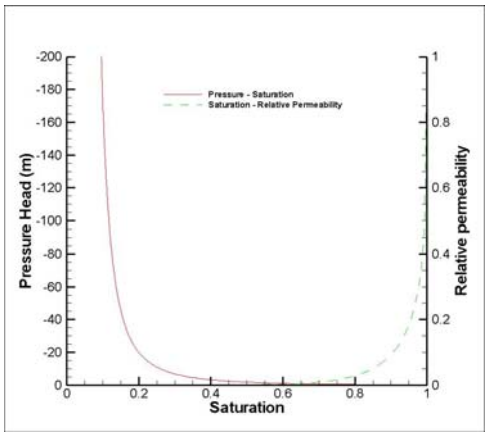

(d): sandy silt

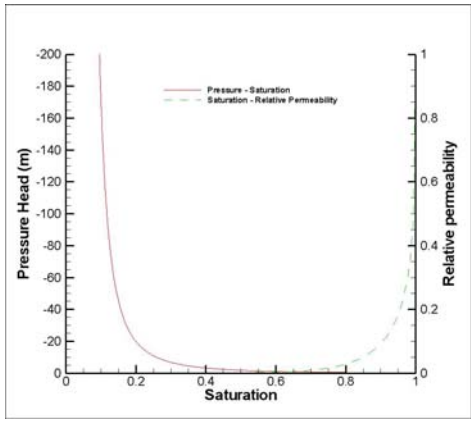

(e): gravelly silt

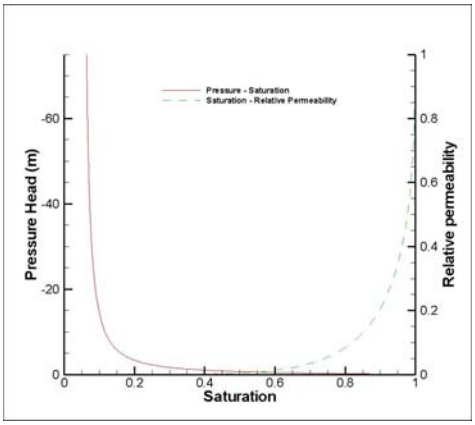

(f): clayey sand

Figure 3.14: Pressure-saturation and relative permeability-saturation relationships for various materials (continued on next page)

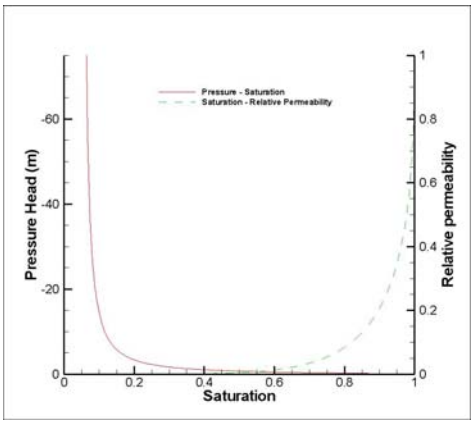

(g): silty sand

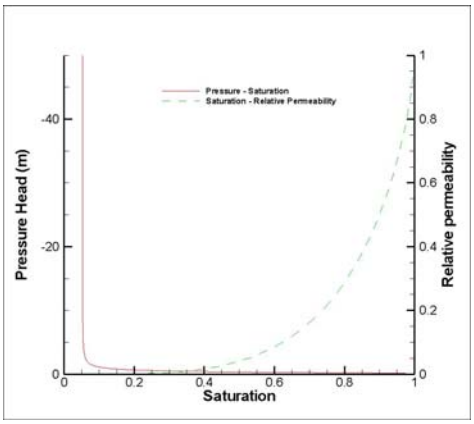

(h): medium sand

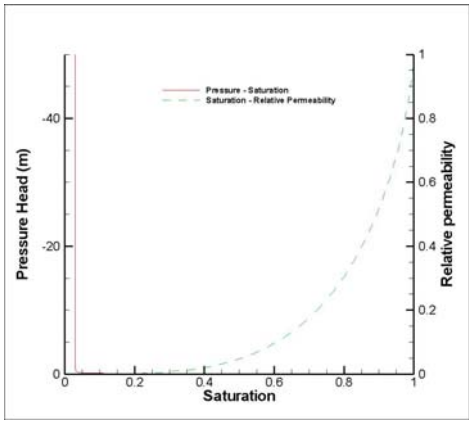

(i): coarse sand

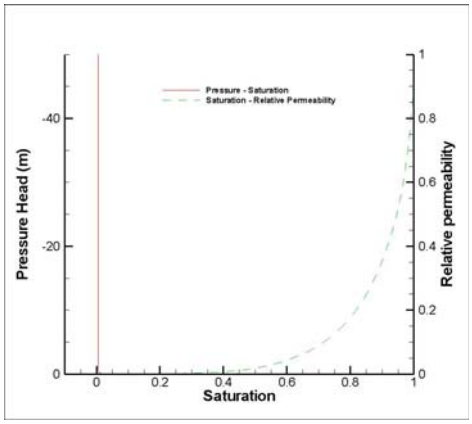

(j): gravel

Fgure 3.14 continued: Pressure-saturation and relative permeability-saturation relationships for various materials

Manning's surface roughness coefficients (Engman, 1986) were isotropic and are provided in Tables 3.5 for various land cover types (Anderson *et al*., 1976) as shown in Figure 3.15. The surface-subsurface coupling length was universally assigned a value of 0.01 m.

Table 3.4: Values of porosity, specific storage, and van Genuchten parameters for various materials

Material	Parameters				
	Porosity	*Specific storage* ($x\ 10^{-5}\ m^{-1}$)	*Residual Saturation*	*Alpha (curve shape)*	*Beta (curve shape)*
Clay	0.47	1.9110	0.098	1.49	1.25
Clayey Silt	0.45	2.3030	0.079	1.581	1.416
Silt	0.43	2.3030	0.050	0.658	1.68
Sandy Silt	0.41	2.3030	0.039	2.667	1.449
Gravelly Silt	0.41	2.3030	0.039	2.667	1.449
Clayey Sand	0.395	1.6170	0.049	3.475	1.746
Silty Sand	0.37	1.6170	0.049	3.475	1.746
Medium Sand	0.360	1.1858	0.053	3.524	3.177
Coarse sand	0.375	7.4480	0.030	29.4	3.281
Gravel	0.28	1.1015	0.005	493.0	2.190

Tables 3.5: Manning's surface roughness coefficient values, 16 GRW land cover types.

Land Cover Type	Roughness coefficient	Land Cover Type	Roughness coefficient
Residential built-up	0.015	Dense mixed forest	0.1
Commercial-industrial built-up	0.012	Plantation (mature)	0.1
Row crops	0.1	Open water	0.03
Small grains	0.2	Wetlands	0.05
Forage	0.13	Bedrock, roads, beaches	0.011
Pasture, sparse forest	0.07	Golf courses	0.45
Dense deciduous forest	0.1	Bare agricultural fields	0.3
Dense coniferous forest	0.1	"other"	0.15

Figure 3.15: Land use map used to assign Manning's surface roughness coefficients (GRCA, 2009)

River gauge data were obtained from Environment Canada and their locations are shown in Figure 3.16.

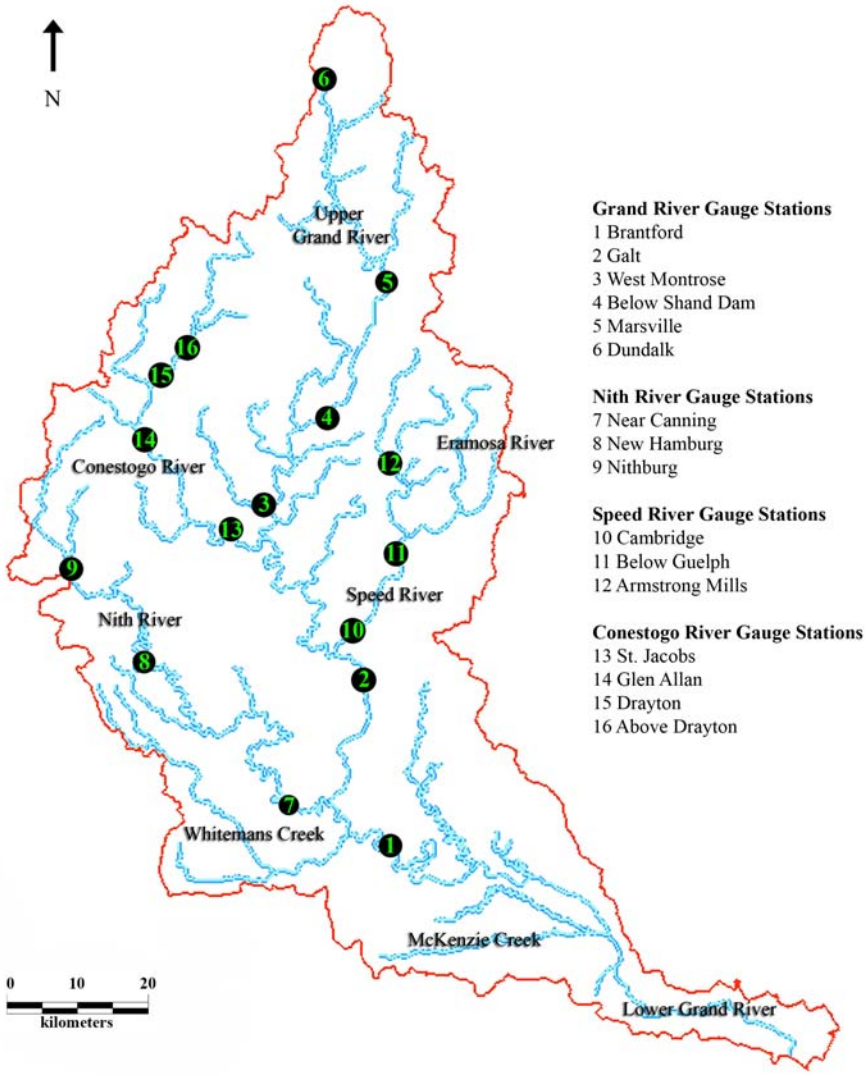

Figure 3.16: Gauge stations and simplified mesh drainage pattern

3.2 Calibration Procedure and Results

In the context of hydrological modelling, calibrating to mean streamflows is one of the important first steps in understanding a watershed's hydrology, in large part because it helps ensure that the input data and resulting water budget reflect observed conditions. Other calibration targets include observed subsurface heads and, more qualitatively, the water table's shape and orientation. Finally, one can match the locations of observed to simulated stream reaches where discharge is especially noticeable. A unique feature of HGS is that it computes the surface drainage network, unlike other models in which the network is explicitly specified.

Calibration typically involves alteration of hydraulic conductivity values specified for discrete hydrogeological units. Also typical is the alteration of parameters especially prone to inaccurate estimation, such as plant evapotranspiration parameters.

Sixteen stream gauge stations (Figure 3.16) were selected for calibration, based on the completeness of their flow records; only stations having recorded flow from 1973 (e.g., Speed River near Armstrong Mills) at the latest to 2004 at the earliest were used to calibrate the model. Calibration of surface flow, rather than the other calibration targets, was the first calibration step because of how readily the former changes in response to parameter adjustment. Expectedly, targets were unmet, by an average of approximately +24%, after arriving at a steady-state condition based on initial estimates of hydraulic conductivity and evapotranspiration

parameters. This strongly suggested, as evidenced by the water table being too elevated throughout most of the system, that estimated hydraulic conductivity values might be too low, at least near the ground surface. Consequently, conductivity values in model layers 1 to 6 were raised by a factor of five. The result was a surface water system that on average was quite close to the observed state, but whose individual gauge station flows still needed to change, mostly negatively, in order for the targets to be very closely approached. The required change after hydraulic conductivity adjustment, however, was less than 2% of the observed flow rate. Because this new streamflow pattern necessitated local-scale parameter adjustment, rather than the large scale adjustment just described, the alteration of conductivity for entire hydrostratigraphic units was echewed. Rather, small adjustments to some of the ZUMs' potential evapotranspiration estimates were deemed to be the most appropriate method to eliminate most of the remaining streamflow discrepancy, especially because this parameter is estimated to increase from south to north in the watershed, and because the high simulated flows were located in the south (e.g., Brantford, Galt). Specifically, potential evapotranspiration in ZUMs 6, 8, 10, 11, 12, and 13 was raised from the original estimated value of 750 mm/year to 800 mm/year, which corresponds to a 600 mm/year actual evapotranspiration estimate (actual rate = 75% of potential rate) and matches the upper bound as calculated by the Ontario Ministry of Natural Resources (1984). Figure 3.17 shows the excellent resulting

agreement between observed and simulated flows. Table 4.3 summarizes the observed and simulated streamflows at the 16 gauge stations.

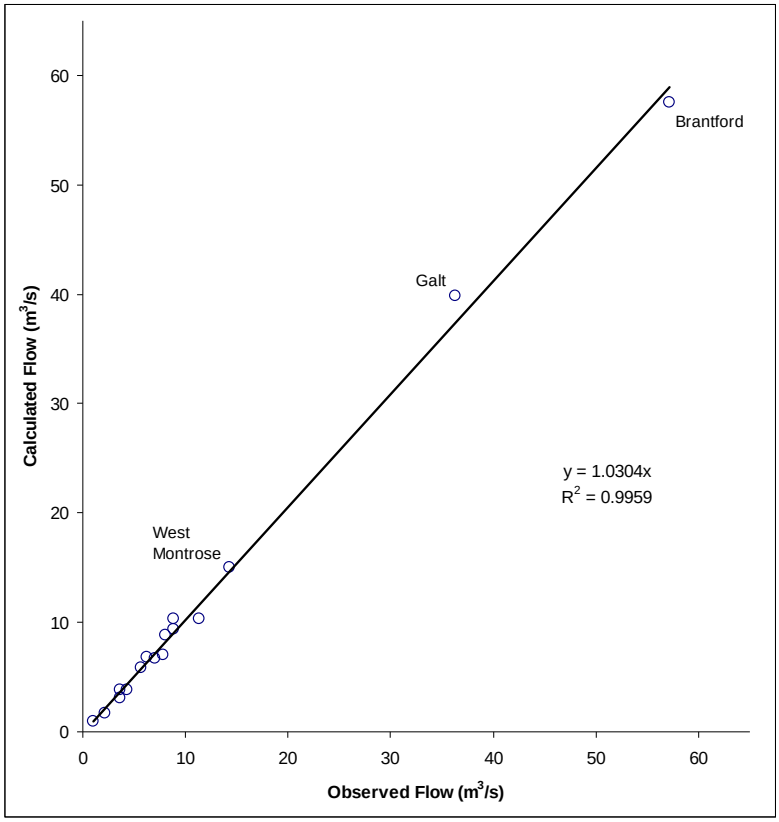

Figure 3.17: Calculated vs. observed long-term average flow in GRW rivers, using 13 zones of uniform actual precipitation

The watershed's simulated river network is shown in Figure 3.18a and matches the observed network (Figure 3.18b) reasonably well, although the model did not closely reproduce lake depths (e.g., Lake Belwood), likely due to the relatively coarse mesh used. Despite the simplified mesh and the somewhat large minimum element target size of 200 m, the steady-state base-case simulation required more than four months CPU time on a 3.4 GHz Pentium 4 personal

computer with 3 GB of RAM, having simulated close to 200 years at completion to arrive at steady-state. It is, however, expected that the parallel version of HGS that is under development would markedly reduce the CPU time.

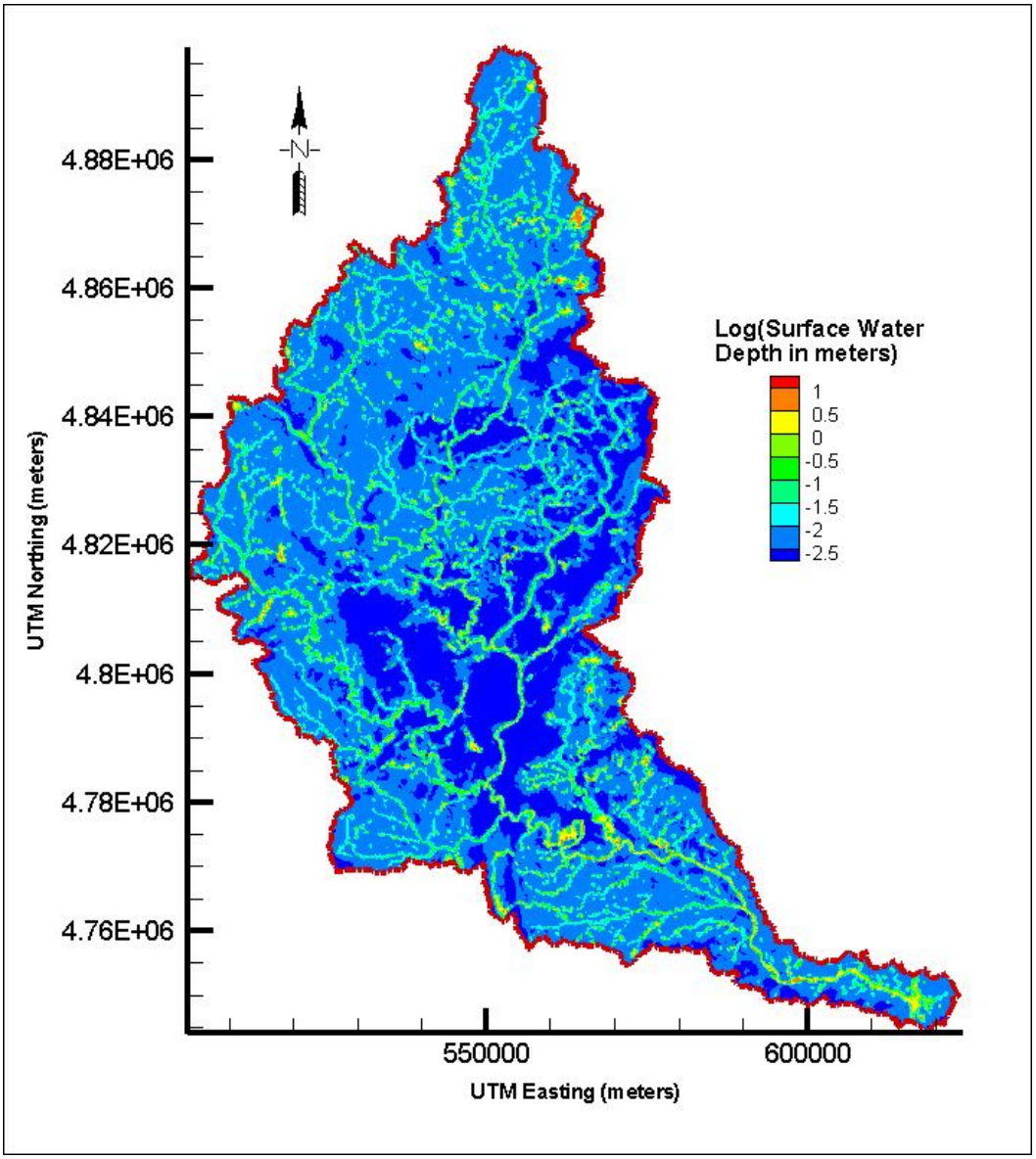

Figure 3.18a: Base-case-simulated river networks of the Grand River Watershed

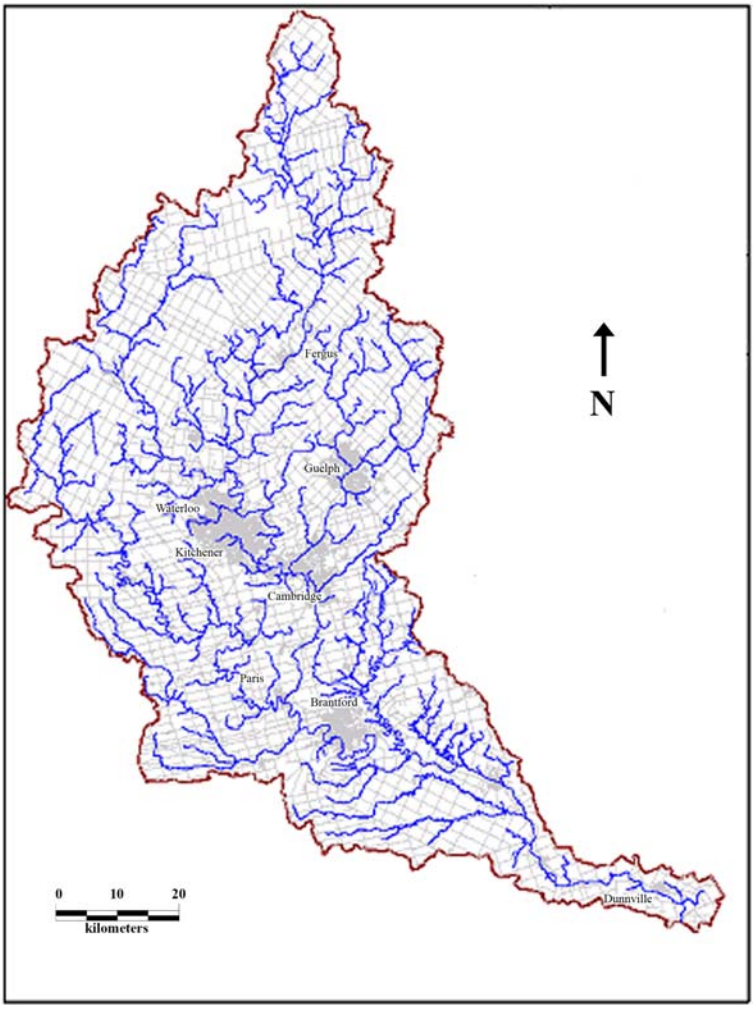

Figure 3.18b: Observed river networks of the Grand River Watershed

Subsurface calibration targets were examined next, since it was assumed that with the surface domain calibrated, the groundwater system likely would need little if any adjustment. That is, because the groundwater system greatly influences streamflow *via* base flow contributions, a well-calibrated surface system can be considered to be evidence of a well-characterized underlying subsurface system. The

number of subsurface water level targets was 387 (Figure 3.19), divided more or less evenly among model layers 2 to 10. Water levels for the uppermost layer and for the two lowermost layers were unavailable. A similar number of targets per layer was sought by randomly choosing every 10th observation well entry from the provided database for relatively data-poor layers, and every 25th entry for the relatively data-rich layers.

Figure 3.20 illustrates the excellent degree to which, in all calibration layers, subsurface heads matched observed ones. Figure 3.21 again shows the good

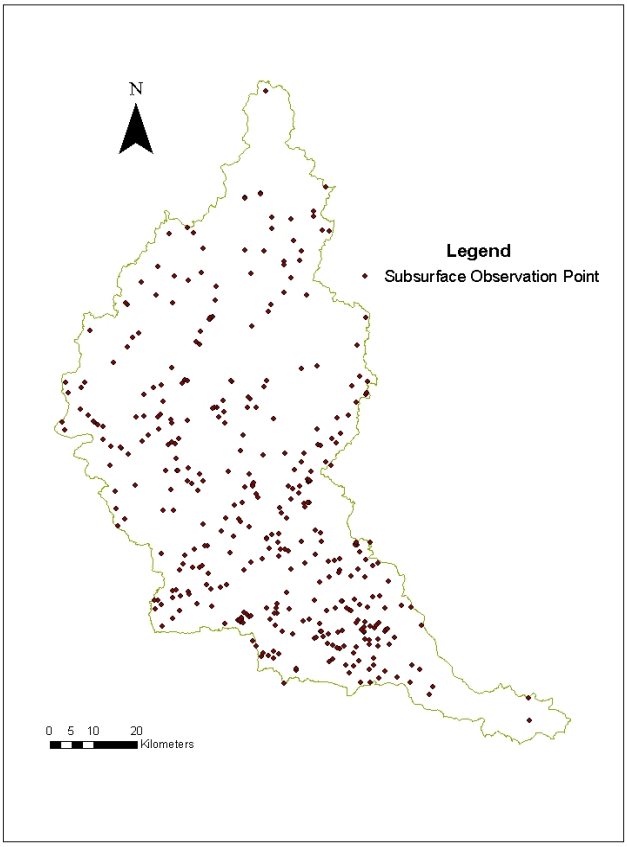

Figure 3.19: Water well records used in model calibration

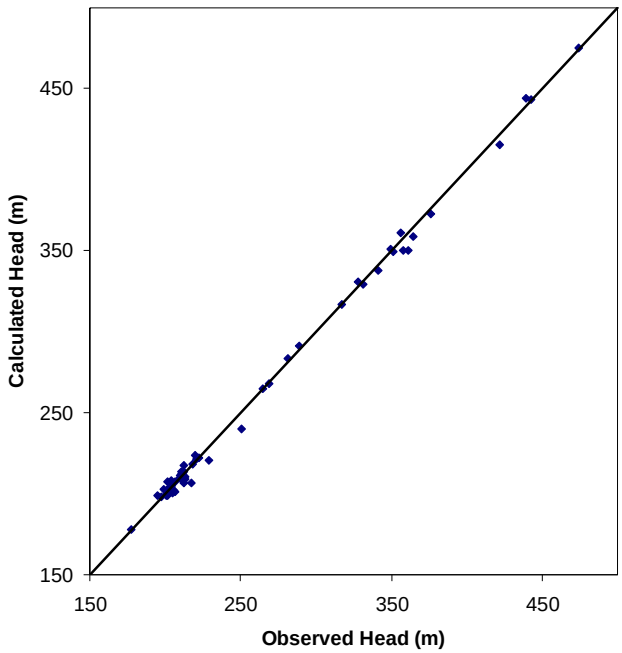

Figure 3.20a: Observed vs. calculated subsurface heads in Layer 2

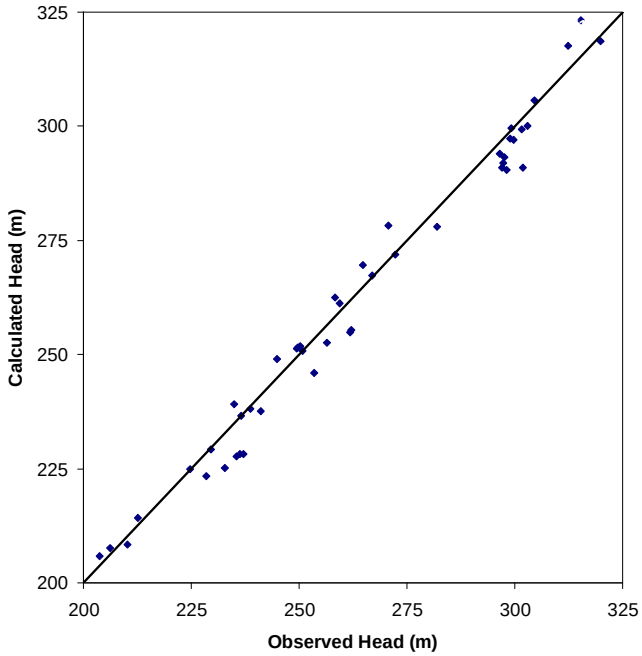

Figure 3.20b: Observed vs. calculated subsurface heads in Layer 3

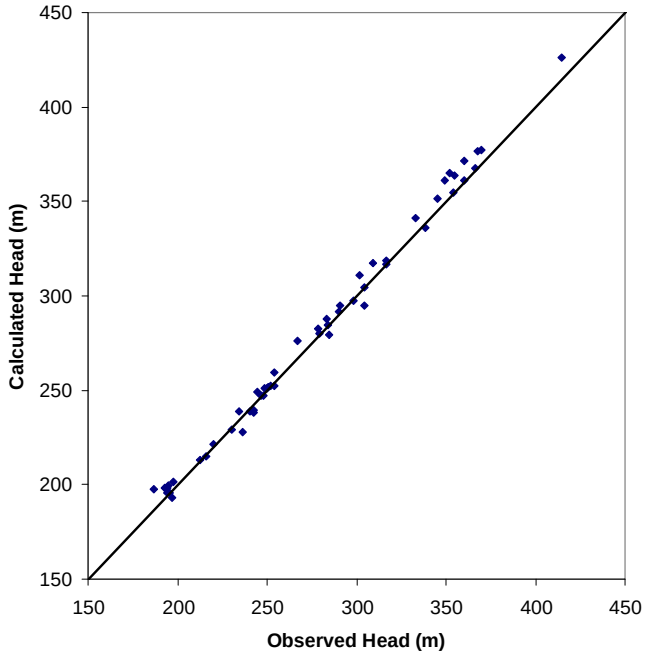

Figure 3.20c: Observed vs. calculated subsurface heads in Layer 4

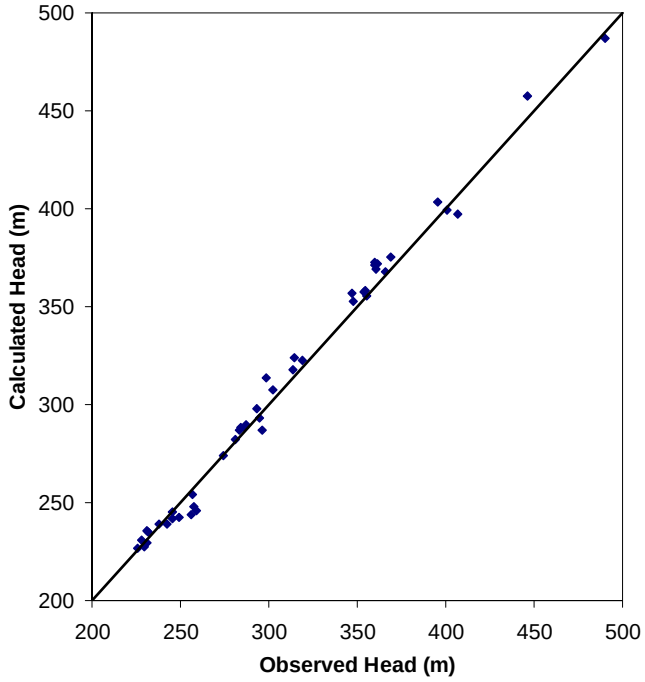

Figure 3.20d: Observed vs. calculated subsurface heads in Layer 5

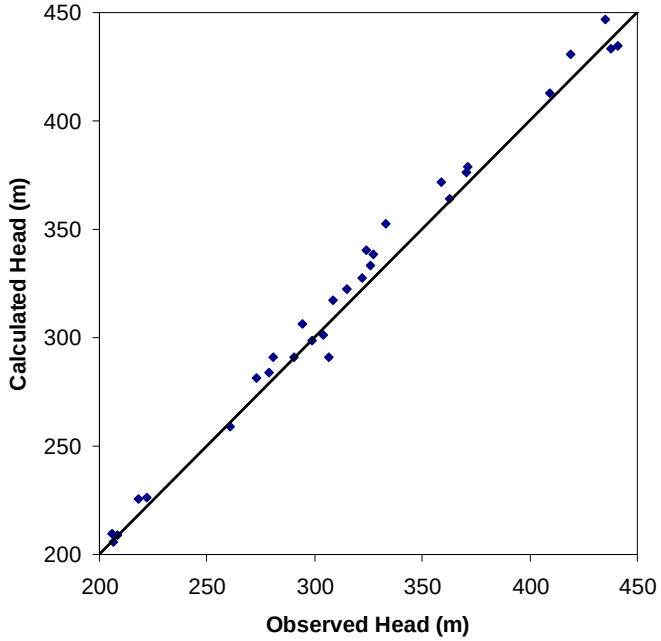

Figure 3.20e: Observed vs. calculated subsurface heads in Layer 6

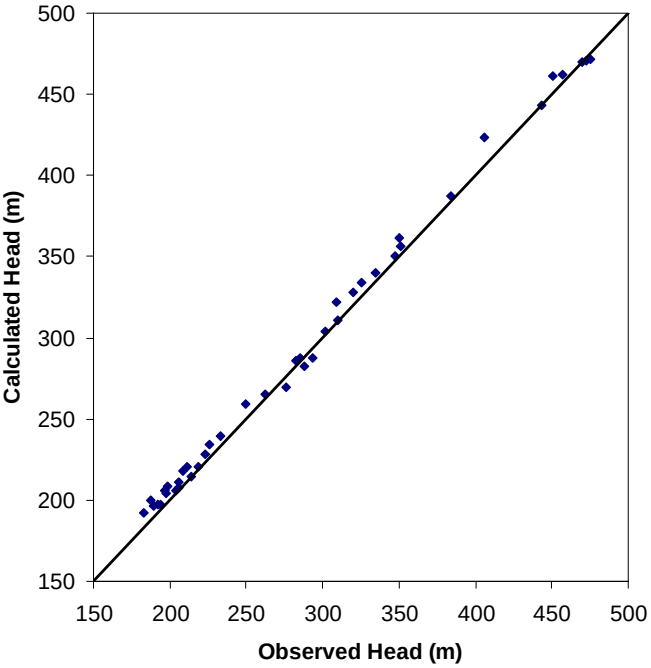

Figure 3.20f: Observed vs. calculated subsurface heads in Layer 7

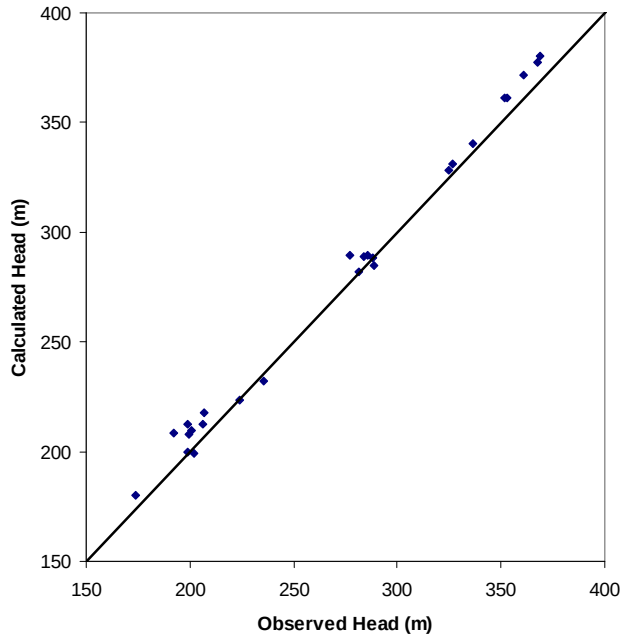

Figure 3.20g: Observed vs. calculated subsurface heads in Layer 8

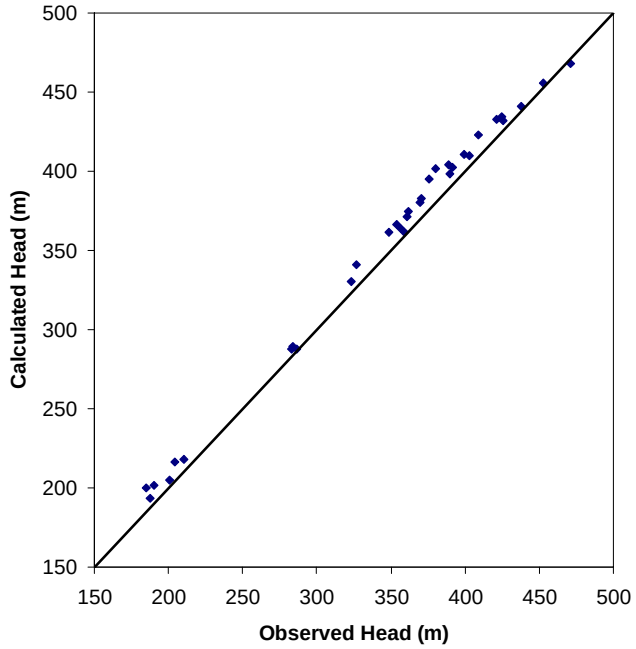

Figure 3.20h: Observed vs. calculated subsurface heads in Layer 9

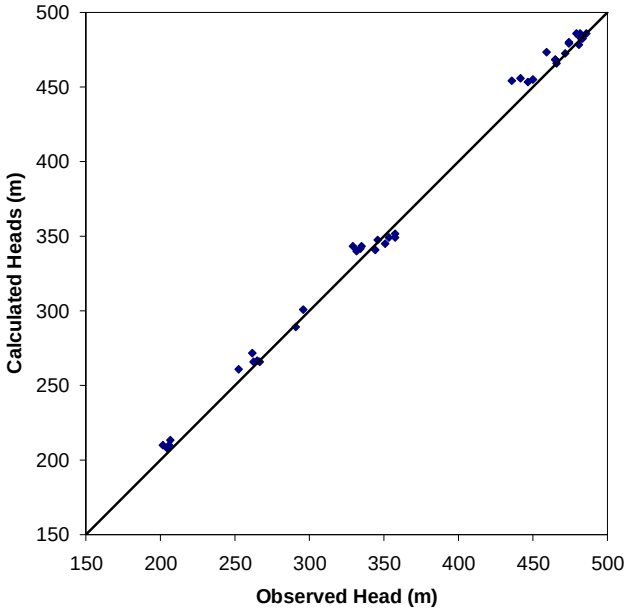

Figure 3.20i: Observed vs. calculated subsurface heads in Layer 10

subsurface matching, although it appears that the area of concentrated tile drainage (Figure 3.4) is the region in which the calibration could be improved further. It is important to note that the observed targets in large part are not temporally averaged and thus do not necessarily represent a long term average state of the groundwater system. However, it is assumed that the groundwater system changes at the decadal timescale, especially at lower depths, in which case even single measurements may be considered to represent the aforementioned average state (AquaResource Inc., 2007).

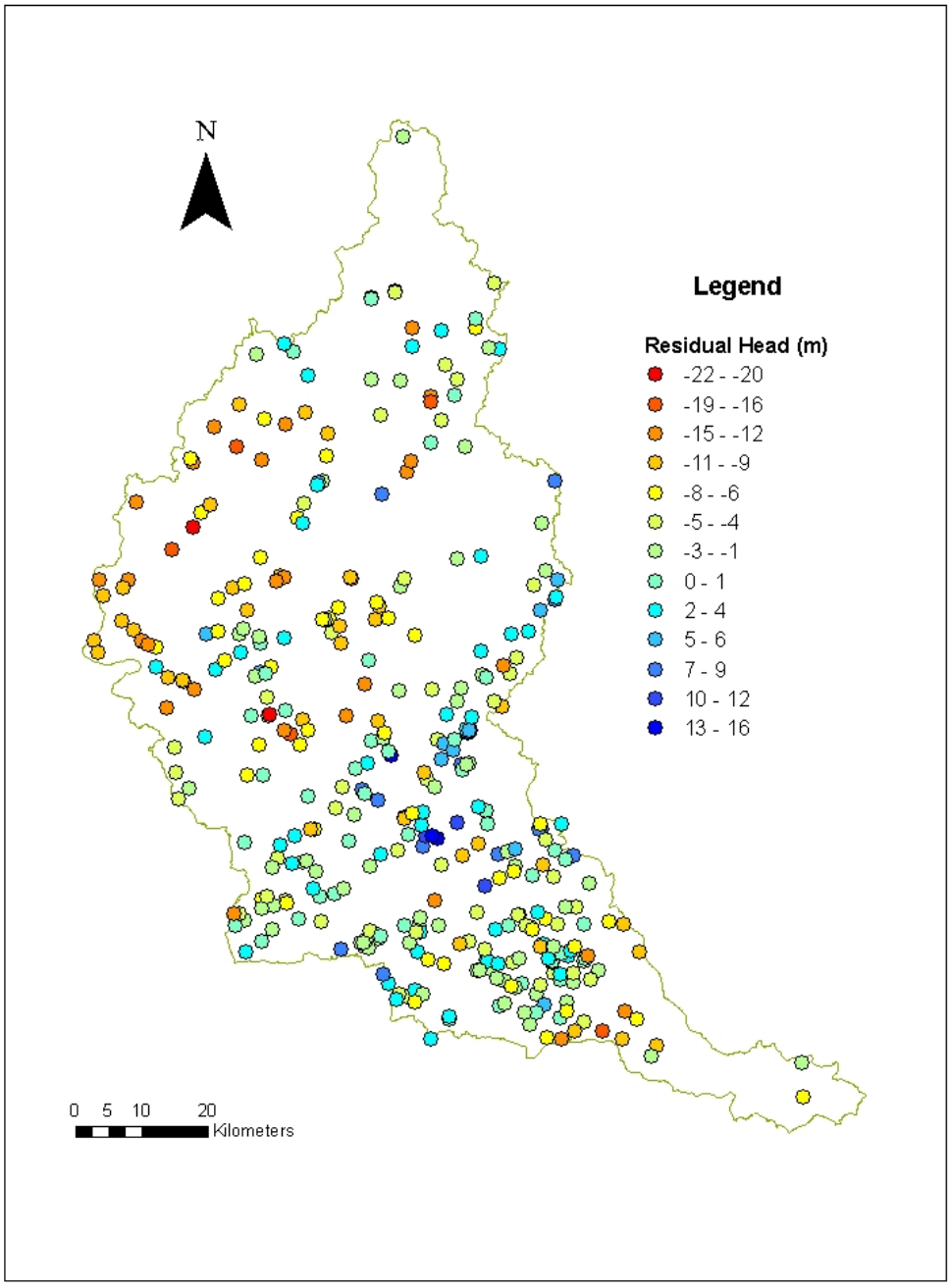

Figure 3.21: Residual subsurface heads

Qualitatively, the success of the calibration can be further evaluated by comparing the observed water table's topography to the simulated one – Figures 3.22 and 3.23 illustrate approximately the same pattern of the depth to the water table. In addition, one can compare the simulated water table to the ground surface elevations (Figures 3.24); the simulated water table should be a subdued version of the ground surface, which indeed is the case.

Furthermore, though again qualitative, comparison of the location of stream reaches gaining appreciable groundwater influx can provide some measure of the effectiveness of the calibration. For example, Figure 3.25 shows patterns of the surface/subsurface exchange flux, which is water either exfiltrating from the ground or infiltrating into it. (Infiltration is not the same as exchange flux, as infiltrating water can be routed back to the surface/atmosphere *via* evapotranspiration.) When it leaves the subsurface domain and enters the surface domain of the model (exfiltration), it does so only into a surface water feature such as a river. Figure 3.26 shows these gaining river reaches as simulated by Graham and Banks (2004), and Figures 3.27 and 3.28 show expanded views of the previous two figures. It is evident from Figures 3.27 and 3.28 that the stream reach shown gains much more groundwater than is typical of most stream reaches throughout the watershed. This reach, part of the Grand River between Paris and Brantford, is known *via* unpublished GRCA spot flow measurements to experience large quantities of exfiltration (groundwater discharge), and thus is an important contributor to the

greatly elevated aquatic biological diversity found there. The watershed's relatively low topographic relief means that the majority of groundwater discharge is confined to such major stream reaches.

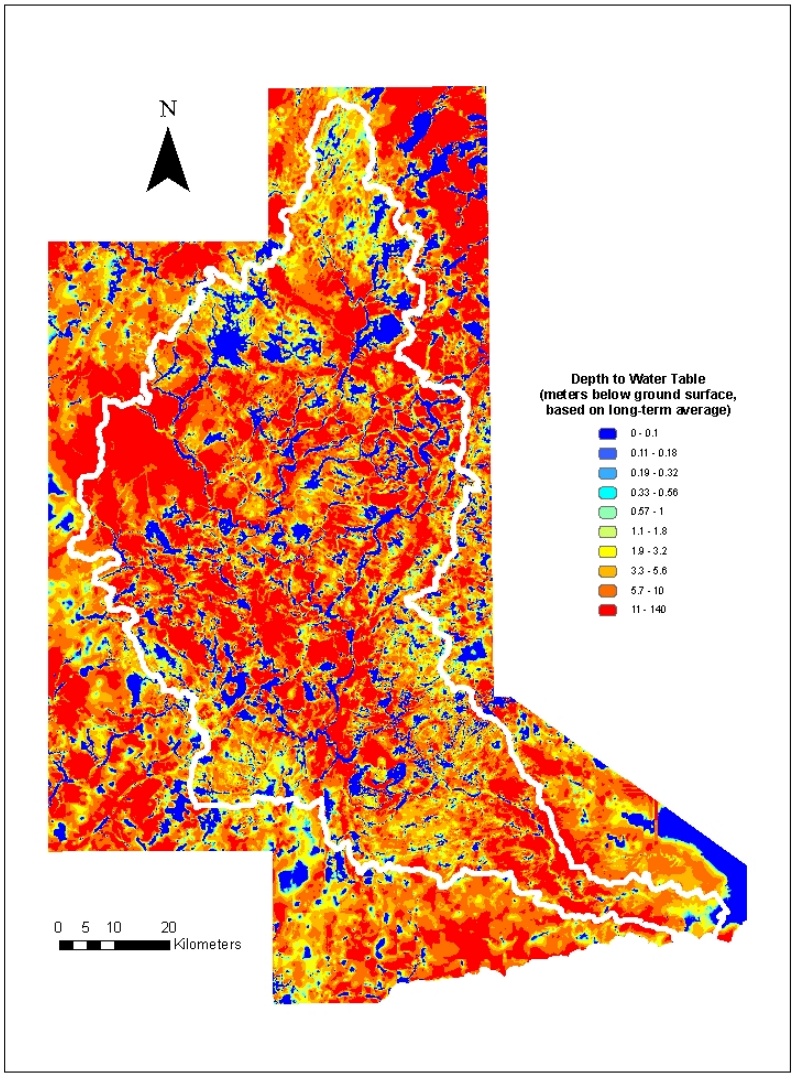

Fpgure 3.22: Observed depth below ground surface to water table, based on long-term average (GRCA, 2000)

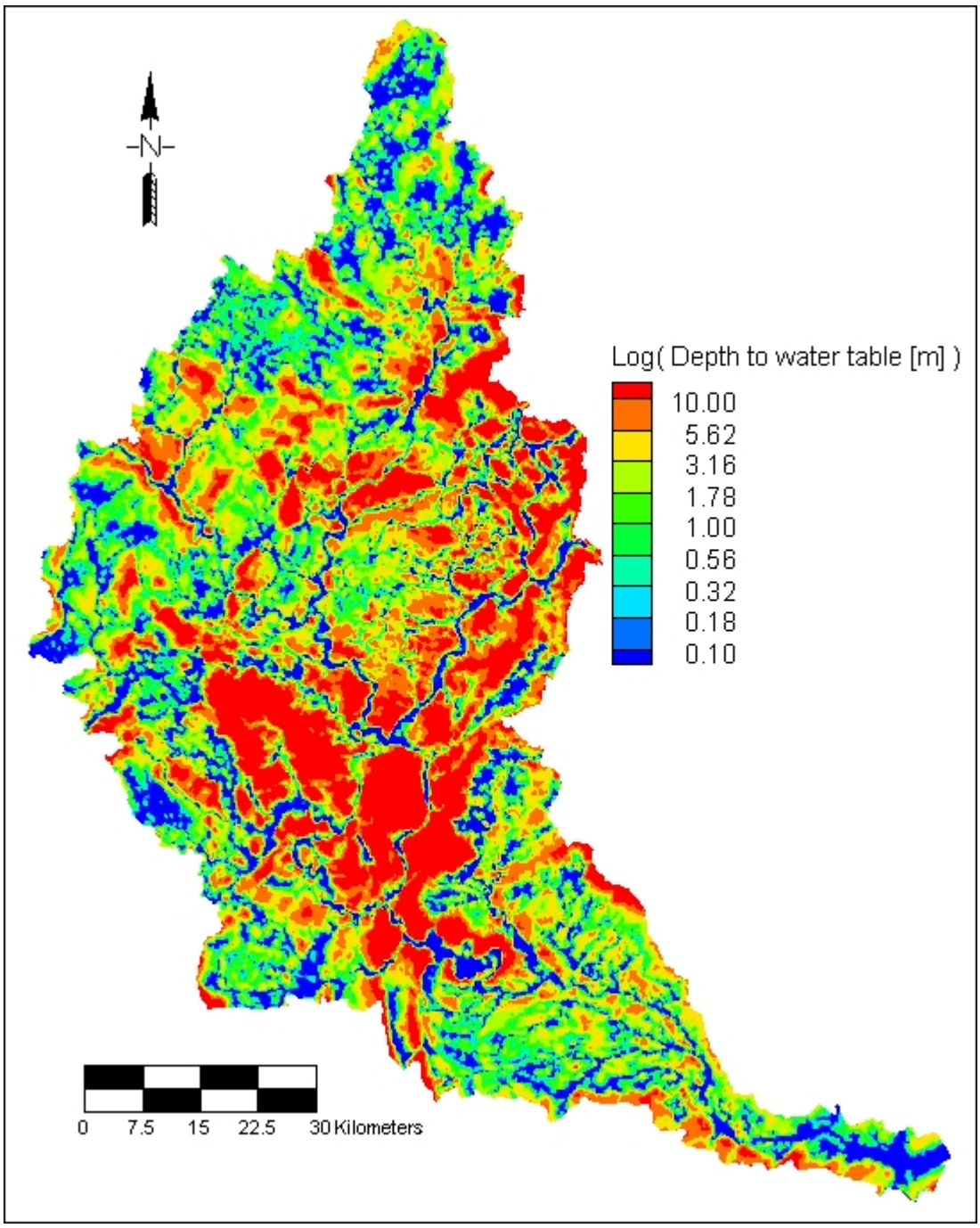

Figure 3.23: Simulated depth below ground surface to water table, base case

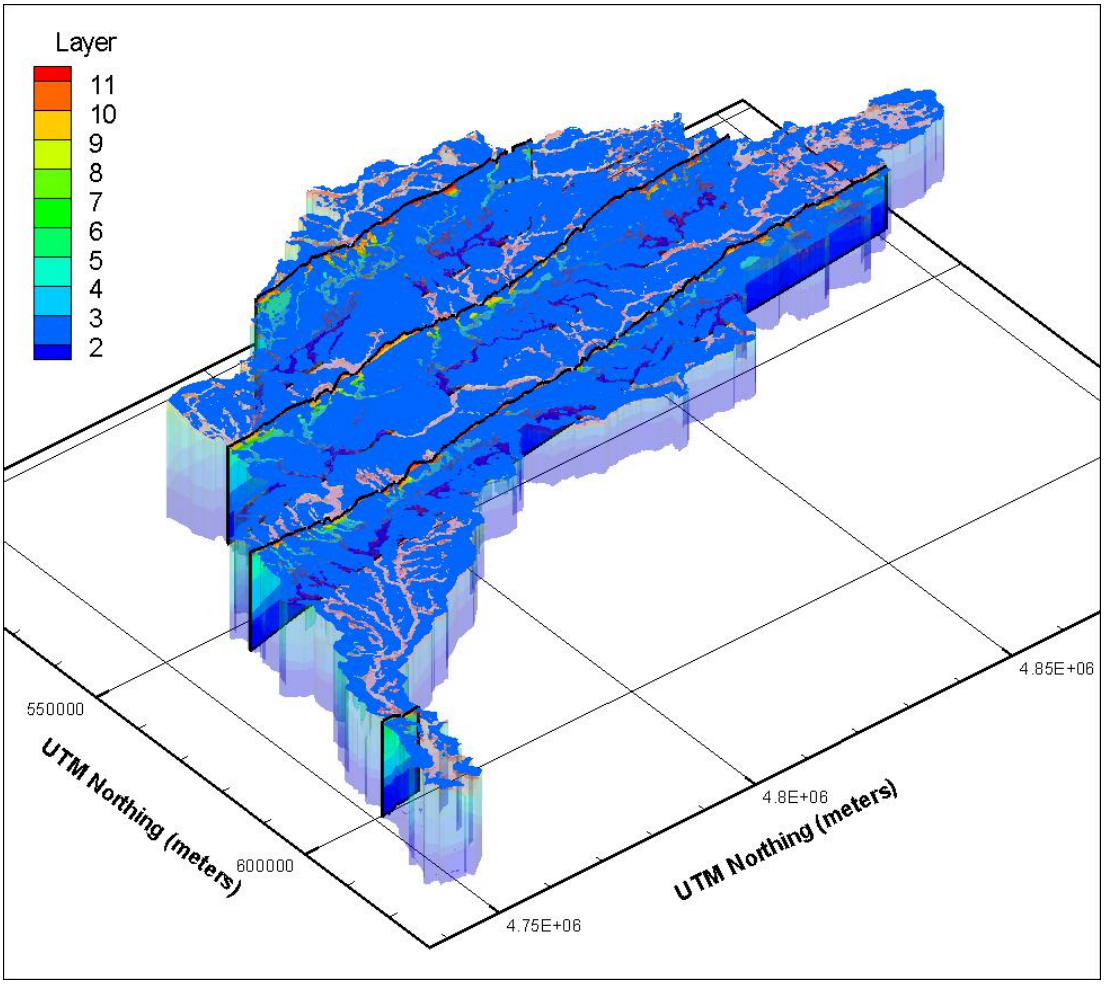

Figure 3.24: Base-case simulated water table topography (blue surface) contrasted against ground surface topography (three vertical slices)

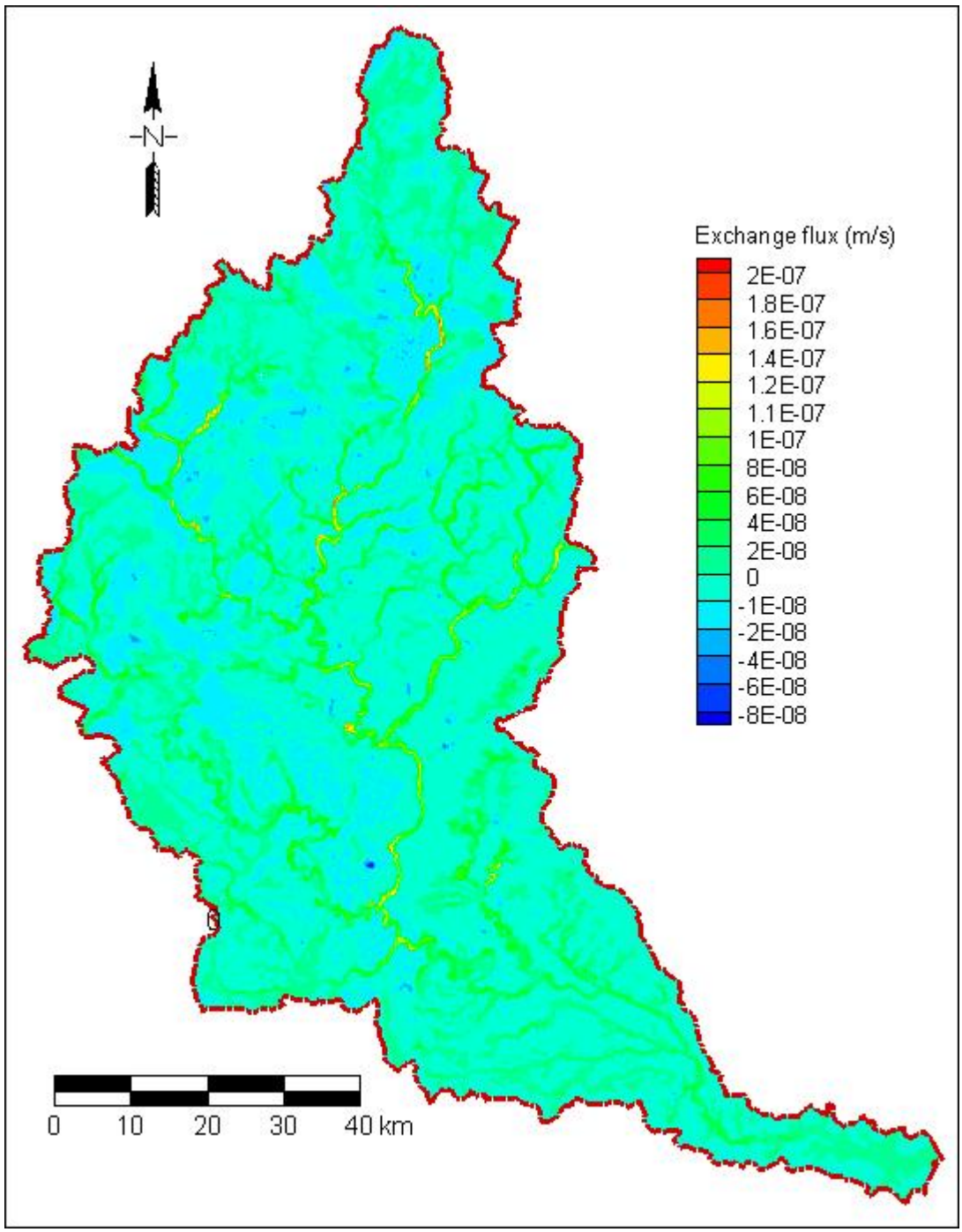

Figure 3.25: Exchange flux, simulated base case (positive values indicate exfiltration into surface domain)

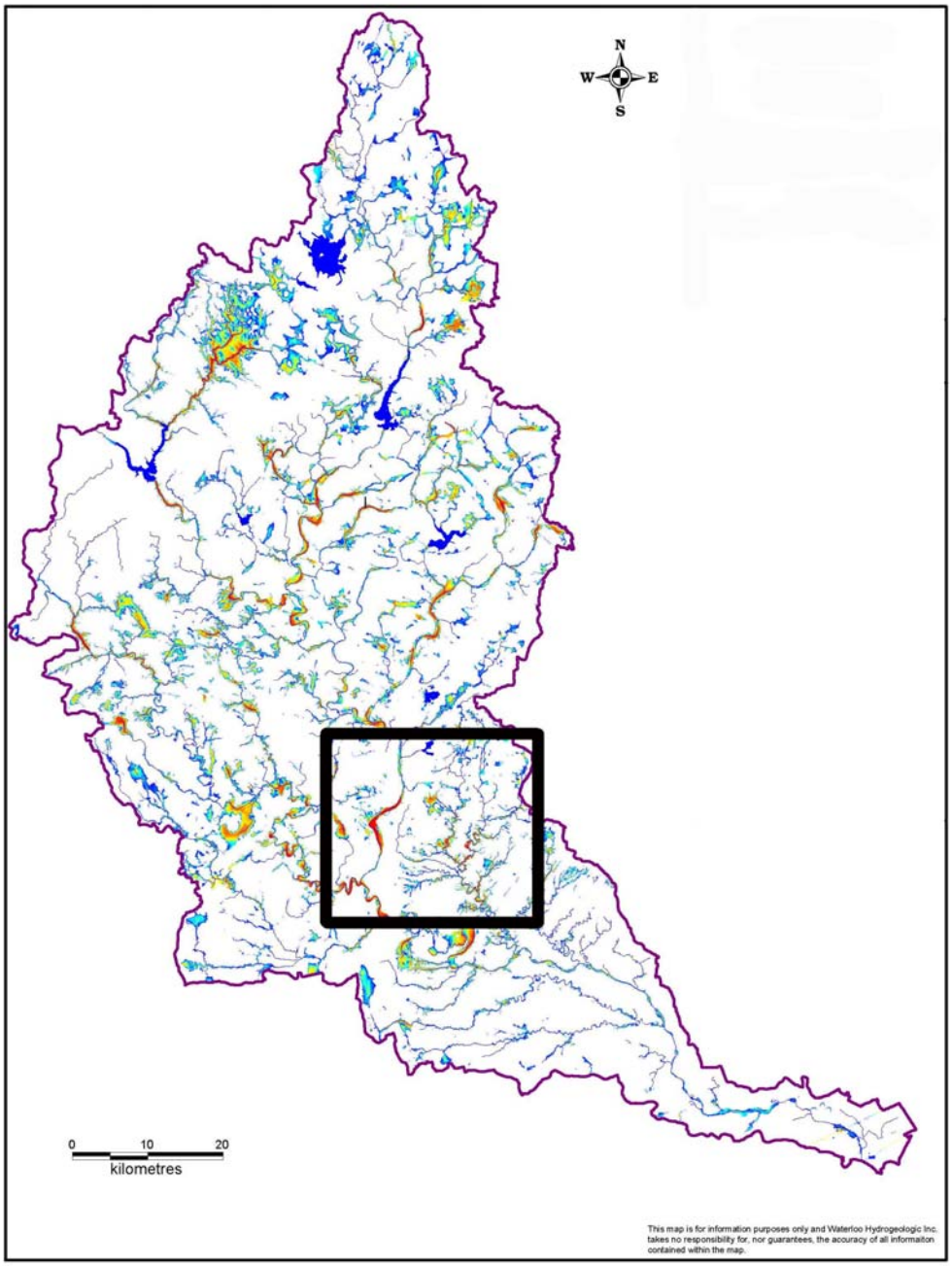

Figure 3.26: GRW discharge-recharge patterns (after Graham and Banks, 2004). Red/orange/yellow indicates gaining stream reaches. Inset depicts area shown in Figure 3.27. Note coincidence between gaining river reaches and the Waterloo Moraine.

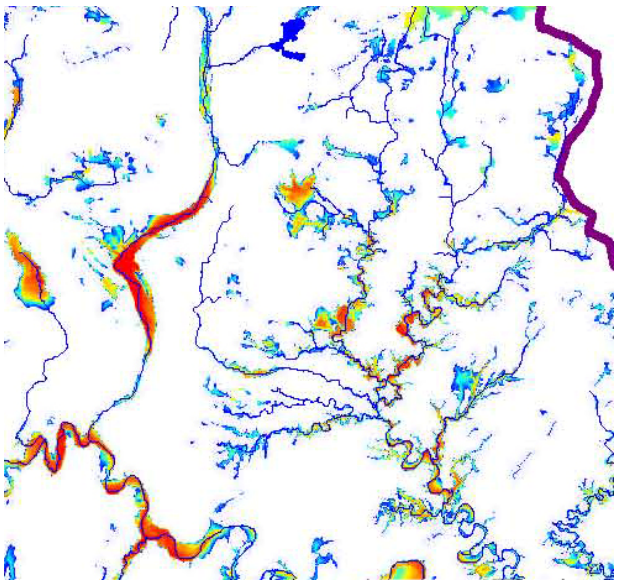

Figure 3.27: Expanded view (see inset of Figure 3.27) of GAWSER-FEFLOW discharge and recharge (after Graham and Banks, 2004). Note similarity of red/orange/yellow (gaining) stream reaches of Figure 3.28.

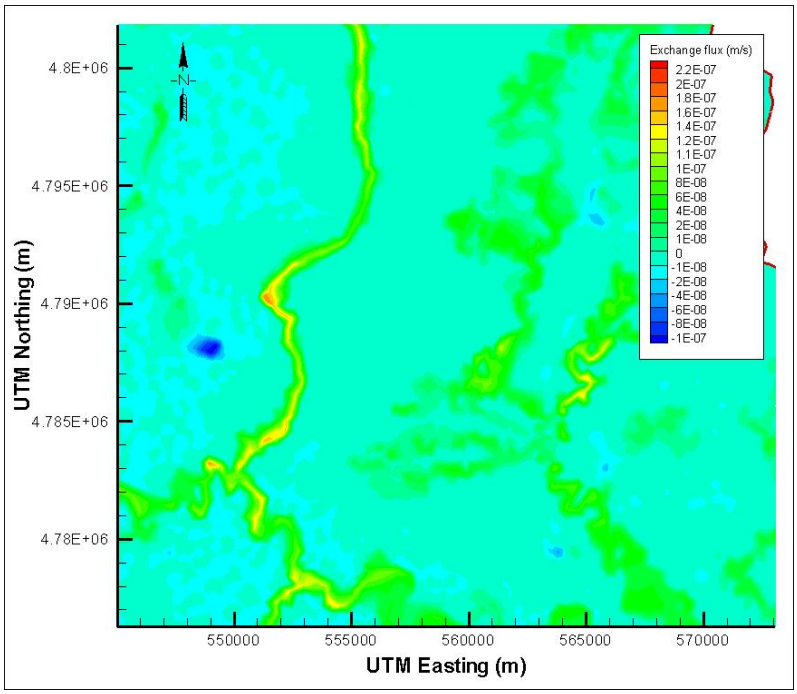

Figures 3.28: Expanded view of HGS-computed exchange flux, base case scenario

Elements of the GRW water budget are shown in Table 3.6. The approximate

Table 3.6: GRW average water budget

Water Budget Parameter	**Value** (m^3/s)	**Value** (mm/year)
Precipitation	200	930
Evapotranspiration	130	605
Surface Flow Out of GRW	67.5	313.5
Infiltration	100	465
Exfiltration	36.5	170
Recharge	39	186
Groundwater Flow Out of GRW	0	0
Groundwater Pumping	3.5	16
Treatment Plant Returns	1.5	4.5

amount of water that evaporates directly from the ground surface totals 321.5 mm/year (53% of total evapotranspiration), and equals the following:

$$\text{evapotranspiration} - (\text{infiltration} - \text{exfiltration} - \text{pumping}) \quad (11)$$

That is, because there is no change in storage, nor modelled flow between the GRW and neighbouring watersheds (not even Lake Erie), the water that infiltrates either must either exfiltrate, evapotranspire, or be pumped from the system. After exfiltration and pumping are subtracted from infiltration, the water left to evapotranspire *via* the subsurface is 283.5 mm/year, which leaves a little over half of the watershed's evapotranspirative loss to occur due to factors not strongly related to vegetation type. This is hardly surprising, as Bolger (2009), for example, found that

the highest evapotranspiration occurred in areas of open water such as river channels and wetland areas.

Recharge, the water that has infiltrated into the ground and then reaches the water table, differs from infiltration in that water undergoing the latter may be diverted away from the water table, for example by evapotranspiration. Indeed, the budget shows that 283.5 mm/year (47% of total evapotranspiration) of infiltrating water evaporates due to the combined effects of transpiration and subsurface evaporation. Recharge's importance relates in large part to its role in maintaining the water supply within aquifers. The average base case value of 186 mm/year (20% of precipitation) closely approximates corresponding values found in Jyrkama (2003) (189 mm/year) and AquaResource Inc. (2007) (180 mm/year). Whereas infiltration and recharge should not be confused with each other, groundwater discharge and exfiltration are identical, occurring exclusively through streambeds, lake beds, and the like.

On average, actual evapotranspiration can be said to account for the greatest percentage (two thirds) of water passing through the system, which agrees with both the M.O.E. estimated upper bound and the steady-state findings of Li *et al.* (2008). At the other extreme is the groundwater component that interacts with neighbouring watersheds, which is explicitly defined to equal zero in the model. As with pumping, there is agreement with AquaResource Inc. (2007) in that both components are minor budget players at the watershed scale in the long-term, although pumping can be an

important component at the local scale and even regionally during times of low streamflow. About one third of the system's water flows through its surface bodies; unfortunately the GRW's surface water outlet – the Grand River at Port Maitland – lacks a gauge station, making it difficult to determine total watershed runoff.

3.3 Discussion

As with most modelling efforts, a balance was struck between proper characterization of the real system (e.g., river morphology) and computational/time costs, and thus several of the GRW's smaller waterways were not assigned nodes prior to mesh creation, after it became clear that the number of nodes in the initially-configured model would be prohibitive. While the calibration results thus cannot be framed in terms of these overlooked areas, the exercise nevertheless showed that average conditions could be simulated for a variety of geologic settings. For example, the Conestogo River at Drayton is dominated by overland runoff, while the Eramosa River system is groundwater-fed. Here, the very hummocky topography allows for increased infiltration to occur. The large Nith subwatershed is composed of tight tills in the upper portion of the basin, but by sandy gravels downstream to the south, and is heavily influenced by the Waterloo Moraine, meaning that the observed reaction to a storm event very much depends on where location in this subwatershed. Because some element lengths are as great as 1 km, the simulation of horizontal surface runoff may be problematic. This may also be true in future transient

simulations based on the present model, but there was no evidence of significant problems in the steady-state findings, as the simulated and observed streamflows and hydraulic heads were represented fairly closely. The base case should thus serve as a useful initial condition for any transient simulations based on this model.

Further limitations of the present approach include those arising from measurement and database issues, as well as conceptual limitations. As to the former, observed river flow records were more complete at certain gauge stations than for others, which led to certain decades at certain stations being over-represented relative to other stations. Similarly, climate data collected at climate stations are assumed to be representative of conditions over a much larger geographic area. However, this assumption falters especially during summer months when extremely localized weather events occur, because the density of the climate stations often cannot capture such events. Furthermore, uncertainty in precipitation measurements can be close to 10% (Metcalfe *et al.*, 1996) with the uncertainty during winter months reaching as much as twice that amount. Errors relating to manual streamflow measurement can be +-10% to 15% (rule of thumb), and measurement error for extreme high and low flows may be significantly larger. However, measurement factors relating to extreme streamflows and to the weather that causes them is much more important in the calibration of transient models. The problem of scale nevertheless remains an important issue, as significant local

variability of many other parameters within the subwatershed can be difficult and often impractical to include in the model.

A potential limitation involved the omission of explicitly defined water control structures from the model. However, the Canning (Nith River) and Drayton (Conestogo River) stations measure streamflow discharging from unregulated basins; the fact that calibration did not need to deviate for these stations with respect other stations on the same rivers suggests that the watershed's flow control structures likely need not be explicitly included in long-term average studies such as the present work.

The choice to manually calibrate the model is only one of several options. P.E.S.T (Doherty, 2001) is one of the most popular automatic parameter estimation algorithms in use, and likely could improve upon the calibration obtained herein. Additionally, it would yield a range of fitted parameter values that would be of use for uncertainty analyses.

Although slight in terms of the watershed's overall water budget, the amount of water extracted *via* pumping can have an important impact at least locally. However, because the coarseness of the model mesh limited the extent to which the shape of the water table around pumping wells (cones of depression) could be simulated in the present work, it is likely that mesh refinement is necessary if the local effects of pumping are to be delineated in the future. It should be noted that the hydrostratigraphy resulting from the chosen mesh design stems, in turn, from an

automated approach that may well lack the refinement necessary to truly describe the layering of the subsurface system.

Well records (water levels), as noted earlier, suffer from a range of uncertainty on the order of 5 meters. This is due to many factors, including clogging of aquifer materials due to the drilling method, measurement while recovery to static conditions are still underway, variability of the water level relative to the time of measurement, measurement error or recording errors, and measurement point elevation errors. While individual values may be in error, the trends illustrated by the multiple data points are nevertheless expected to be realistic. Because natural fluctuations in groundwater levels are generally minor (~ 2m or less where stress conditions are consistent), carefully measured water levels are considered to be more certain than most other calibration targets (AquaResource, 2007).

The GRW water budget includes values of three unprescribed processes: actual evapotranspiration, infiltration, and exfiltration, and is quite similar to the findings of Jyrkama (2003) and AquaResource Inc. (2007). For example, the former, with similar base case precipitation input had average evapotranspiration of 512 mm/year. The latter estimated evapotranspiration at 491 mm/year, but its incomplete water budget does not facilitate the determination of the evapotranspiration deficit relative to the estimate given herein. Given this agreement between most of the water budget components among the three studies, and given the fact that evapotranspiration is among the most difficult parameters to estimate, some studies

understandably may employ less physically-rigorous modelling methods for the sake of both time/cost savings and the inclusion of hydrologic processes that are difficult to quantify and simulate. While a HGS snowmelt function is in development, it should be stressed that the equilibrium approach herein is much less negatively affected by the neglect of snowmelt processes, relative to a transient study.

When treating surface water bodies such as lakes, typical subsurface models represent these features as specified head boundaries where lakes are known to form, where the lakes are known to exist, whereas the present approach allows for lakes to form naturally. The fact that they did not properly form is simply an artefact of the mesh coarseness and the lack of data on the bathymetry of the lake bottoms.

Chapter 4: Steady-State Simulation of Grand River Watershed Hydrology Under Future Climate Conditions

4.1 Scenario Details

More than 90% of the multiple GCMs considered in IPCC (2007) predict that GRW precipitation will increase during winter, up until 2090. However, important output differences exist among the models: while the Canadian Coupled Climate Model and the Hadley Coupled Climate Model both show increased precipitation amounts resulting primarily from increased frequency of heavy precipitation events, the former model emphasizes this frequency increase from December to July, while the latter emphasizes it during the rest of the year (Sousounis and Grover, 2001). Further, fewer than 66% of said models agree on the direction of summer precipitation change. As such, GCM output should at best be considered to represent a plausible range of future climate. In the present work, synthetic scenarios based in part on (Fagherazzi *et al*., 2007) were constructed by perturbing the historical record for precipitation, by an arbitrary amount (e.g., 10% increase) (Barrow *et al*., 2004; Mearns *et al*., 2003). The GCM-based climate change scenarios are used only to bound the synthetic ranges, given the infrequent agreement among GCMs regarding precipitation predictions.

Once a calibrated steady-state solution was arrived at, the actual precipitation value of each ZUM was modified by a certain percentage in each synthetic climate change scenario. This is shown in Table 4.1, where for each scenario the thirteen

ZUM-based values have been averaged in the table to convey a watershed-wide estimate. For example, the IPCC (2000) concluded that at least forty future climate scenarios were equally likely. Note that while von Storch *et al*. (1993) recommend that at least four GCM grid boxes should be used to define the domain of any study investigating the effects of GCM scenarios, this is impossible for the GRW, due to the very coarse GCM spatial resolutions presently available.

Table 4.1: Synthetic climate change scenarios

Scenario	**Change in actual precipitation throughout simulation, relative to 1960-1999 levels**	**Actual Precipitation, averaged over 13 ZUMs** (mm/year)
1	-5%	884
2	+5%	976
3	+10%	1023
4	+15%	1070
5	+20%	1116

As in Arnell and Reynard (1996), the chosen scenarios represent the potential range of regional climate change 50 years from now, enabling a realistic range of possible impacts to be quantified. The scenarios were developed with the aid of Environment Canada's Canadian Climate change Scenarios Network (CCCSN) visualization tool. Because summer precipitation changes differed between the various GCMs, the synthetic scenarios range from a precipitation increase of 20% to a decrease of 5%, which spans the GCM output range. Zhang *et al*. (2000) showed that over the past century and for southern Canada, from 1900-1998, the annual mean

temperature and precipitation have increased between 0.5 to 1.5°C, and 5% to 35%, respectively.

4.2 Projected Changes in Hydrological Regime

Figures 4.1 to 4.4 and Table 4.3 show the surface runoff response to each of the five climate change scenarios, contrasted against that for the base-case (1960 to 1999). Under Scenario 1 (5% less precipitation than average), GRW gauge stations experience an average discharge decline of approximately 15.3% relative to the baseline simulation. On average, the stations on the Grand River showed the greatest percentage decrease (20%), with the other three main drainage systems more or less grouping together. This decline clearly is due to flow decline close to where the Grand River begins, at the Dundalk station which reported a discharge decrease of more than 40%, suggesting that even drier climates could very well cause the river there to unprecedentedly cease flowing. All other scenarios involved a forced precipitation *increase*, causing the Grand River to react much more similarly to the responses of the Nith, Conestogo, and Speed drainage systems. The Speed River reacts more than any other, up to a difference of 9%. Within subcatchments, too, there is always a negligible difference in discharge response between stations; for example, the Cambridge station flow response was always similar to that of the Armstrong Mills station.

The results of scenario 2 (5% more precipitation) shows all stations experiencing a 12% or 13% discharge increase, except for the Speed River which on average experiences a discharge change that is 2% greater than the other subcatchments, and as high as 15% at two of its stations. This inter-subcatchment trend, whereby Speed River discharge continues to change the most in response to climate forcing, is amplified in transitioning from Scenario 2 to Scenario 5, where the forced precipitation level is +20% and discharge is calculated to be between 49% and 59% of the base case, depending on the station being considered. That is, the Speed River's 2% greater response in Scenario 2 increases to a 4% greater response in Scenario 3. It increases to 7% and roughly 9% in Scenarios 4 and 5, respectively, and so increasingly diverges with each 5% increase in precipitation. One possibility is that the prevalent bedrock outcropping in the Speed subcatchment is responsible for the river's somewhat different response to climate forcing. Conversely, the responses Nith, Conestogo, and Grand Rivers do not diverge from each other.

Figures 4.5 to 4.7 show that among the five climate change scenarios, the water table's pattern of highs and lows does not change appreciably. Transitioning from the extreme of -5% precipitation directly to that of +20, there is a slight difference, but the difference between Scenarios 1 and 2, or 4 and 5 for example are too slight to easily observe. This strongly suggests that general horizontal groundwater flow directions within the GRW, at least in the uppermost aquifer, are

unlikely to change unless forced by climates significantly more extreme than those simulated here.

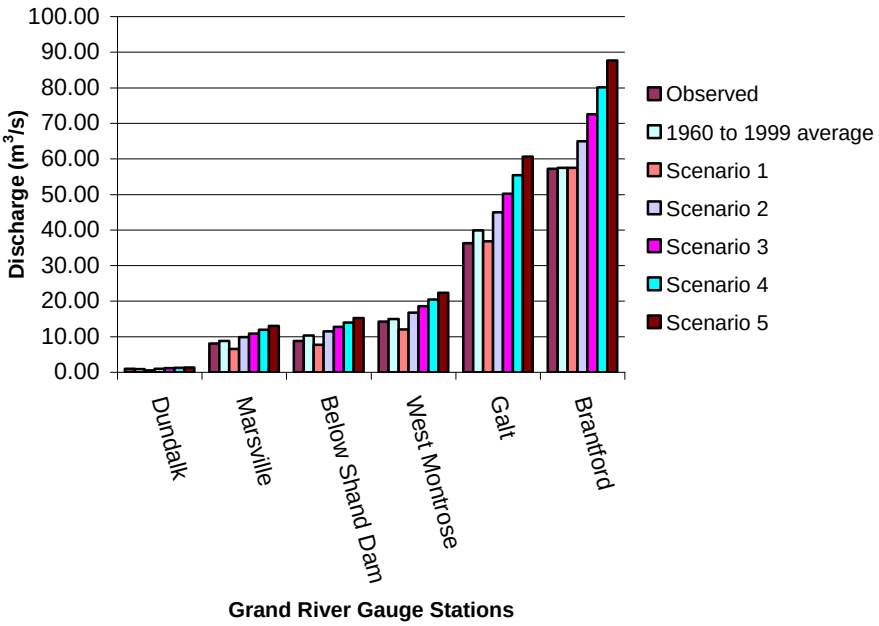

Figure 4.1: Observed Average Grand River Discharges vs. Climate Change Scenario Discharges

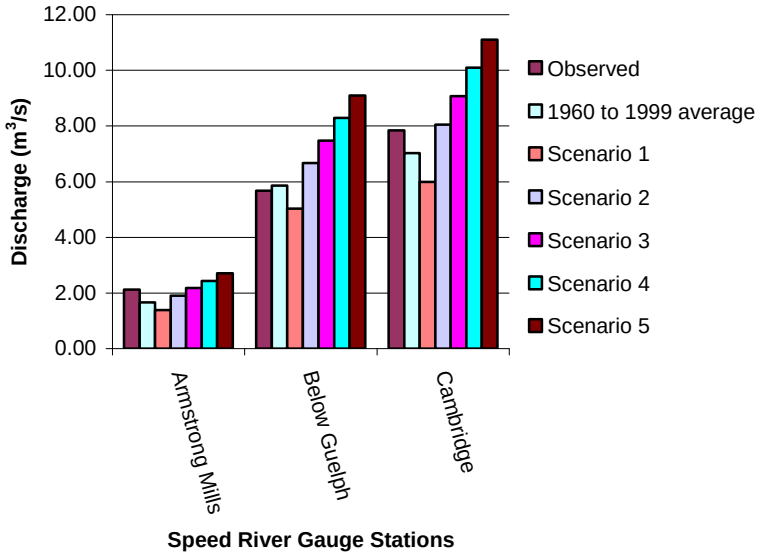

Figure 4.2: Observed Average Speed River Discharges vs. Climate Change Scenario Discharges

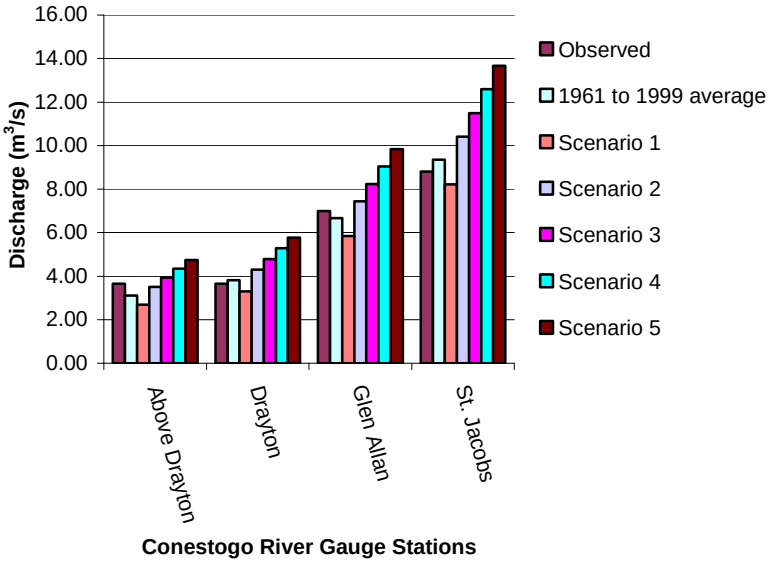

Figure 4.3: Observed Average Conestogo River Discharges vs. Climate Change Scenario Discharges

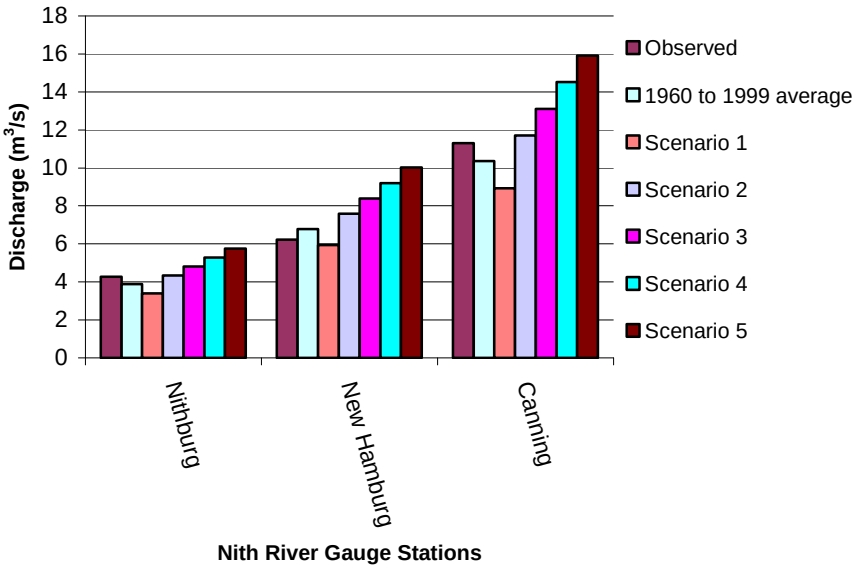

Figure 4.4: Observed Average Nith River Discharges vs. Climate Change Scenario Discharges

However, when one considers the climate-forced change in the depth-to-water table, the degree of change is much more noticeable. Relative to the base scenario, nodally-averaged depths change by a minimum of about +48 cm (i.e., a lowered water table) and a maximum of about -108cm, as shown in Table 4.2. The absolute maximum difference is about -4.5 m, and is located in the Waterloo Moraine. The change in nodally-averaged water table depth among the increased-precipitation scenarios decreases approximately linearly ($r^2 = 0.99$) with each 5% precipitation increment, although a second-order polynomial fit gives an r^2 of unity. That is, there is a difference of -0.28 m between Scenarios 2 and 3, but this difference decreases

Table 4.2: Change in depth-to-water table caused by climate change. Negative values indicate a rising water table relative to the base case scenario.

Scenario	Nodally-averaged change in depth-to-water table (m)	Maximum water table depth (m)
Base		
1	+0.48	62.92
2	-0.36	60.88
3	-0.64	59.99
4	-0.88	59.15
5	-1.08	58.43

to -0.24 m between Scenarios 3 and 4, and decreases to -0.20 m between the two highest-precipitation scenarios. An explanation for this slight trend is that, as the water table rises to the ground surface, the former's gradient becomes more and more pronounced especially in areas of undulating topography and along streambanks, such that water is discharged to the surface domain at an increasing rate (see section just below on discharge patterns). The effect is to thereby dampen the rate at which the water table can rise. Maximum depth to the water table is best described by the polynomial expression of Figure 4.8, which shows that increasing precipitation has a slightly progressively weaker effect on the maximum. Below the water table and for Scenarios 2 to 5, inter-scenario average hydraulic head change (Table 4.4) ranged from a maximum of -53 cm between Scenarios 2 and 3 to a minimum of only -8cm between Scenarios 3 and 4, rather than between the expected 4-to-5 scenario transition. The minimum of -8 cm might be explained by a stage being reached between Scenarios 3 and 4, perhaps due to the presence of particular topographic

features, where near-surface pore space already was very close to saturation. This would cause the change in the pressure component of hydraulic head to plateau (see saturation-pressure relationships).

Groundwater discharge (exfiltration in Table 4.5) responded to climate forcing as alluded to earlier: more water in the system leads to greater hydraulic gradients especially in topographically pronounced areas (e.g., streambanks), and to a corresponding increase in discharge to the surface zone. This discharge change is clear when comparing the base case or Scenario 1 to Scenario 5 (Figures 3.25, 4.9, and 4.10, respectively); Figure 4.11 compares all the simulations.

Table 4.3: Calculated river discharges resulting from climate change scenarios

Gauge Station	Observed Average Flow (m^3/s)	Base Case (m^3/s)	fraction of observed average flow	Climate Scenario 1 (-5% P) (m^3/s)	fraction of base simulation flow	Climate Scenario 2 (+5% P) (m^3/s)	fraction of base simulation flow	Climate Scenario 3 (+10% P) (m^3/s)	fraction of base simulation flow	Climate Scenario 4 (+15% P) (m^3/s)	fraction of base simulation flow	Climate Scenario 5 (+20% P) (m^3/s)	fraction of base simulation flow
Dundalk	0.98	0.91	0.93	0.54	0.59	1.02	1.12	1.13	1.24	1.24	1.36	1.35	1.48
Marsville	8.06	8.80	1.09	6.56	0.75	9.84	1.12	10.91	1.24	11.98	1.36	13.05	1.48
Below Shand Dam	8.83	10.30	1.17	7.75	0.75	11.54	1.12	12.79	1.24	14.04	1.36	15.28	1.48
West Montrose	14.3	14.98	1.05	12.04	0.80	16.80	1.12	18.64	1.24	20.49	1.37	22.34	1.49
Galt	36.3	39.88	1.10	36.81	0.92	45.02	1.13	50.22	1.26	55.42	1.39	60.61	1.52
Brantford	57.2	57.53	1.01	57.48	1.00	64.99	1.13	72.56	1.26	80.15	1.39	87.72	1.52
	AVERAGES-->		**1.06**		**0.80**		**1.12**		**1.25**		**1.37**		**1.50**
Armstrong Mills	2.12	1.66	0.78	1.39	0.84	1.91	1.15	2.18	1.31	2.44	1.47	2.71	1.63
Below Guelph	5.67	5.86	1.03	5.03	0.86	6.67	1.14	7.48	1.28	8.29	1.41	9.10	1.55
Cambridge	7.84	7.03	0.90	5.99	0.85	8.05	1.15	9.07	1.29	10.09	1.44	11.11	1.58
	AVERAGES-->		**0.90**		**0.85**		**1.14**		**1.29**		**1.44**		**1.59**
Nithburg	4.27	3.88	0.91	3.39	0.87	4.34	1.12	4.81	1.24	5.29	1.36	5.76	1.48
New Hamburg	6.22	6.78	1.09	5.93	0.87	7.58	1.12	8.40	1.24	9.21	1.36	10.03	1.48
Canning	11.3	10.36	0.92	8.93	0.86	11.71	1.13	13.11	1.27	14.51	1.40	15.91	1.54
	AVERAGES-->		**0.97**		**0.87**		**1.12**		**1.25**		**1.37**		**1.50**
Above Drayton	3.66	3.11	0.85	2.68	0.86	3.51	1.13	3.93	1.26	4.34	1.40	4.74	1.52
Drayton	3.66	3.82	1.04	3.30	0.86	4.30	1.13	4.79	1.25	5.29	1.38	5.77	1.51
Glen Allan	6.98	6.67	0.96	5.84	0.88	7.44	1.12	8.24	1.24	9.04	1.36	9.83	1.47
St. Jacobs	8.81	9.35	1.06	8.22	0.88	10.41	1.11	11.50	1.23	12.59	1.35	13.67	1.46
	AVERAGES-->		**0.98**		**0.87**		**1.12**		**1.25**		**1.37**		**1.49**

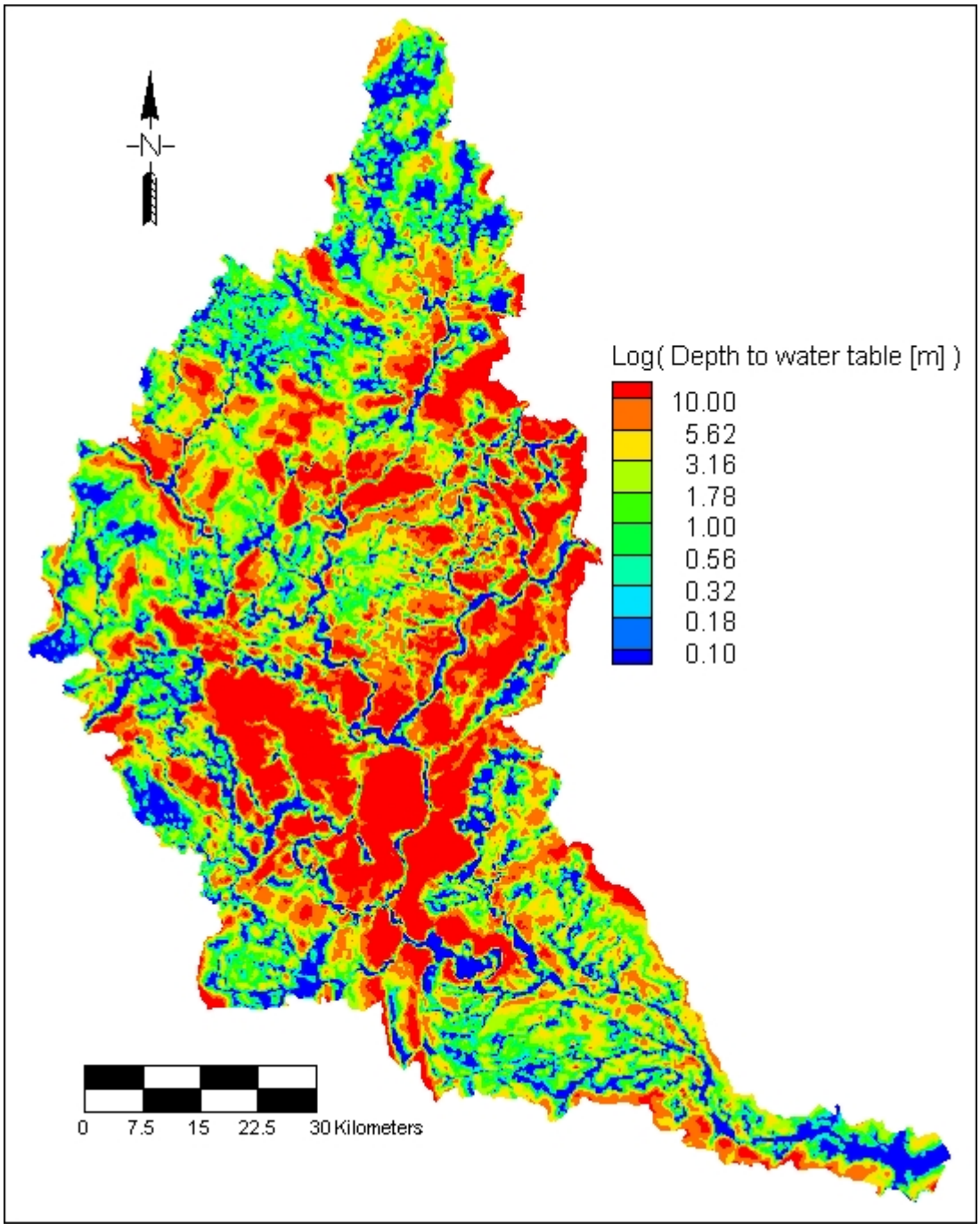

Figure 4.5: Simulated depth below ground surface to water table, Scenario 1

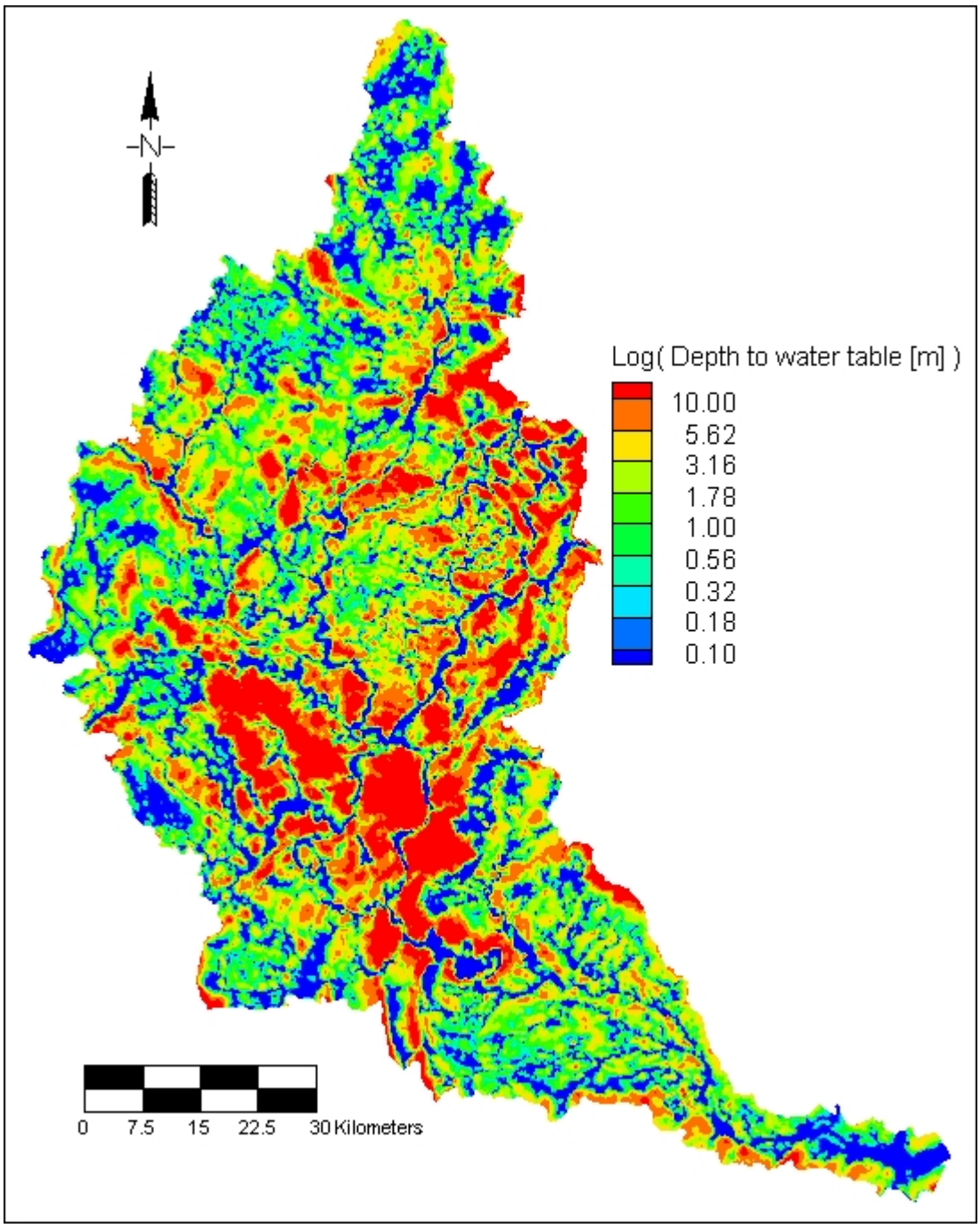

Figure 4.6: Simulated depth below ground surface to water table, Scenario 5

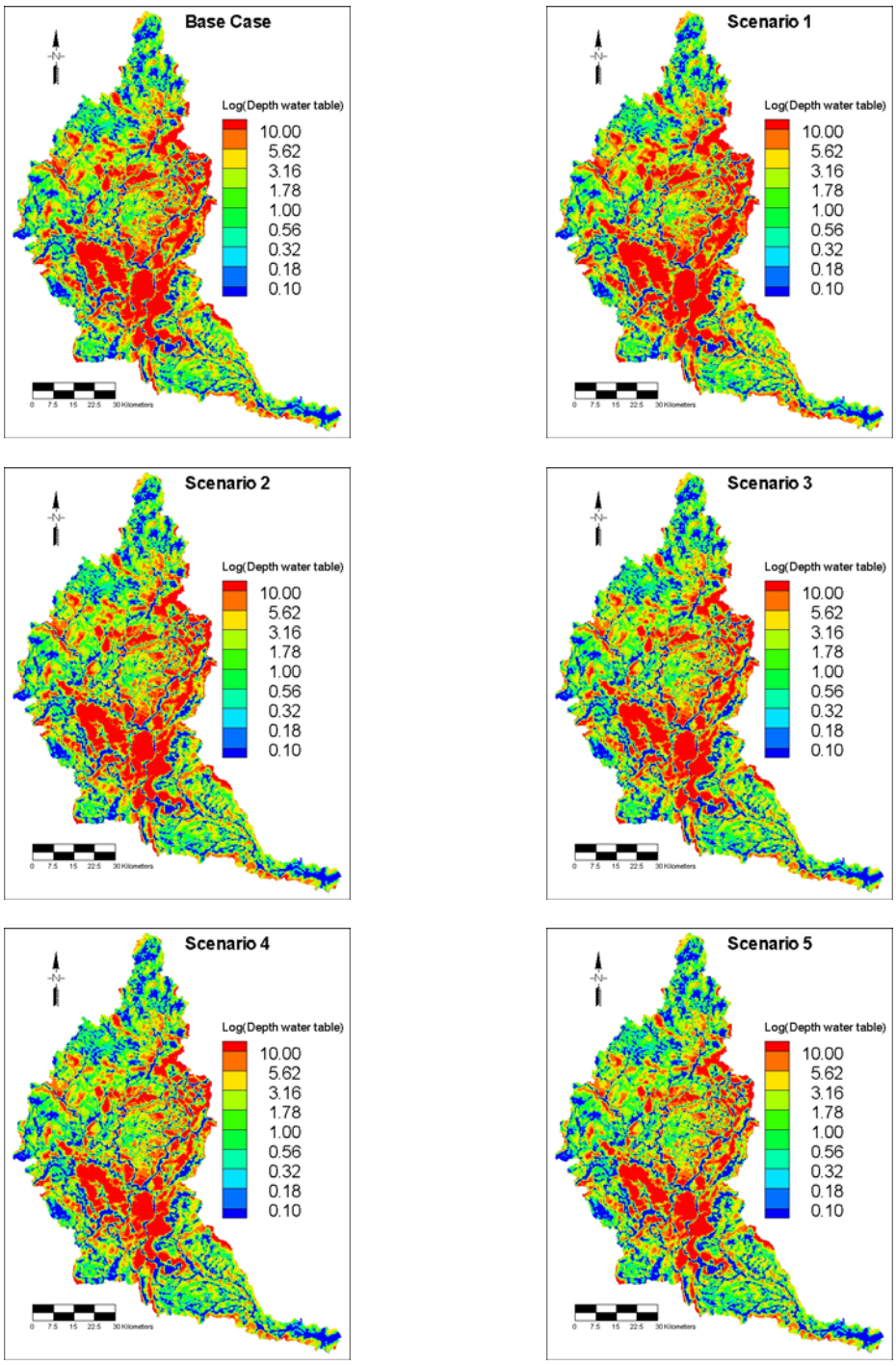

Figure 4.7: Simulated depth below ground surface to water table, base case and all climate scenarios

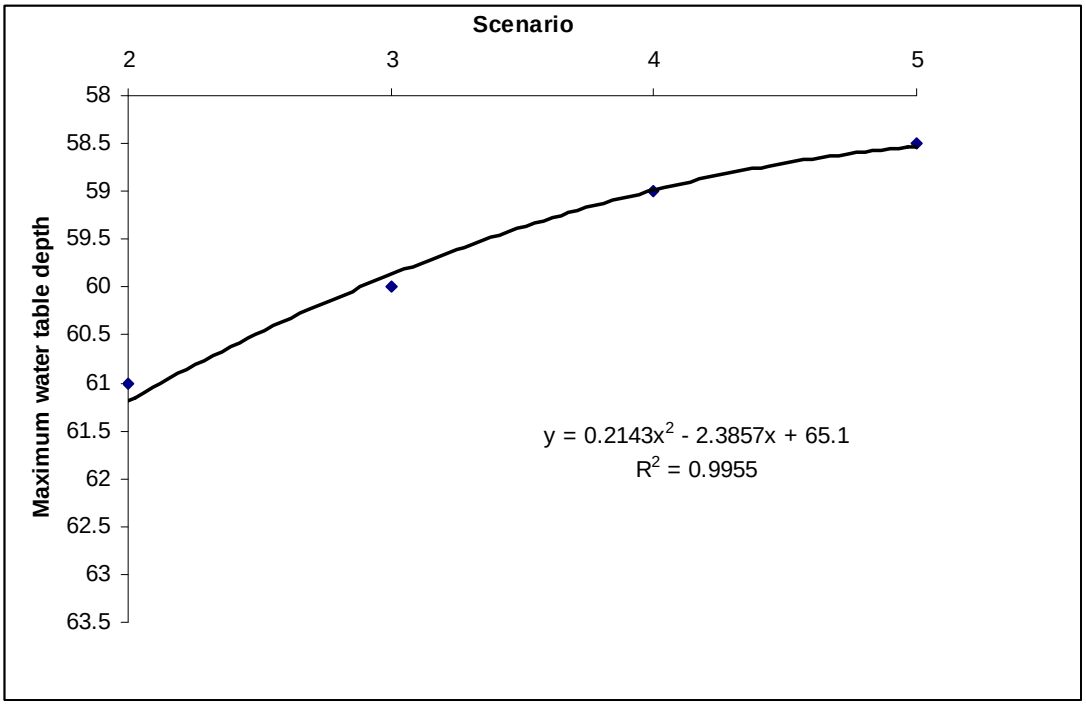

Figure 4.8: Climate change's effect on maximum water table depth.

Table 4.4: Change in nodally-averaged hydraulic head, relative to base climate case.

Simulation	Average hydraulic head change (m)	Head minimum (m)	Head maximum (m)
Base	-	172.59	527.57
Scenario 1	-0.55	172.50	527.30
Scenario 2	+0.41	172.66	527.76
Scenario 3	+0.94	172.72	527.92
Scenario 4	+1.02	172.78	528.04
Scenario 5	+1.25	172.83	528.15

Groundwater recharge (Table 4.6) responded to climate forcing linearly (r^2 = 0.99) among scenarios 2 to 5. Moreover, the magnitude of the decline or increase in

recharge changed in direct proportion to the change in precipitation. For example, recharge declined by about 5% relative to base case when precipitation was reduced

Table 4.5: Climate change-induced variation in exchange flux. Negative values indicate water removal from the surface domain.

Scenario	**Minimum Exchange Flux** (mm/year)	**Maximum Exchange Flux** (mm/year)
Base	-3564	6654
1	-3879	6496
2	-3311	6780
3	-2926	6875
4	-2942	6938
5	-2781	7001

by 5% (Scenario 1), and when precipitation was increased by 5%, recharge closely followed suit, in agreement with Nash and Gleick (1993), who also increased precipitation by 20% while holding all else constant. An implicit result of this is that evapotranspiration did not change from one scenario to the next, which contrasts with the findings of Jyrkama (2003), who found that evaporation under similar conditions (e.g., +20% precipitation) would cause evapotranspiration to increase by 12% (or about 61 mm/year) over forty years. Over the same time span, runoff was projected to increase by 12% (or less than 10 mm/year) and the average recharge rate by approximately 53% (100 mm/year) when comparing to the base case. This indicates that approximately 30 mm/year of the recharge increase would be utilized by processes other than evapotranspiration and runoff. Despite the present work's

lack of a forecast in increased evapotranspiration, its corresponding precipitation scenario (Scenario 5: +20%) predicts only a 21.5% (or 40 mm/year) increase in runoff over fifty years; an increase in evapotranspiration (see discussion just below) obviously would only lower this estimate.

Table 4.6: Climate change and average GRW groundwater recharge

Scenario	**Recharge** (mm/year)	**Change relative to base case** (mm/year)
Base	186	-
1	176.5	-9.5
2	198	12
3	207	21
4	216.5	30.5
5	226	40

4.3 Discussion

In terms of both input and output, the steady-state surface and subsurface GRW hydrological system was modelled such that it fell in line with the findings of other research (Jyrkama and Sykes, 2007; AquaResource, 2007) on said watershed. As expected, increasing the precipitation rate will generally increase all other hydrological rates, as there is more water available in the system to meet process demand. The hydrological response is predicted to be approximately linear with respect to the degree of climate change, and thus enables water managers to reasonably predict the outcomes of climate change beyond the bounds presented in the present work.

Focussing on the surface response to precipitation change, the expected increase in runoff should provide some comfort to water managers searching for ways to meet, for example, both the rising drinking water demands and the waste dilution needs of the burgeoning population. This is true even though seasonal variation was not taken into account, because managers have at their disposal numerous flow control structures with which to capture and store the extra flow predicted herein. For example, with 20% more precipitation, no single river tributary experienced less than a 49% increase in discharge. Thus, in any one year, one might expect a potential discharge increase of approximately half of the long-term average. Without flow control, such flow increases would make erosion control much more challenging, and fisheries managers might struggle to cope with the effects of increased sediment load, not to mention increased flow (flooding), on the watershed's freshwater fish and other biota. Increases in river discharge are expected to coincide also with intensification of discharging groundwater mainly into river corridors, where coldwater fish may benefit to the detriment of species less tolerant of the colder temperatures associated with discharging groundwater. A notable and negative biota-related consequence of the only "dry" scenario is that flow along the most upstream section of the Grand River could actually become ephemeral. Biota may have to cope also with subsurface effects of climate change. Vegetation, – especially wetland vegetation – may struggle to effectively adapt to the predicted falling (but more likely rising) water table, in turn affecting dependent animal

species. A lower water table also could mean less evapotranspiration from the GRW, because shallow-rooted plants may be less able to supply the atmosphere with transpired water. This was not seen herein, as only one slightly dry scenario was

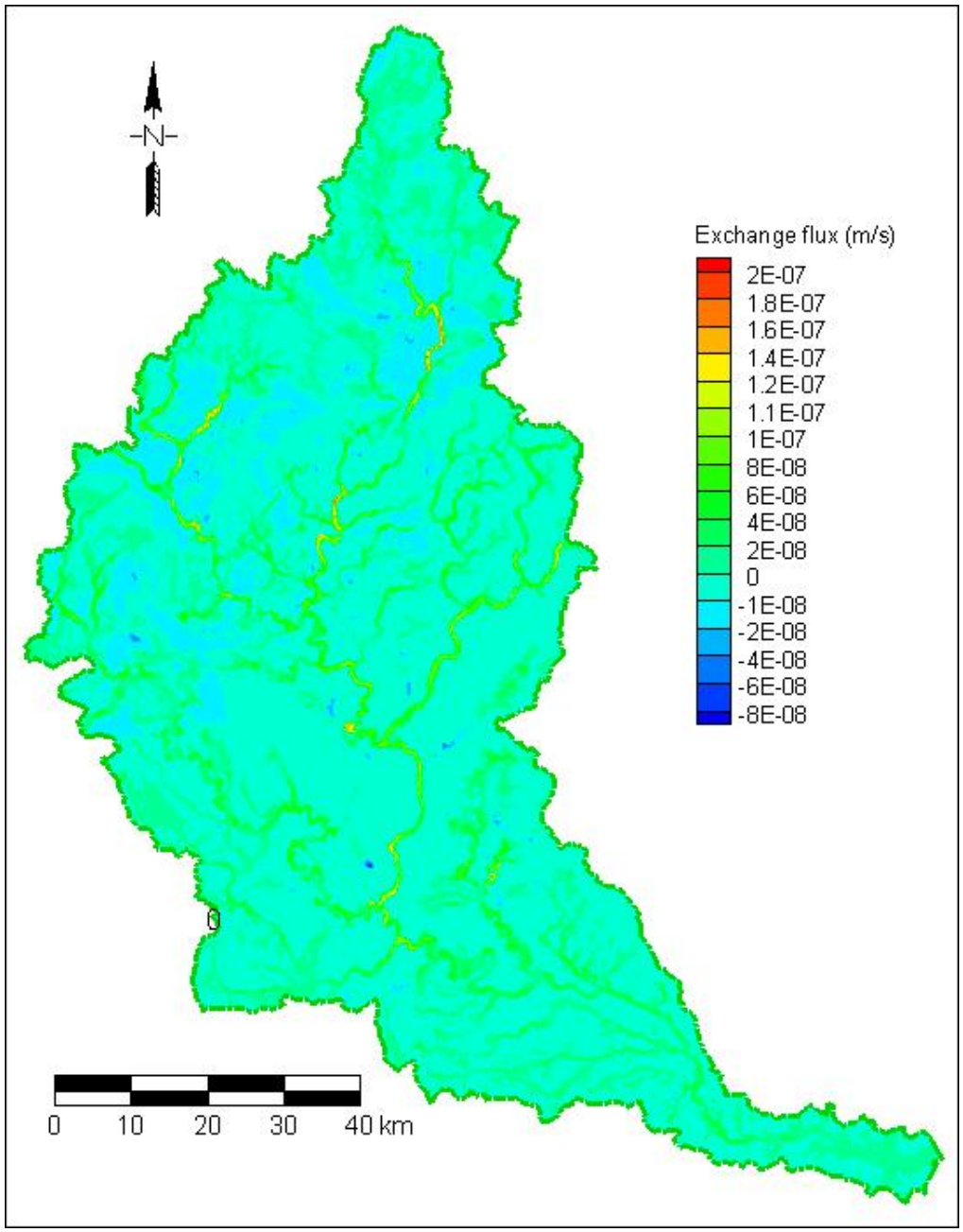

Figure 4.9: Exchange flux, scenario 1

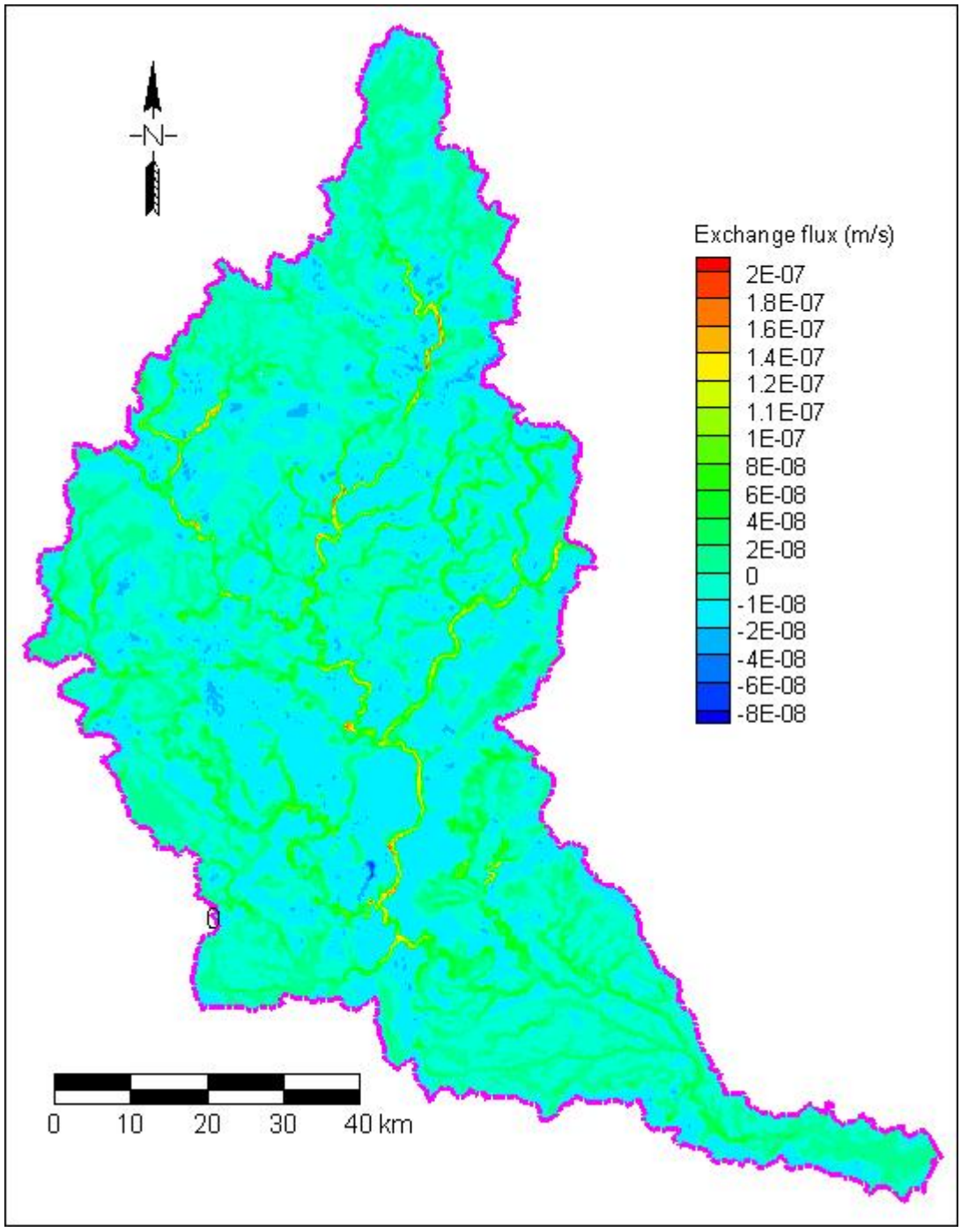

Figure 4.10: Exchange flux, scenario 5

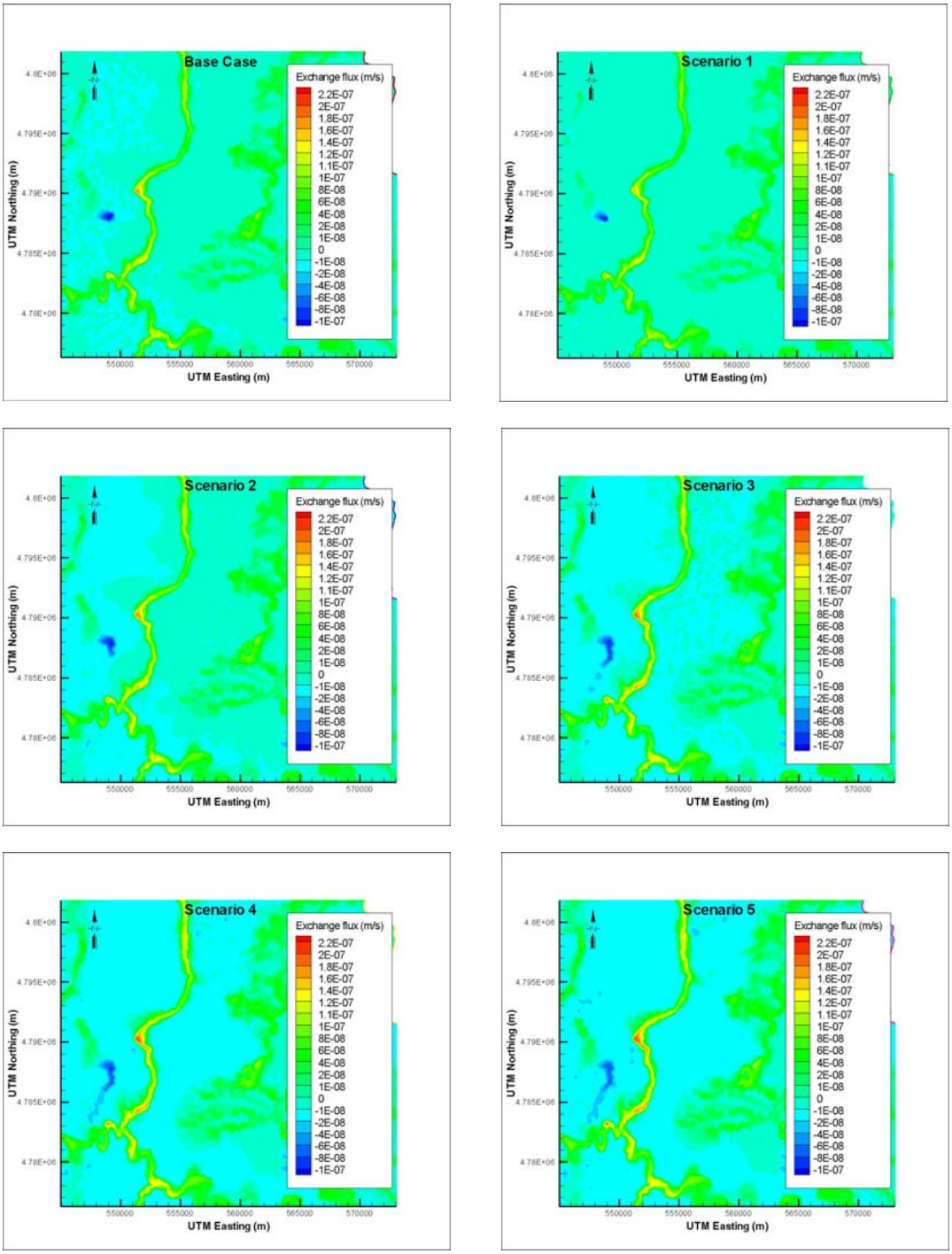

Figure 4.11: Expanded views of exchange fluxes, base case and all climate scenarios

examined.) Water table drops could affect the efficiency of anthropogenic groundwater extraction, too, though the maximum drop observed in the present work is unlikely to render any but the shallowest wells unusable. At the other extreme, while the greatest effects of climate change were expected near the water table, hydraulic head changed even at great depth, and this might have a slight impact on water pumping from the deeper aquifers.

The height of the water table, as well as stream baseflow supply, is affected by precipitation infiltrating the ground and recharging the groundwater system as it reaches the water table. Again, the approximately linear response with respect to precipitation should not only give managers some confidence to predict scenarios not simulated presently, but also provide them with guidance concerning the protection of recharge zones. That is, if groundwater can serve as an even greater water supply than presently is the case, it may be worthwhile to be even more wary of projects that limit the watershed's ability to replenish its groundwater.

Evapotranspiration was modelled such that it could increase, with increasing precipitation, only as a result of the water table moving upwards to the root zone and maximum evaporation depth. However, while the water table indeed moved upwards in Scenarios 2 to 5, actual evapotranspiration fully met potential evapotranspiration, no doubt due to the system constantly receiving precipitation and thus constantly having all surfaces (e.g., vegetation) coated with water. That is, it was found that much of the water budget's evapotranspirative loss is via surface

water, meaning that the present work cannot be used to predict future evapotranspiration trends without first altering potential ET, and/or running transient simulations which would allow the system's surfaces to be "dry" more often than not. The inclusion of scenarios involving temperature change very likely would have shown, by way of potential ET change, evapotranspiration increases and thus would have provided valuable information, as in Jyrkama (2003). Although a consistent prediction of climate models is that global warming will increase total evaporation, due to increases in surface temperature and higher wind speeds promoting greater potential evaporation, the greatest change will likely result from an increase in the water-holding capacity of the atmosphere (IPCC, 2001). While potential evaporation will almost certainly increase with temperature, the former's increase may be muted by the moderating influence of large water bodies, such as the Great Lakes to the west of the GRW. Evaporation, occurring over these bodies and increased due to longer ice-free times, may decrease the atmosphere's water holding capacity (i.e., the potential evaporation) in the study area. Adding to the uncertainty regarding future evapotranspiration, Eckhardt and Ulbrich (1998) showed that changes to the physiological response of plants can both intensify and lessen evapotranspiration processes. The limited understanding of some of the many land-based and atmospheric balances and counter-balances will continue to make it difficult for modellers to choose from among the myriad resulting climate change scenarios.

Predicted changes in land use may serve to counter many of the outcomes presented here. Predicted groundwater recharge increases, for example, may be offset by increased groundwater pumping and by land use changes that result from urban expansion. Similarly on the surface, increased water demand may translate into increased water takings from the predicted higher rivers, potentially resulting in no net change in the surface water balance.

Chapter 5: Summary and Conclusions

Understanding the impact of potential changes in the hydrologic cycle due to climate change is essential for ensuring the quality and sustainability of water resources in the future. While steady-state results based on long-term meteorology do not enable the detailed prediction of acute watershed hydrological regimes, they do elucidate general trends that should be of use to water managers. In general, because groundwater systems respond at relatively slow rates, particularly at the watershed scale, a steady-state approximation is reasonable and provides a general understanding, while also providing reasonable initial conditions for the next generation of climate change-related modelling, as well as general watershed modelling. The provision of initial conditions for the Grand River Watershed is especially valuable, given its size and complexity.

Surface and subsurface results indicate that the modelling effort provided a realistic representation of the long-term surface and groundwater flow system at a regional scale. The hydrological change expected based in part on similar studies *via* climate forcing was reproduced in the present work, mainly because of the successful model calibration. General trends in these forced changes in most cases allow predictions to be made regarding the effects of even more extreme climate forcing not included here. This study should provide valuable results for any future "vulnerability, impacts and adaptation" assessment focussing on climate change and hydrology in the GRW catchment, and perhaps provide a more general understanding

so that other catchments might be better understood in the context of climate change (Barrow *et al*., 2004). It should additionally allow for further, more complex comparison to the FEFLOW-GAWSER approach, to the HELP3 approach of Jyrkama (2003), and to any physically or non-physically robust and/or coupled surface water-groundwater model. This increase in complexity will be manageable *via* increasing computing capability combined with more detailed data to refine the models presented here. Gradually, the limitations of the present study (e.g., omission of regional flow groundwater boundaries and of explicitly defined smaller streams) will be eliminated. More direct linkage to other models (e.g., GCMs) with feedback incorporated may then provide a much larger scale of hydrological understanding. Conversely, improvements such as mesh refinement should make it easier to focus calibration and prediction capabilities in even the most localized portions of the watershed. However, the limiting factor of the fully-integrated approach is that it requires a very fine discretization of spatial and often temporal domains, to some extent limiting this robust numerical approach to the simulation of small catchments for relatively short durations (Bouwers, 2007). Until the necessary computing power and/or code efficiency (e.g., parallelization) becomes available, a reasonable approach appears to be a compromise and combination of a very refined mesh and somewhat non-physically based, yet coupled modelling.

References

Alcamo, J., P. Döll, T. Henrichs, F. Kaspar, B. Lehner, T. Rösch, and S. Siebert. 2003. Global estimates of water withdrawals and availability under current and future "business-as-usual" conditions, Hydrol. Sci. J., 48, 339-348.

Anderson, J.R., E.E. Hardy, J.T. Roach, and R.E. Witmer. 1976. "A Land Use and Land Cover Classification System for Use with Remote Sensor Data." Geological Survey Professional Paper 964. United States Printing Office, Washington, 36 pp.

AquaResource Inc. 2007. "Integrated Water Budget Report - Grand River Watershed". Prepared for the Grand River Conservation Authority, Ontario. 200 pp.

Arnell, N.W. and N.S. Reynard. 1996. The effects of climate change due to global warming on river flows in Great Britain. J. Hydrol., 183(3-4):397-424.

Arnell, N.W. 2003. Effects of IPCC SRES* emissions scenarios on river runoff: a global perspective. Hydrology and Earth System Sciences 7(5): 619-641.

Barrow E., B. Maxwell, and P. Gachon (eds.), (2004): Climate Variability and Change in Canada: Past, Present and Future, ACSD Science Assessment Series No. 2, Meteorological Service of Canada, Environment Canada, Toronto, Ontario, 114 pp.

Bolger, B.L. 2009. Simulating the Predevelopment Hydrologic Condition of the San Joaquin Valley, California. Ph.D. Thesis, Department of Earth Science, University of Waterloo, Waterloo, Ontario, Canada.

Bouwer, H. and R.C. Rice, 1983. Effect of stones on hydraulic properties of vadose zones. In Proceedings of the Characterization and Monitoring of the Vadose (Unsaturated) Zone, National Water Well Association, Worthington, Ohio.

Boyd, D., S. Cooke, and W. Yerex. 2009. "Exploring Grand-Erie Connections: Flow, Quality and Ecology". 9th Annual Grand River Watershed Water Forum.

Brouwers, M.H. 2007. "A Case Study for Assessing the Hydrologic Impacts of Climate Change at the Watershed Scale". M.Sc. Thesis, University of Waterloo, Ontario, 121pp.

Carsel, R.F. and R.S. Parrish. 1988. Developing Joint Probability Distributions for Soil Water Retention Characteristics. Water Resources Research 24: 755-769.

Canadell, J., R.B. Jackson, J.R. Ehleringer, H.A. Mooney, O.E. Sala, E.-D. Schulze. 1996. Maximum rooting depth of vegetation types at the global scale. Oecologia 108: 583–595.

Chen, Z., S.E. Grasby, and K.G. Osadetz. 2004. "Relation between Climate Variability and Groundwater Levels in the Upper Carbonate Aquifer, Southern Manitoba, Canada." Journal of Hydrology 290(1-2): 43-62.

Davies, J.A. 1972. Actual, potential and equilibrium evaporation for a beanfield in southern Ontario. Agricultural Meteorology 10:331-348. doi:10.1016/0002-1571(72)90036-2

Diersch, H.-J.G. 2002. WASY Software FEFLOW-Reference Manual. WASY Ltd., Berlin, 78pp.

Doherty, J. 2001. PEST-ASP Users' manual. Watermark Numerical Computing, Brisbane, Australia.

Downer, C.W. and F.L. Ogden. 2004. Appropriate vertical discretization of Richards' equation for two-dimensional watershed-scale modelling. Hydrological Processes 18: 1-22.

Eckhardt K. and U. Ulbrich. 2003. Potential Impacts of Climate Change on Groundwater Recharge and Streamflow in a Central European Low Mountain Range. Journal of Hydrology 284(1-4): 244-252.

Engman, E. T., 1986, Roughness coefficients for routing surface runoff. J. of Irrig. and Drain. Eng., 112(1): 39-53.

Fagherazzi, L., D. Fay, and J. Salas. 2007. "Synthetic hydrology and climate change scenarios to improve multi-purpose complex water resource systems management". Found in "Water Resources Management IV". Brebbia, C.A. and A. Kungolos, Eds., WIT Press, Southampton, U.K., 720pp.

Gellens, D and E. Roulin. 1998. Streamflow response of Belgian catchments to IPCC climate change scenarios. Journal of Hydrology 210(1-4): 242-258.

Goderniaux, P., S. Brouyère, H.J. Fowler, S. Blenkinsop, R. Therrien, P. Orban, and A. Dassargues. 2009. Large scale surface-subsurface hydrological model to

assess climate change impacts on groundwater reserves. Journal of Hydrology 373 (1-2): 122-138.

Graham, J.E. and W.D. Banks. 2004. "Grand River Watershed Geological and Hydrogeological Model Project". Waterloo Hydrogeologic, Inc.

Grand River Conservation Authority (GRCA). 2000. http://www.grandriver.ca. 400 Clyde Road, PO Box 729, Cambridge, Ontario, Canada, N1R 5W6.

Holysh, S., J. Pitcher, and D. Boyd. 2001. "Grand River Regional Groundwater Study Technical Report". Grand River Conservation Authority, Ontario.

Howard, K.W.F. and A. Griffith. 2009. Using transient models to confront the impacts of climate change on groundwater reserves in sub-Saharan Africa. Hydrol. Sci. J. 54(4).

IPCC (Intergovernmental Panel on Climate Change). 2000. In: Nakicenovic, N. and R. Swart (Eds.), Special Report on Emissions Scenarios. Cambridge University Press, Cambridge, United Kingdom.

IPCC. 2001. In: McCarthy, J.J., O.F. Canziani, N.A. Leary, D.J. Dokken, and K.S. White (Eds.), "Climate Change 2001: Impacts, Adaptation, and Vulnerability". Cambridge University Press, Cambridge, United Kingdom.

IPCC. 2007. "Climate Change 2007: Impacts, Adaptation and Vulnerability". Contribution of Working Group II to the Fourth Assessment Report of the Intergovernmental Panel on Climate Change. Parry, M.L., O.F. Canziani, J.P. Palutikof, P.J. van der Linden, and C.E. Hanson, Eds., Cambridge University Press, Cambridge, UK, 976 pp.

Jha, M., Z. Pan, E. S. Takle, and R. Gu. 2004. Impacts of climate change on streamflow in the Upper Mississippi River Basin: A regional climate model perspective. Journal of Geophysical Research 109: D09105.

Jones, J.P. 2005. "Simulating hydrologic systems using a physically-based, surface-subsurface model : issues concerning flow, transport and parameterization". Ph.D. Thesis, Department of Earth Science, University of Waterloo, Waterloo, Ontario, Canada.

Jones, R.N., F.H.S. Chiew, W.C. Boughton, and L. Zhang. 2006. Estimating the sensitivity of mean annual runoff to climate change using selected hydrological models. Advances in Water Resources 29 (10): 1419-1429.

Jyrkama M.I. 2003. “A Methodology for Estimating Groundwater Recharge”. Ph.D. Thesis, Department of Civil Engineering, University of Waterloo, Waterloo, Ontario, Canada.

Jyrkama M.I. and J.F. Sykes. 2007. The Impact of Climate Change on Spatially Varying Groundwater Recharge in the Grand River Watershed (Ontario). Journal of Hydrology 338: 237-250.

Kundzewicz, Z.W., L.J. Mata., N. Arnell, P. Döll, B. Jiménez, K. Miller, T. Oki, Z. Şen, and I. Shiklomanov. 2008. The implications of projected climate change for freshwater resources and their management. Hydrol. Sci. J. 53(1), 3–10.

Li, Q., A.J.A. Unger, E.A. Sudicky, D. Kassenaar, E.J. Wexler, S. Shikaze. 2008. Simulating the multi-seasonal response of a large-scale watershed with a 3D physically-based hydrologic model. Journal of Hydrology 357 (3–4): 317–336.

Loáiciga, H.A., J.B. Valdes, R. Vogel, J. Garvey, and H. Schwarz. 1996. Global warming and the hydrologic cycle. Journal of Hydrology, 174 (1-2): 83-127.

Loáiciga, H.A. 2003. Climate Change and Groundwater. Annals of the Association of American Geographers 93(1): 30-41.

Mace, A., D.L. Rudolph, and R.G. Kachanoski. 1998. Suitability of Parametric Models to Describe the Hydraulic Properties of an Unsaturated Coarse Sand and Gravel. Ground Water v36(3): 465-475.

McLaren, R. 2008. GRID BUILDER – A pre-processor for 2-D, triangular element, finite-element programs. Groundwater Simulations Group, University of Waterloo, Waterloo, Ontario.

Mearns, L.O., F. Giorgi, P. Whetton, D. Pabon, M. Hulme, and M. Lal. 2003. “Guidelines for use of climate scenarios developed from Regional Climate Model experiments”. Data Distribution Centre of the International Panel of Climate Change, 38 pp.

Mercer, J.W., S.D. Thomas, and B. Ross. 1982. Parameters and Variables Appearing in Repository Siting Models. Division of Waste Management, Office of Nuclear Material Safety and Safeguards, U.S. Nuclear Regulatory Commission. Washington, D.C.

Metcalfe, J.R., B. Routledge, and K. Devine. 1996. Rainfall Measurement in Canada: Changing Observational Methods and Archive Adjustment Procedures. Journal of Climate 10(1): 92–101. DOI: 10.1175/1520 0442(1997)010<0092:RMICCO>2.0.CO;2

Milly, P.C.D., K.A. Dunne, and A.V. Vecchia. 2005. Global pattern of trends in streamflow and water availability in a changing climate. Nature 438 (7066): 347-350.

Minville, M., F. Brissette, and R. Leconte. 2008. Uncertainty of the impact of climate change on the hydrology of a nordic watershed. Journal of Hydrology 358: 70-83.

Nash, L. and P. Gleick. 1993. The Colorado River Basin and Climatic Change: The Sensitivity of Streamflow and Water Supply to Variations in Temperature and Precipitation. U.S. Environmental Protection Agency, EPA230-R-93-009, Washington, D.C. 121 pp.

Nyenje, P. M. and O. Batelaan. 2009. Estimating effects of climate change on groundwater recharge and base flow in the upper Ssezibwa catchment, Uganda. Hydrol. Sci. J. 54(4).

Ontario Ministry of Natural Resources (1984). Water Quantity Resources of Ontario. Toronto. Queen's Printers for Ontario.

Panday,S. and Huyakorn, P.S. 2004. A fully coupled physically-based spatially-distributed model for evaluating surface/subsurface flow. Advances in Water Resources, 27: 361-382.

Partington, D., A.D. Werner, P. Brunner, C.T. Simmons, G.C. Dandy, and H.R. Maier. 2009. Using a fully coupled surface water - groundwater model to quantify streamflow components. 18th World IMACS / MODSIM Congress, Cairns, Australia 13-17 July, 2009.

Schroeder P.R., T.S. Dozier, P.A. Zappi, B.M. McEnroe, J.W. Sjostrom, and R.L. Peyton. 1994b. "The Hydrologic Evaluation of Landfill Performance (HELP) Model: Engineering Documentation for Version 3. EPA/600/R-94/168b, U.S. Environmental Protection Agency Office of Research and Development, Washington.

Schroeter, H. 1989. GAWSER Training Guide and Reference Manual. School of Engineering, University of Guelph, Ontario, Canada.

Scibek J. and D.M. Allen. 2006. Modeled impacts of predicted climate change on recharge and groundwater levels. Water Resources Research 42 (11), art. No. W11405, doi:10.1029/2005WR004742.

Scurlock, J.M.O., G.P. Asner, and S.T. Gower. 2001. Worldwide Historical Estimates of Leaf Area Index, 1932-2000, prepared for the Oak Ridge National Laboratory, Oak Ridge, Tennessee. ORNL/TM-2001/268.

Singer, S.N. 1997. "Summaries of Geologic and Hydrogeologic Studies Containing Information Relevant to the Grand River Basin". Ontario.

Sousounis P.J. and E.K. Grover. 2002. Potential Future Weather Patterns over the Great Lakes Region. Journal of Great Lakes Research 28(4): 496-520.

Sudicky, E.A., J.P. Jones, Y.-J. Park, A.E. Brookfield, and D. Colautti. 2008. Simulating complex flow and transport dynamics in an integrated surface-subsurface modelling framework, Geosciences Journal, 12(2), 16 pp.

Therrien, R., R.G. McLaren, E.A. Sudicky, and S.M. Panday. 2007. HydroGeoSphere: a three-dimensional numerical model describing fully-integrated subsurface and surface flow and solute transport, Groundwater Simulations Group, University of Waterloo, Waterloo, Ontario, Canada, 360 pp.

van Genuchten, M.Th., F.J. Leij, and L.J. Lund., Eds. 1989. Indirect Methods for Estimating the Hydraulic Properties of Unsaturated Soils. Proceedings of the International Workshop on Indirect Methods for Estimating the Hydraulic Properties of Unsaturated Soils. University of California, Riverside, California.

von Storch, H., E. Zorita, and U. Cubasch. 1993. Downscaling of global climate change estimates to regional scales: An application to Iberian rainfall in wintertime. J. Climate 6: 1161-1171.

Zhang X., L.A. Vincent, W.D. Hogg, and A. Niitsoo. 2000. Temperature and Precipitation Trends in Canada During the 20th Century. Atmosphere-Ocean 38(3): 395-429.

Appendix A: Pumping well locations and pumping rates

UTM Easting	UTM Northing	Pumping Rate (L/day)
557299	4802613	2462400
557332	4802671	2462400
557283	4802706	2462400
557312	4802757	2462400
528456	4800028	144000
528560	4800075	118080
559660	4795343	65000
559678	4795373	65000
538429	4812255	4546000
555060	4859714	393000
523373	4822056	576000
523373	4822139	576000
531210	4819179	687384
531200	4819129	687384
524445	4807493	144000
524533	4807508	144000
562968	4822422	12960
555995	4806225	196650
556235	4792616	209000
556259	4792611	262000
563705	4798651	20410
563728	4798440	20410
563624	4798256	20410
563832	4798267	20410
538818	4805693	5271000
524277	4807753	194400
539488	4821131	393120
539516	4821145	393120
560431	4798971	2618000
560391	4798971	524000
575409	4789660	164000
549952	4784823	617143
570846	4760082	981936
538911	4810431	2291184
537670	4812254	72000
537701	4812271	72000
556365	4805063	2160000
558375	4804749	3283200

UTM Easting	UTM Northing	Pumping Rate (L/day)
557325	4804292	3268800
557836	4822990	15000
557917	4822988	299000
557585	4792061	51000
523188	4801569	3543000
537923	4800213	982800
549409	4838788	34000
549436	4838776	34000
549546	4838999	34000
554943	4838900	34000
549370	4838819	7000
549434	4838931	7000
557140	4806113	5184000
557128	4806110	5184000
555245	4799693	24000000
544383	4813559	1015200
544534	4813823	1015200
544485	4813802	1015200
558989	4799533	2291229
551115	4838278	1963911
539490	4810810	2128000
544524	4807050	4550000
541552	4813578	2291184
532950	4809489	9092000
532941	4809593	10473984
535307	4812505	3142200
537492	4803557	9092000
532534	4809830	5564000
538887	4812296	5246000
538806	4805716	6819000
522504	4805921	131000
529885	4809192	272760
529588	4809465	272760
506873	4823367	554612
522240	4802232	1081948
552386	4785942	2618496
548413	4890190	1181960
544033	4804487	4582000

Appendix A (continued)

UTM Easting	UTM Northing	Pumping Rate (L/day)
506628	4824064	1425600
538773	4812233	5236992
547169	4812065	9164736
546753	4812386	1136500
546835	4812176	1136500
549454	4820234	157110
549457	4820230	3700000
548902	4810685	3700000
549044	4810856	3700000
538545	4818192	81828
557572	4825924	294580
538787	4812245	3273120
522313	4825864	523699
522397	4825906	523699
555860	4806624	1636560
545076	4806748	539220
550217	4807980	1960000
555204	4798117	6547000
550887	4765789	720000
541521	4808278	3273185
570737	4786861	327312
540359	4816066	368500
535506	4823860	6546240
550603	4839932	409140
518481	4813788	1503000
518773	4813453	1503300
527988	4819395	885600
527962	4819437	885600
546065	4836321	1136500
540670	4807663	418405
539724	4810627	21275284
540837	4821487	310667
540829	4821478	310667
540782	4821527	310667
557400	4801615	364870
544002	4803857	2289600
522188	4825500	720286
522528	4825874	916474
542225	4826091	237600

UTM Easting	UTM Northing	Pumping Rate (L/day)
548169	4773753	109500
558112	4859697	458000
530291	4794530	1145000
530308	4794513	1145000
526188	4856503	44640
557749	4797831	321120
557284	4859752	196000
551033	4844501	195840
555091	4859714	654000
557275	4770962	123000
544173	4774858	102285
537461	4837989	1690908
537491	4837967	1690908
537484	4838121	1690908
537435	4838042	1690908
537499	4838084	1690908
537548	4838114	1690908
558458	4808933	490968
562971	4822422	23040
562971	4822424	12960
562963	4822429	10080
557025	4823001	328000
529250	4827800	265000
560771	4820357	3400000
560399	4823213	10300000
561615	4819162	3300000
559925	4823346	3100000
558194	4819722	3200000
560986	4819785	2300000
538362	4817291	371000
540585	4810399	71000
557700	4835799	589000
570784	4815980	60000
562210	4852957	182000
559836	4811222	548000
560055	4810875	122000
537687	4806011	3458000
537714	4806040	4320000
537573	4806489	4320000

Appendix A (continued)

UTM Easting	UTM Northing	Pumping Rate (L/day)
548102	4806061	82100
558406	4826477	916000
542837	4774099	216000
548934	4801969	1620300
548964	4801644	1620300
548940	4801662	1620300
528414	4809122	1227000
549884	4791652	58250
568756	4829813	982500
568756	4829810	982500
566388	4816161	656000
566318	4816054	130000
566425	4815893	65000
547142	4835875	1963000
527515	4790696	163656
527509	4790718	120120
534859	4810217	184500
562403	4822865	110000
534677	4793524	207000
534564	4793458	207000
557809	4823006	15000
551512	4843819	30000
543958	4834940	1637000
553771	4812203	655000
553898	4812349	1637000
565174	4820242	882000
539080	4814310	333000
569534	4814390	132000
569499	4814701	323000
569537	4814528	185000
560340	4825750	3273000
567950	4822200	3273000
554813	4770994	1145000
554813	4770994	1145000
535684	4794136	264000
535684	4794136	264000
535714	4794134	318000
535714	4794134	318000
530453	4822212	826200
553900	4775032	2290000

UTM Easting	UTM Northing	Pumping Rate (L/day)
549235	4813543	181500
549159	4813543	181500
549103	4813513	181500
552979	4847310	136950
552769	4847410	136950
553123	4847275	136950
536181	4826521	1310000
536181	4826521	1310000
567598	4812203	114600
567476	4812030	515600
567808	4811999	802000
540792	4814806	150000
557972	4781203	1278000
535656	4826289	1962000
567996	4822441	6547000
568384	4847833	1113000
568935	4812721	3600000
565010	4818350	6546000
568231	4822980	6546000
525205	4804343	420000
559967	4818962	13750000
552838	4851283	523000
522721	4851267	872000
550061	4840788	1963911
537467	4816423	1636560
535853	4787331	615000
551856	4839132	1963872
534025	4828530	1407500
533395	4778824	1310400
533420	4778827	1310400
533389	4778888	1310400
551270	4799187	523000
551402	4799113	656000
554681	4820016	5237000
538499	4852043	1130500
538494	4852048	1130500
550121	4784706	1636560
550138	4784666	1636560
561749	4817173	5237000
550113	4784788	1669000

Appendix A (continued)

UTM Easting	UTM Northing	Pumping Rate (L/day)
526940	4844707	1963872
530535	4822038	68190
530572	4820871	523000
530480	4821000	3282000
530453	4822212	136380
558681	4816893	654623
565102	4821177	7856000
567991	4822718	6546000
569900	4779324	65712
550393	4839498	1832947
549217	4841523	1963872
560265	4819845	6050000
565004	4819478	540000
555140	4860586	1145000
555130	4860582	1308000
545764	4837476	1136500
562351	4828140	1907640
569203	4814403	392774
547335	4809929	654637
547420	4810066	654637
543790	4793376	1044200
543790	4793376	1044200
547973	4812619	11000
547889	4812595	11000
547993	4812609	11000
547882	4812614	410000
552679	4846312	1178320
513195	4824105	327600
513202	4824177	163200
535853	4787331	360000
536897	4787372	336960
550471	4772335	1146000
547153	4770544	3816000
548170	4770886	818500
547535	4769093	704000
547535	4769093	704000
547535	4769093	704000
547535	4769093	704000
547230	4770180	3928000
551304	4764355	130925

UTM Easting	UTM Northing	Pumping Rate (L/day)
551360	4764282	130925
533014	4777874	196000
533059	4777871	524000
533078	4777889	131000
542256	4800883	164000
553904	4765563	1363000
549291	4771186	5236992
538262	4777496	278400
543628	4772241	409140
543819	4773665	2620000
547360	4776021	1309300
563010	4820588	175000
563036	4821307	252000
563398	4821157	110000
557537	4767409	383000
546278	4769498	261850
546190	4769481	261850
545894	4769408	261850
545868	4769436	261850
554664	4762966	654525
554664	4762966	654525
558059	4786055	100000
581686	4780055	164000
581642	4780071	818500
582132	4780057	818500
548754	4815632	164000
548769	4815586	164000
567174	4837007	327312
566898	4836647	327312
550603	4765259	982000
550582	4765234	1227000
562478	4820358	737000
562551	4820377	525000
561928	4819232	1309000
544667	4777255	556000
555452	4767523	1178323
545446	4771840	982000
563447	4822456	65000
553900	4769009	212753
553927	4769108	212753

Appendix A (continued)

UTM Easting	UTM Northing	Pumping Rate (L/day)
546832	4770289	3272000
548436	4775248	851000
536887	4813553	259200
556651	4804577	126000
556519	4762870	409140
547033	4769638	2273
551316	4808472	818280
552053	4812678	2160000
547553	4769124	649000
552165	4775780	2589120
551224	4773909	2589000
549631	4773202	68190
549631	4773202	68190
549631	4773202	68190
549631	4773202	68190
549631	4773202	68190
549631	4773202	68190
549631	4773202	68190
549631	4773202	68190
566033	4845329	654000
537113	4795456	186480
537057	4794542	186480
537052	4794562	186480
537031	4794549	186480
537010	4794632	186480
536960	4794520	186480
537182	4794563	186480
559242	4792452	65462
559246	4792542	327312
557026	4804566	819000
548334	4800724	404920
576560	4829760	653800
576517	4829590	653800
588721	4754158	195840
568312	4816988	657000
558978	4786247	64800
531366	4806544	2619000
531366	4806475	47000
535805	4802225	82000
549441	4817845	126060

UTM Easting	UTM Northing	Pumping Rate (L/day)
549354	4817908	299970
550951	4784324	409000
550654	4784077	409000
560679	4809412	195482
560640	4809381	263673
560725	4809296	272765
560725	4809289	272765
560648	4809366	209120
560679	4809389	100014
532856	4805847	266400
566513	4799640	1309000
532087	4786336	130925
555074	4872470	1152000
557245	4777150	200000
545928	4798234	17500
545986	4798456	37500
566329	4798568	12231
566663	4799588	12231
566282	4798695	12231
566430	4799551	12231
566615	4800491	12231
566267	4799226	12231
567068	4798709	12231
566663	4800168	12231
566391	4798791	12231
566406	4798945	12231
567448	4799583	12231
566183	4799256	12231
566918	4798887	12231
548198	4774298	144000
536850	4813250	674000
551000	4807300	49000
551100	4807300	49000
551300	4807300	117000
551300	4807400	117000
550900	4807800	117000
551400	4807300	117000
551100	4807800	13000
534860	4802900	272000
552457	4779301	691000

Appendix A (continued)

UTM Easting	UTM Northing	Pumping Rate (L/day)
552220	4779189	492500
551093	4800879	200000
551093	4800879	1000
547590	4798226	3000
564140	4815443	552900
539175	4810390	2619000
545061	4806746	539220
545076	4806746	539220
571022	4812087	110000
537463	4800378	419580
540346	4816059	368500
517813	4813877	52500
517855	4813854	52500
557427	4815114	79200
570188	4811581	250000
569847	4811446	200000
547976	4800065	89000
547738	4799810	150000
543788	4797428	47000
543683	4797421	81000
555293	4778358	9002
549872	4801566	115000
554500	4780500	687600
554501	4780501	655200
558858	4823140	1635000
558098	4775775	392774
569462	4812611	72800
550764	4782665	388800
585689	4770498	6546240
585713	4770494	1636560
550238	4841057	92160
560466	4788078	490968
560466	4788078	490968
560000	4823000	136800
540818	4808768	164000
563512	4821997	816000
567192	4858827	229118
567364	4859360	78600
551467	4783891	164000
555310	4799583	14400

UTM Easting	UTM Northing	Pumping Rate (L/day)
555345	4799590	7200
563024	4821986	3600
563000	4821986	3600
536314	4826693	389000
535066	4809215	638333
535062	4809181	638333
535182	4809237	638333
535126	4809310	638333
534997	4809009	638333
535169	4809202	638333
536240	4826594	328000
540680	4811303	2074
540719	4811320	2074
540718	4811262	15552
540723	4811239	15552
540719	4811234	34560
540704	4811300	32832
540730	4811269	2074
535339	4825062	4540000
535347	4825062	1934100
567410	4791650	202000
561092	4820909	11520
561018	4820862	11520
560985	4820923	11520
560982	4820975	11520
557049	4801038	14400
557183	4801047	72000
557018	4801061	14400
535399	4825774	1962000
534911	4809434	689114
534949	4809129	689114
535439	4808712	689114
535035	4809241	689114
535065	4809198	689114
534881	4809094	689114
534850	4809082	689114
536326	4826996	27360
536337	4826964	27360
536342	4826918	17280
536351	4826901	27360

Appendix A (continued)

UTM Easting	UTM Northing	Pumping Rate (L/day)
536292	4826881	27360
536350	4826851	33120
536343	4826829	48960
536325	4826791	17280
536315	4826763	21600
536324	4826744	103680
536312	4826727	33120
536315	4826995	17280
558706	4801766	980000
536205	4827249	426000
536418	4826594	230000
559540	4807988	85000
559838	4808018	85000
559451	4808040	85000
576597	4788127	380000
535531	4803398	250000
557585	4792061	51000
535531	4803398	108000
547642	4876206	345600
547600	4876100	21600
561037	4828551	339586
525786	4856366	170202
526220	4856511	44640
526254	4856516	44640
536050	4817700	40000
575090	4786794	81200
549657	4791403	58250
553905	4845247	327000
554167	4845115	1308000
553930	4845624	654000
554212	4845252	425000
547680	4813810	818280
526367	4808466	65500
569384	4813245	392500
569536	4813137	67000
569616	4813435	68500
569389	4813250	392500
536853	4817847	230000
536861	4817909	230000
556401	4821896	1640000

UTM Easting	UTM Northing	Pumping Rate (L/day)
560587	4820072	3000000
549515	4821114	820800
549528	4821187	2232000
530898	4803907	13638000
537976	4779881	98000
537982	4779887	49000
549210	4891762	1636560
559023	4807929	163500
559051	4807935	163500
549906	4784965	617143
549915	4784943	617143
549934	4784906	617143
549952	4784832	617143
549975	4784787	617143
549984	4784759	617143
538162	4805871	3950000
537994	4805866	3950000
537941	4805666	3950000
538080	4805434	3950000
538289	4805669	3950000
538380	4805873	3950000
540774	4808694	6547000
536149	4853714	459000
560507	4788389	2592150
560609	4788365	2592150
560532	4788366	2592150
548198	4839686	1962000
542787	4799007	179000
542778	4799004	179000
537262	4810650	3413000
537262	4810650	2462500
584022	4823893	5237000
532496	4809797	4582000
538787	4812245	3274000
557890	4859897	491040
558232	4860045	393120
558096	4859676	457920
535323	4853051	1080000
535319	4853057	1964160
548439	4890899	460800

Appendix A (continued)

UTM Easting	UTM Northing	Pumping Rate (L/day)
548650	4892679	159840
545434	4834906	12270000
544880	4792807	5480000
568055	4822967	8791200
567924	4823094	8791200
567996	4822441	8791200
536978	4853376	393000
548059	4784377	1426000
537504	4853848	413000
556869	4820737	1964000
536538	4805046	6550000
506735	4823859	718268
546953	4812094	1136500
547063	4812012	1136500
537022	4853000	393000
537518	4853322	1080000
552179	4785512	6547000
552147	4785618	983000
551998	4807023	130000
549716	4817654	142000
538975	4814875	81000
560520	4828020	65000
560760	4827800	65000
566601	4800523	545042
553036	4785502	324000
553216	4785322	324000
550012	4803179	1800000
547642	4876206	345600
547600	4876100	21600
547359	4809952	196383
540648	4827761	655200
540588	4808860	16365600
557513	4758603	54000
569822	4827964	1310000
537691	4806544	4320000
521161	4846256	1310000
521161	4846251	1310000
550114	4784789	1669000
527002	4845081	1963872